UNIVERSITY OF CALIFORNIA, SAN DIEGO

Origin of basalt-hosted epithermal gold-silver mineralization in the Fire Creek Deposit, Northern Nevada Rift from a whole-rock to grain-scale perspective

A Thesis submitted in partial satisfaction of the requirements for the degree of Master of Science

in

Earth Sciences

by

Jorge Perez

Committee in charge:

Professor James M.D. Day, Chair
Professor Geoffrey W. Cook
Professor Jeffrey S. Gee

2013

The Thesis of Jorge Perez is approved, and it is acceptable in quality and form for publication on microfilm and electronically:

Chair

University of California, San Diego

2013

DEDICATION

I would like to thank everyone who has contributed to this project, whether it be a grammatical correction, project suggestion, interpretation or analytical assistance. I would like to thank my girlfriend, Lauren Ovalle. She stood by me on my academically frustrating nights, made my everyday life easier and cheered me up with that amazingly epic smile. I love you and can't wait to jump along to our next adventure. I would like to thank my family Christina, Salvador, Jose and Angel. Their unconditional support and encouragement has been a part of my everyday academic career. I would like to dedicate this thesis to my parents, Jose and Eva Perez. This next section is in Spanish and I hope that it expresses my gratitude towards them. Quiero dedicar esta tesis a mis padres, José y Evangelina Perez. Sin una educación formal vinieron a este país en 1974 buscando el Sueño Americano. Mis padres reconocieron la importancia de una educación y me han motivado a lograr mi licenciatura y maestría. Nunca podre expresarles lo agradecido que estoy por todos los esfuerzos que han hecho y todo lo que me han enseñado: el trabajo constante, paciencia, ser honesto, tener confianza y nunca darme por vencido. Los quiero agradecer por dejarme soñar. Nunca estuviera en esta posición de prosperar sin sus esfuerzos, gracias. I would like to thank Geoff Cook for inspiring students every day and for guiding me as an undergraduate and graduate student. I would like to thank James Day for allowing me to be a part of his lab and partaking in the Fire Creek project. His ability to involve his students in every step of the research has led to a profound understanding in analytical methods, field work and developing original thought. I would like to thank my officemates Caitlin & Tyler (A.K.A. El Vampiro) who helped make these two last year's manageable.

TABLE OF CONTENTS

LIST OF FIGURES

LIST OF TABLES

ABSTRACT OF THE THESIS

Origin of basalt-hosted epithermal gold-silver
mineralization in the Fire Creek Deposit, Northern Nevada Rift
from a whole-rock to grain-scale perspective

by

Jorge Perez

Master of Science in Earth Sciences

University of California, San Diego, 2013

Professor James M.D. Day, Chair

Fire Creek, located in northern Nevada, is host to a low-sulfidation, epithermal Au-Ag deposit that is spatially and temporally associated with mid-Miocene volcanism. This study implements a whole-rock to mineral-scale analysis in order to evaluate the ore's paragenesis. Volcanic units at Fire Creek are a co-genetic suite of basalts to trachydacites which were subjected to three distinct pulses and possess Au-Ag in two distinct forms. Two generations of gold and Ag bearing sulfide grains are present and the average Au varies from 28.3-6.7 ppm; Ag varies from 46.6-33.0 ppm. Other studies on mid-Miocene northern Nevada low-sulfidation epithermal Au-Ag

deposits have reported general conditions for deposition or have focused on rhyolitic-hosted ores. These studies lack in-*situ* trace- and major-element analysis in order to provide a high precision model on mid-Miocene low-sulfidation, epithermal Au-Ag deposits. This study presents the first known highly siderophile element (HSE) analysis on electrum (Au and Ag alloy) grains and has coupled textural observations with in-*situ* chemical analysis in order to characterize individual pulses and develop a general paragenesis for northern Nevada mid-Miocene epithermal deposits.

1. INTRODUCTION

Epithermal environments represent an important economic class of mineral deposit and are host to some of the largest concentrations of Au-Ag mineralization in the world (McLemore, 1994). Epithermal deposits are characterized by dominantly meteoric fluids (with a slight magmatic component), forming at low to moderate temperatures (50-300 °C) and pressures (<500 bar) in the upper crust. They are typically volcanic-hosted and are related to volcano-plutonic activity (Pirajno, 2009).

Northern Nevada is host to numerous epithermal deposits and is an important precious metals source for the United States (John, 2001). Epithermal Au-Ag deposits are found throughout the northern Nevada region and can be hosted by volcanic centers associated with mid-Miocene bimodal basalt-rhyolite magmatism. Amongst these deposits is Fire Creek, a pre-dominantly basalt-hosted epithermal Au-Ag deposit which lies on the Northern Shoshone range in Lander County, Nevada (Figure 3). Fire Creek is currently an active mine host to a low sulfidation, epithermal Au-Ag deposit which has been through several stages of prospecting since the 1930's (Raven et al., 2011). Although there are several known bimodal basalt-rhyolite formations in the region, Fire Creek is rare because the Au and Ag are hosted by basalts. Fire Creek also displays several paragenetic pulses that allow for the establishment of temporal and geochemical relationships at the study site.

Epithermal deposits can be divided and characterized by the oxidation state of sulfur; low-sulfidation deposits are dominated by H_2S (reduced; lower temperature) and high-sulfidation deposits are dominated by SO^{2-} (oxidized; higher temperature) (Pirajno, 2009). Extensive research has been performed on low sulfidation epithermal Au-Ag deposits (e.g., Vikre, 1985; Noble et al., 1988; White et al., 1995; Sillitoe et al., 1996; Simmons et al., 2000; John, 2001; John et al., 2003A; Wallace, 2003; Leavitt et al., 2004; Kamenov et al., 2007; Saunders et al., 2008; Hames et al., 2009). Through these studies, general conditions, characteristics, and styles for epithermal ore formation have been defined. In northern Nevada, mid-Miocene low-sulfidation epithermal Au-Ag deposits originated from a mantle source associated with the impingement of the Yellowstone hotspot (Kamenov et al., 2007). The origin was established by comparing Pb isotope ratios in both ores and the Columbia River basalts. Although the data appear conclusive, the studied ores were all hosted by rhyolitic units which do not necessarily encompass the whole mid-Miocene suite. Pb concentrations also appear to vary systematically within distinct pulses at Fire Creek which may modify the Pb concentrations.

Although many studies have been performed on the overall nature of northern Nevada bimodal basalt-rhyolite deposits and their origin, no extensive work has been conducted on trace element pulse characterization. Highly siderophile elements (HSE: Os, Ir, Ru, Rh, Pt, Pd, Re, Au), for example, are a potentially powerful suite of elements that can be used to understand Au-Ag mineralization because of

their intimate association with Au. This suite of elements tends to have strong affinities for metals and sulfides relative to silicates and so can be used to track both sulfide and alloy generation processes in Au-Ag deposits. While absolute concentrations of the HSE are potentially diagnostic tools for mineral-resource exploration, these elements also display variable partitioning behavior between highly compatible Os, Ir, Ru and Rh relative to compatible Pt and Pd and to moderately incompatible Re and Au during melting and crystallization (Day, 2013). This partitioning behavior makes these elements particularly powerful tools for tracing magmatic processes and for understanding the processes by which Au and other precious metals were sourced to form economic deposits.

This study differs from others focused on Northern Nevada epithermal Au-Ag mineralization as it not only examines the nature and style of mineralization in detail, but also examines in-*situ* major and trace elements in order to characterize individually identified pulses of mineralization. Petrographic observations are coupled with siderophile element abundances for different pulse generations to address the chemical nature of the fluid and its effects on prior pulses. The combination of these methods has allowed for a diverse pulse characterization and for the development of a refined mechanism of Au-Ag deposition at Fire Creek.

2. GEOLOGICAL SETTING

2.1 Regional Geology

Fire Creek lies at the northern end of the Shoshone Range near the western edge of the middle Miocene Northern Nevada rift (NNR), forming part of the Northern Great Basin (Figure 1). The NNR represents the surface manifestation of WSW\ENE crustal extension during the Miocene, likely related to pre-Cenozoic deep crustal faults that were reactivated by impingement of the Yellowstone hotspot (e.g., Zoback & Thompson, 1978; John and Wallace, 2000). Basement rocks in the northern Shoshone Range consist of Ordovician, Silurian and Devonian deep water marine, siliclastic sedimentary rocks (John et al., 2003B). Unconformably overlying the basement are the early Oligocene Caetano Tuff and a mid-Tertiary sequence of sedimentary rocks consisting of coarse debris flows, conglomerates, siltstone, mudstone and minor limestone that were deposited prior to the onset of mid-Miocene rifting (John and Wallace, 2000; John et al., 2003A).

Two distinct ore emplacement episodes are evident in the Northern Great Basin. The first episode produced Cu, Mo, and Au deposits, W skarns, and sedimentary rock-hosted Au deposits associated with early Mesozoic to late Cenozoic subduction-related calc-alkaline magmatism (Ward, 1995; John, 2001; John et al., 2003B). At ~30 Ma subduction ceased along a significant portion of western North America (Atwater, 1970; Dickinson and Snyder, 1979). After a period of ~13-14 m.y., intraplate bimodal magmatism became prominent, associated with impingement

of the Yellowstone hotspot on the North American plate at 16.6 Ma (Geist & Richards, 1993; John and Wallace, 2000; Camp and Ross, 2004) (Figure 1).

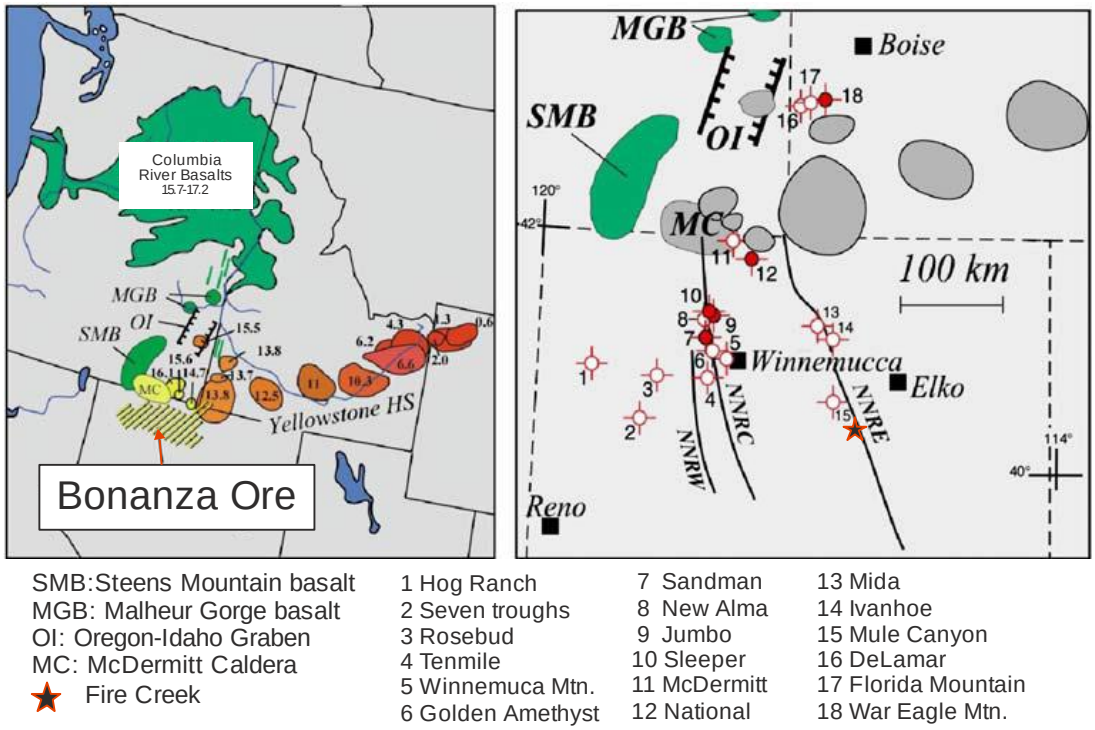

Figure 1: Distribution of mid-Miocene magmas, the Northern Nevada rift and the Yellowstone hotspot track. Northern Nevada rift encompasses central (NNRC), western (NNRW) and eastern (NNRE) offshoots. The Fire Creek deposit lies along the NNRE in close proximity to Mule Canyon, Ivanhoe and Midas. Numbered locations indicate other deposits in the area (Modified from Saunders et al. 2008).

Accompanying Yellowstone hotspot-associated bimodal volcanism was the reactivation of Cenozoic faults forming the NNR due to active Basin and Range extension (Theodore et al., 1998; John and Wallace, 2000; John et al., 2003A; Leavitt et al., 2004). These reactivated Cenozoic faults appear to have acted as conduits to voluminous basaltic dike swarms that propagated south to form prominent north-northwest trending aeromagnetic anomalies in the NNR, and that are considered to have formed concurrently with the Columbia River basalts (Zoback et al., 1994; Mabey et al., 1966; Robinson et al., 1970). The basaltic dikes appear to have fed mid-

Miocene bimodal volcanic centers that host epithermal Au-Ag deposits in northern Nevada (John, 2001; Ponce & Glen, 2002; John et al., 2003A; Hames et al., 2005). The ages of Au mineralization have been synthesized from numerous deposits in Northern Nevada; these deposits were likely emplaced in a relatively narrow time period between 16.5-15 Ma (Figure 2). Based on these ages and the similar styles of bimodal volcanism in the NNR, there is clear evidence for both spatial and temporal association of the mid-Miocene epithermal Au-Ag deposits in the NNR with the Yellowstone hotspot track.

The origin of the Yellowstone hotspot magmas that produced the Columbia River Basalts, the dikes and ultimately the ores along the NNR has been the subject of much debate. While numerous models have been proposed, no one model can account for all aspects of mid-Miocene North-Western American volcanism. However, in all cases these models implicate a mechanism for slab tearing which allowed for magma to ascend and impinge upon continental crust (Geist & Richards, 1993; Camp & Hanan, 2008; Coble & Mahood, 2012; Christiansen et al., 2002; Liu & Stegman, 2012).

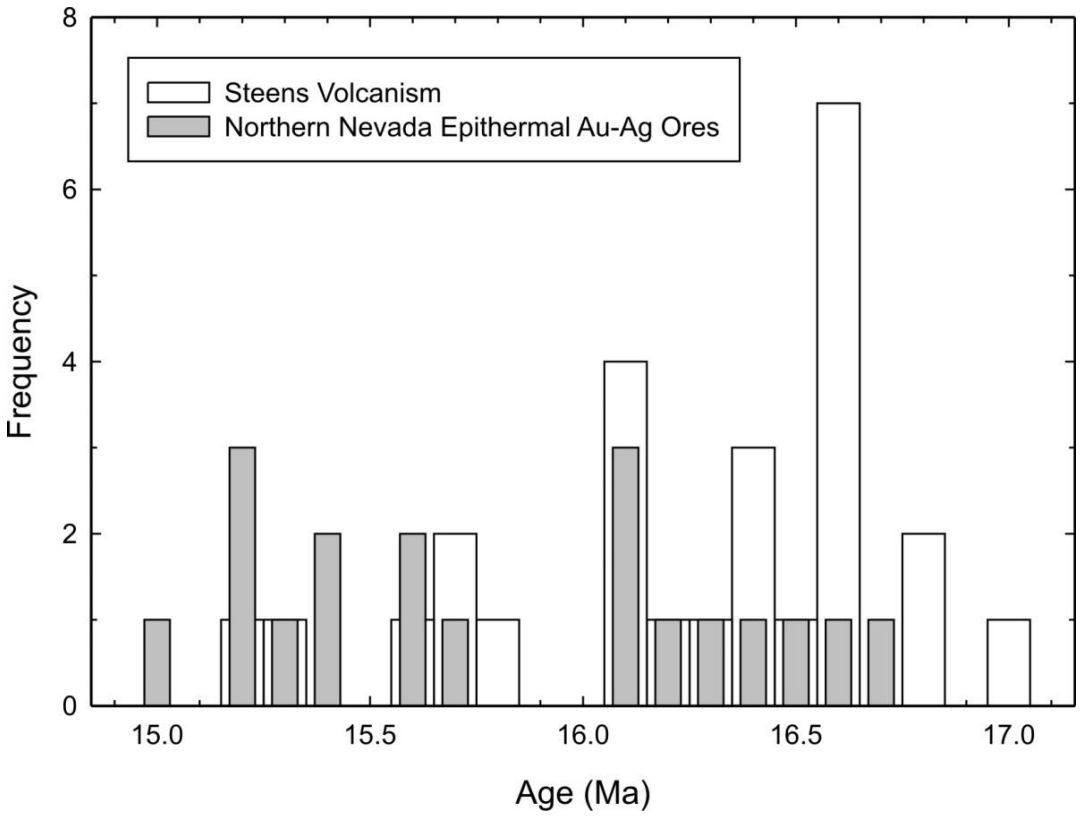

Figure 2: Age distribution of northern Nevada epithermal ores and Steens Volcanism. Data shows that the ores were all generally deposited in a narrow time period and are temporally associated with Steens Volcanism. Dates acquired from Table 1.

2.2 Local Geology

Fire Creek - the field area of focus for this study - is located in the Northern Nevada Rift (NNR) on the northern end of the Shoshone range (Figure 1 & 3). At Fire Creek a series of mid-Miocene basaltic to andesitic lava flows are cut by multiple basaltic to andesitic dikes. These units host a significant low-sulfidation epithermal Au-Ag vein ore deposit. Raven et al. (2011) have reported up to eleven units identified in drill cores from the surface exploration program (Figure 4); these units vary from basaltic to dacitic lava flows to pyroclastic rocks and are typically underlain by Paleozoic sediments. Only a few surface expressions of mineralization are present in

the study area (Figure 5) and a trachydacitic cap rock (Tb1) outcrops that post-dates Au-Ag mineralization. A summary of the unit descriptions and relations is provided in Figure 4.

Structurally, Fire Creek is associated with high angle normal faulting and horst and graben structures commonly attributed to Basin and Range tectonism (John and Wallace, 2000; Raven et al., 2011). These normal faults have strikes ranging from N 10° to N 30° east (Raven et al., 2011). The exact mechanism for the creation of these faults is highly debated, but could represent the surface manifestation of reactivated Cenozoic faults (e.g., John et al., 2003A). The faults likely served as a convenient conduit for hydrothermal activity and are associated with fluid transfer related to emplacement of ore veins (Wallace, 2003).

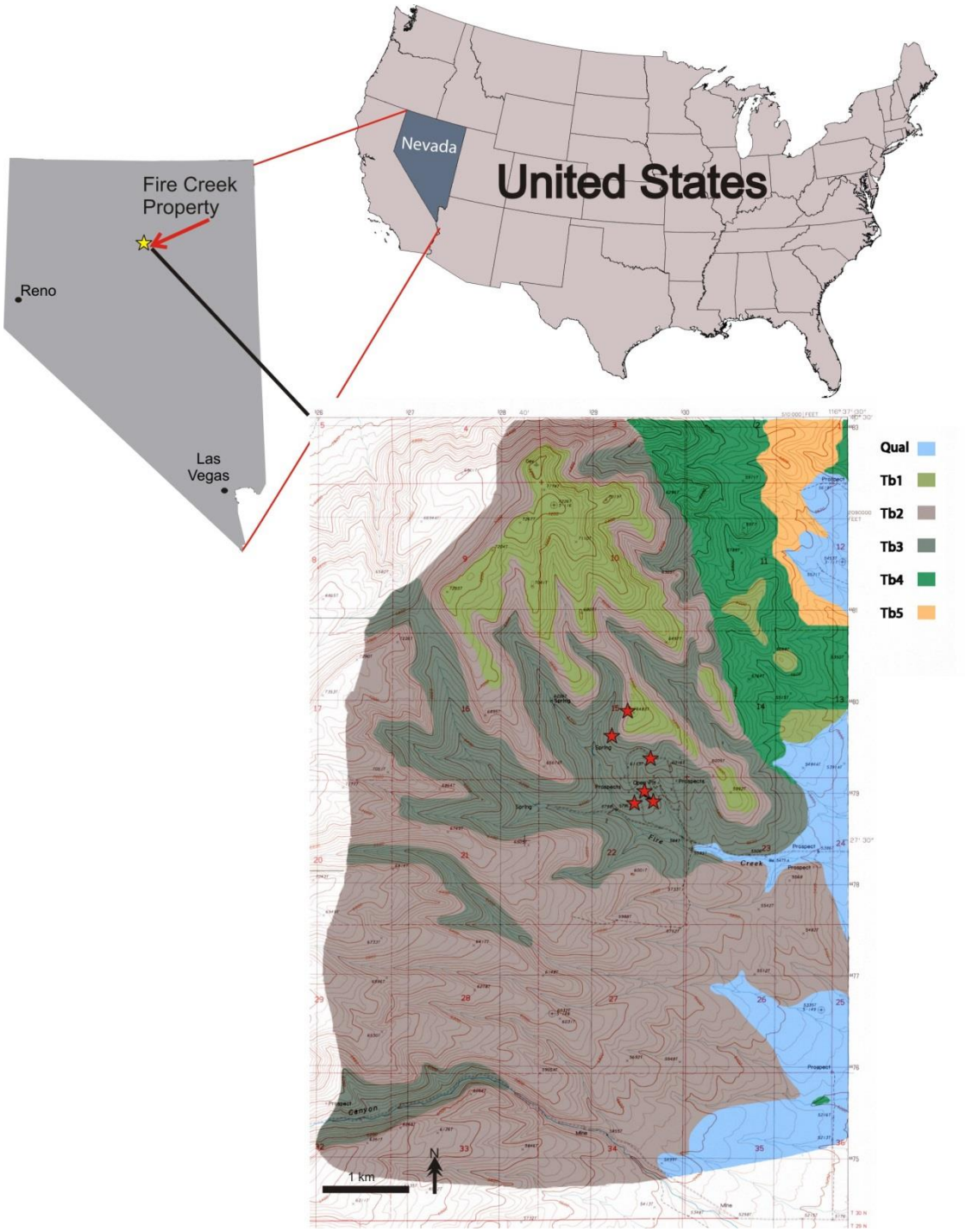

Figure 3: Geological map of Fire Creek property. The contour map was provided by the USGS and the geological units were mapped by Klondex mines. Stars represent surface sample locations for this study. Tb4 is a vitrophyric to aphanitic pisolitic porphyry. Tb5 is an aphanitic to very fine grained basalt. Qal is quaternary alluvium. Stratigraphy column in Figure 4 represents typical units that may be encountered during drilling.

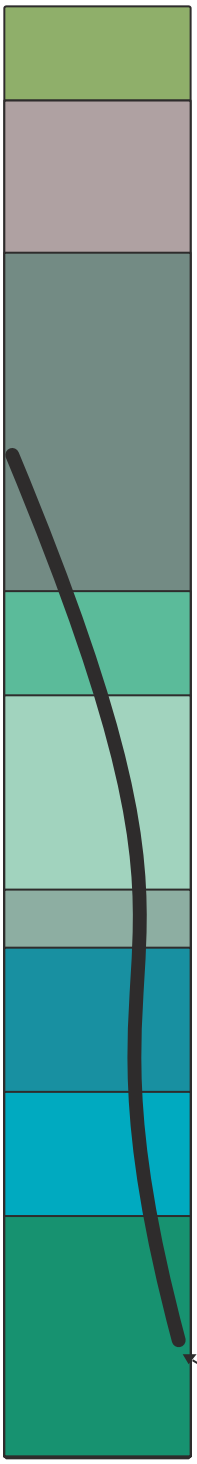

Tb1: Interbedded andesite-basalt flow sequence. Tb1 consist of very fine grain sugary with very rare phenocrysts of plagioclase and biotite. A tan to brownish gray mottling of the rock is apparent, as is a characteristic platy parting with highly variable orientations. Interbedded with the andesites are aphanitic, vesicular, basalt flows from 2 to 5m thick.

Tb2: Black to dark gray and brownish gray, aphanitic to very fine grain sugary to weakly glassy basalt flows with minor to 10% plagioclase phenocrysts. The rock typically contains 3-7% disseminated crystalline magnetite.

Tb3: Multiple light red-gray to gray, brown and black, platy to massive, vesicular, aphanitic, and porphyritic basalt flows. Aphanitic flows contain 1-3% magnetite and pyroxene in an aphanitic groundmass. Porphyritic flows contain up to 25% phenocrysts of plagioclase and pyroxene from 0.2 to 5mm in size in a very fine grain to glassy groundmass. Brown to tan ash rich tuff units occur at several horizons.

LAT: Tan to creamy-tan, non-welded, lapilli, lithic ash flow tuff with 10 to 40% basalt lithics and pumice fragments. Crystals are rare to absent and is often interbedded with underlying Tbma near base.

Tbeq 1: Holocrystalline, dense, very fine to fine grained, equigranular and porphyritic basalt flows with vesicular flow tops. Subhedral and anhedral intergrowths of plagioclase and pyroxene with very minor amounts magnetite in the groundmass with 5-15% plagioclase phenocrysts. Interbedded tan to creamy-tan, non-welded, lapilli, lithic ash flow tuff with 10 to 40% basalt lithics and pumice fragments. Crystals rare to absent and is often interbedded with underlying Tbma near base. Area is only present only in the Northeast Area.

Tbma: Black aphanitic to glassy basalt, uniformly dense and structureless. Thin lithic tuff flows in the far north area.

Tbeq or Tbeq 2: Holocrystalline, dense, very fine to fine grained, equigranular and porphyritic basalt flows with vesicular flow tops. Subhedral and anhedral intergrowths of plagioclase and pyroxene with minor magnetite in the groundmass with 5-15% plagioclase phenocrysts. Tbeq 2 is only present in the Northeast Area.

Tvft: Black to blackish gray and dark green, vitric to unwelded glass rich lithic tuffs and glassy basalt flow breccias.

Tuff & Basalt: Interbedded lithic tuffs and lesser sugary textured basalt flows, with rare small lacustrian sedimentary beds. Tuffs are non-welded, rhyolitic, lapilli to rarely bomb, lithic as flow tuffs with basalt lithics of variable composition and texture comprising up to 40% of tuff. Basalts are very fine grain sugary with rare phenocrysts and vesicles. Lacustrian sediments are composed of locally carbonaceous siltstone, chert, and waterlain tuffs.

Dike: Black to dark greenish gray, dense, massive, brittle, aphanitic to glassy basalt. It was emplaced contemporaneous with Tb2 and Tb3.

Figure 4: Generalized stratigraphic section for Fire Creek. Unit descriptions and relative order are as described by Raven et al. (2011). Colors correlate with the geological map in Figure 3.

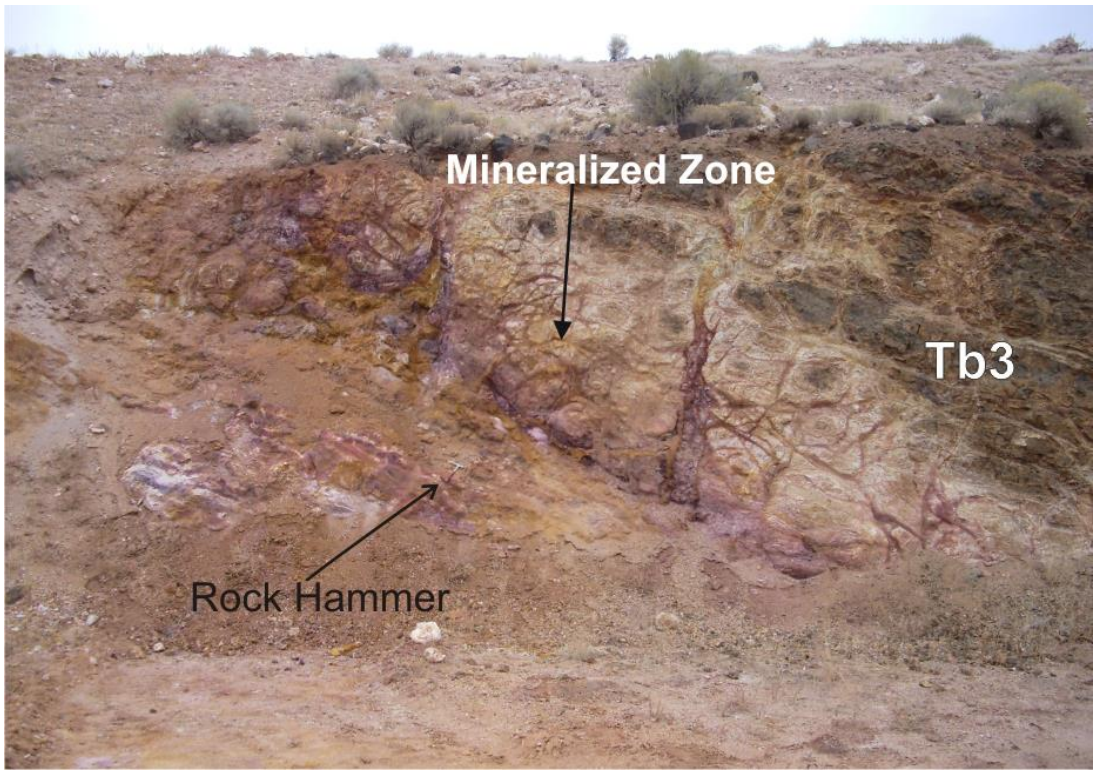

Figure 5: Exposed portion of the vein showing pervasive hydrothermal alteration within unit Tb3. Alteration decreases away from the vein and an opal cap is present on the surface.

3. ORE PROCESSES AND PREVIOUS WORK

Most of Earth's siderophile elements (Ag, Ni, As, Mo, Pt, Au, etc.) were partitioned into the core during the differentiation of Earth. Despite the expected metal-silicate partitioning of siderophile elements between core and mantle, abundances of these elements in the upper mantle are higher than expected. This has been explained through post-core formation late accretion of siderophile element-rich impactors (c.f., Chou, 1978; Day, 2013). During partial melting of the mantle, siderophile elements can be transferred into mantle melts and are extracted to the crust at mid-ocean ridges, subduction zones and intraplate magmatic regions. These volcanic centers can host economically viable ore deposits, if conditions responsible for pre-concentration are met within the magmatic system. A combination of magma source, mechanism transport and deposition variability may lead to a plethora of possible ore deposit types (porphyry, skarn, epithermal, etc.) (c.f., McQueen, 2005).

The term 'epithermal' refers to a type of ore deposit which is formed from dominantly meteoric fluids at low to moderate temperatures (>300 °C) and shallow depths (1-2 km) (Hedenquist and Lowenstern, 1994). Epithermal deposits can be divided into two categories; low- and high-sulfidation deposits. High-sulfidation deposits form from high-temperature magmatic fluids intermixed with meteoric fluids proximal to magma chambers, forming oxidized and acidic fluids. These high-S deposits are typically found in subduction settings (e.g., Sillitoe & Hedenquist, 2003). Low sulfidation epithermal systems (such as at Fire Creek) formed from reduced

fluids (primarily meteoric) with a nearly neutral pH and low salinity somewhat distal from coeval magma chambers that may be genetically related to them, and typically form in extensional settings. The main metals associated with low sulfidation deposits are Au and Ag, whereas high sulfidation deposits also include Cu, As, Sn and Sb as major metals (Sillitoe & Hedenquist, 2003).

Northern Nevada hosts a variety of ore deposits, with many that are temporally and spatially linked to two distinct magmatic assemblages: western andesite and bimodal basalt-rhyolite (John, 2001). These deposits consist of high- and low-sulfidation epithermal Au-Ag and porphyry Cu-Au deposits. The western andesite assemblage was produced by subduction along the western continental margin which formed water-rich, calc-alkaline magmas and is host to high- and low-sulfidation and porphyry deposits. The bimodal basalt-rhyolite assemblage was formed from tholeiitic magmas with low water content in a continental rift environment and is host to low-sulfidation Au-Ag deposits. This latter deposit-type forms the specific focus of this work and hence the main metals that will be discussed in this context are Au and Ag.

The Fire Creek deposit is a low sulfidation epithermal deposit associated with mid-Miocene bimodal basalt-rhyolite volcanism which was initiated approximately 6.6 Ma near the Nevada, Oregon, and Idaho intersection (Dickenson 2006; Brueseke et al. 2007; Saunders et al. 2008). Multiple mid-Miocene low sulfidation deposits in Northern Nevada have been investigated (e.g., Vikre 1985; Noble et al., 1988; Conrad et al., 1993; John et al., 2003A, Kamenov et al., 2007; Hames et al., 2008), but all

have suffered from limited sampling from ‘mature’ mines that were well into excavation at the time of study. A primary reason for examining Fire Creek is that it is currently under development for mining operations and so allowed for a highly robust, pristine sample set to be acquired that samples representative geological variability throughout the site. Another important distinction between the various low-sulfidation mid-Miocene NNR deposits, such as Midas, Sleeper, Buckskin National, Buckhorn, Mule Canyon and Fire Creek are their lithological host rocks (Table 1). Consequently, as will be demonstrated here, the differing styles of mineralization, ore geochemistry and gangue mineralization may be strongly affected by the associated host lithologies.

A major controversy persists as to the source of Au and Ag in NNR epithermal Au-Ag deposits. One model posits that the majority of Au and Ag was leached from underlying sedimentary units and deposited in distinct styles based on stable isotope data (John et al., 2003A). In this model, the magma source merely served as a heat source that drove hydrothermal activity and leached Au an Ag from the underlying sedimentary units. In an alternative model, based on Pb isotope data for numerous NNR deposits, it has been proposed that the Au and Ag are in fact sourced from the magmas themselves (Kamenov et al., 2007). This model is posited because the Pb isotope ratios in gangue minerals are consistent with hydrothermal leaching of major elements from metasedimentary rocks, but that lead isotope ratios within Au ores themselves are similar to that of the Columbia River Basalts (CRB; Kamenov et al., 2007; Hames et al., 2009). Determining the source of the Au and Ag is a vital goal

because it is possible that the mineralization is directly related to the CRB magmatic system.

Table 1: Geochronology of bonanza Au-Ag Deposits, Northern Great Basin (modified from Saunders et al., 1996 & Saunders et al., 2008).

Deposit	Age (Ma)	Dominant Host Rock	Reference
Sleeper	16.1-14.3±0.07	Rhyolite	Conrad et al. 1993
Midas	15.4-15.3±0.08	Rhyolite	Leavitt et al. 2004
Fire Creek	-	Basalt	This work
Mule Canyon	15.6±0.04	Basalt	John et al. 2003
Hog Ranch	15.2-14.8±0.04	Rhyolite	Bussey 1996
Ivanhoe	15.19±0.05	Rhyolite	Wallace 2003
Buckskin-National	15.8-15.4±0.2	Rhyolite	Vikre 1985
Buckskin National	16.06±0.3	Rhyolite	Vikre 2007
DeLamar (ID)	15.7±0.5	Rhyolite	Halsor et al. 1988
War Eagle Mtn.I (ID)	16.31±0.04	Granitoid	Hames et al. 2009
War Eagle Mtn.II	15.61±0.04	Granitoid	Hames et al. 2009
Jumbo	16.53±0.04	Meta-sediments	Kamenov et al. 2007
Sandman	16.17±0.04	Meta-sediments	Kamenov et al. 2007
Tenmile	16.52±0.04	Meta-sediments	Kamenov et al. 2007
New Alma	16.03±0.03	Meta-sediments	Kamenov et al. 2007
McDermitta	15.6±0.4	Rhyolite	Noble et al. 1988
Seven Troughs	13.82±0.02	Rhyolite	Hudson et al. 2006

4. METHODS

4.1 Sampling

All samples in this study were attained from the Fire Creek Property, Lander County, Nevada, with permission from Klondex Mines Ltd in 2011 (hereafter referred to as 'Klondex'). Samples include cores and surface samples. Klondex generously permitted sampling of one half or one quarter of available cores, with preservation of the remaining core for assay or for a further economic indicator. For the purpose of this work, two cores were selected from a wide range of available cores provided from the Klondex exploratory coring program. The two cores, and the intervals selected for study within those cores, were selected based on: (1) the full range of recognized lithological diversity at the Fire Creek Property; (2) degree of alteration and relation to mineralization, and (3) access to the range of mineralization observed at Fire Creek.

Sample FC 0703 is a 12.2 m interval of core removed at a depth of 274-281 m (based on the present surface morphology at the site). This interval represents a section of both high-grade and low-grade ore, and is representative of the main zone (the main zone is a term used by Klondex to indicate a system of veins which are being targeted). Sample FC 0427 contains portions of a 548.64 m sample of core which represents non-mineralized to slightly mineralized samples. These samples were chosen in order to better develop an understanding of pre-mineralizing magmatic processes. Core samples were labeled according to the Klondex labeling system and further refined in order to record and log petrographic and geochemical

information at finer scales. All core samples were also recorded by Klondex and projected on to a cross-section (Figure 6).

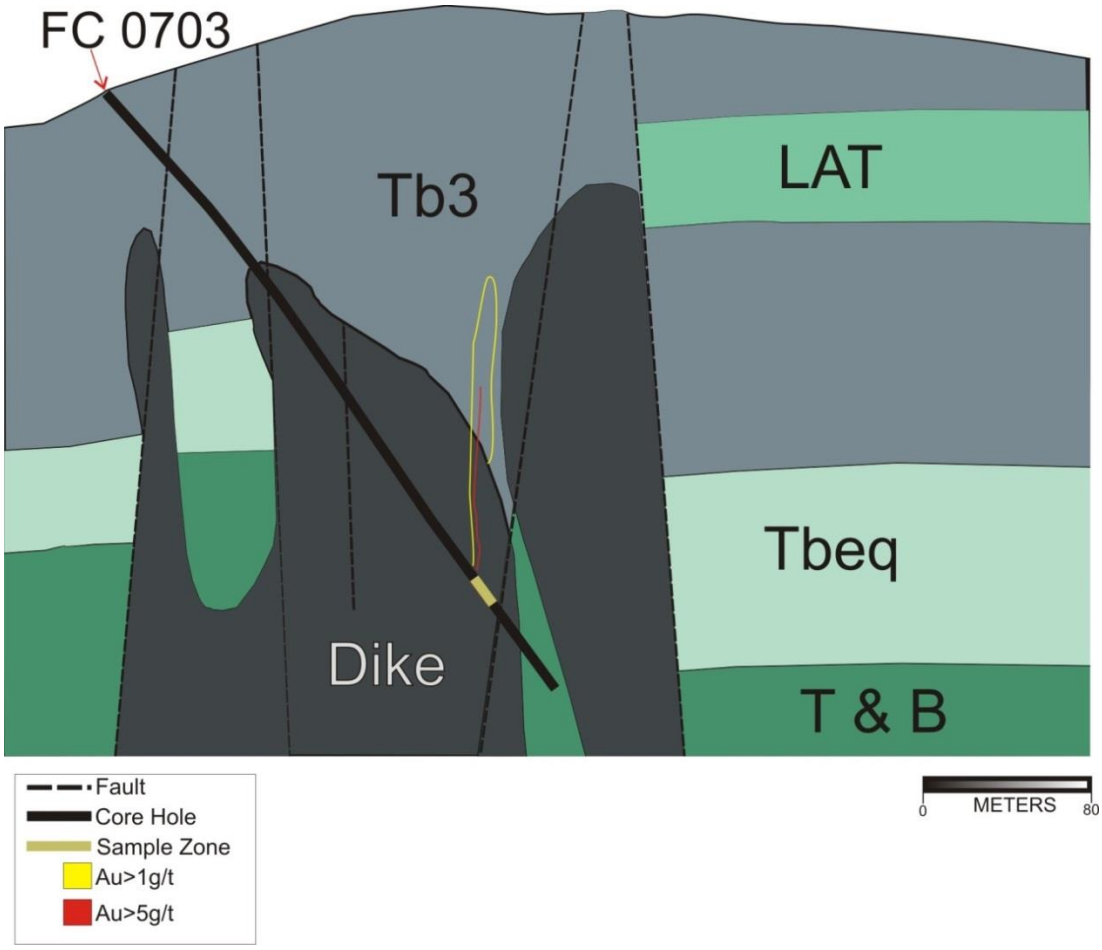

Figure 6: Cross section of Fire Creek with core hole FC 0703 (black line).Units present are indicated on the figure and described on figure 4. Tan region of core hole indicates the location and the sample section (Sample FC 0703; ~12m) which was attained for this study. Red and yellow zones indicate low to high grade zones of ore indicated by Klondex. Image was modified from a cross section attained from Klondex.

A total of 12 samples were collected at surface exposures or within the recently constructed mine adit at the site. This collection was performed to obtain representative samples of sub-surface and surface lithologies associated with bi-modal volcanism in the area and which host the mineralization. These samples were

recorded, photographed and located (using GPS) on site (with the exception of samples taken underground, which were located based on mine maps). Samples collected in exposed portions of the mine were selected on the basis of being representative of typical Fire Creek units (Raven et al., 2011) and/or any exposed mineralized sections. Two samples localities that are representative of a mineralized portion of the study area are shown in Figure 5.

Magnetic susceptibility measurements were acquired in the field (FC 1101-1105) and on FC 0703 (core interval) using a hand-held magnetic susceptibility meter (GF Instruments SM 20). These measurements were conducted by placing the susceptibility meter flush to the sample and taking >3 individual measurements of different portions of the sample to obtain a mean relative magnetic susceptibility measurement. These measurements were noted alongside petrographic, location and sample observations. Magnetic susceptibility was used as a proxy for regions of alteration (Figure 7; Table 3 & 4).

4.2 Petrology & Petrography

Detailed petrologic observations were logged every ~5 cm for core unit FC 0703 (12m of core). Magnetic susceptibility measurements were also made along FC0703. Observations made included rock type, degree of alteration, hardness, color, mineralogy, pulse type and width of veins. Petrographic observations led to the selection of 19 zones from which polished sections were made. All cores were received by Klondex in boxes with designated numbers and five, 0.6m intervals.

Polished sections were named according to their box number, row number, and petrographic note number (example: 50-2-2; Figure 7). Two non-mineralized sections were chosen from Tbeq and the dike. These zones were selected with the aim of representing a wide range of mineralization and unaltered host rock. A total of 19 mineralized and 2 non-mineralized sections were made. The sections were all cut at Scripps Institution of Oceanography (SIO) and the billets were sent to San Diego Petrographics where they were made into polished sections.

Detailed petrography was performed on all polished sections in reflected, polarized and cross-polarized light. Samples contained multiple vein generations (with distinct mineral phases), high and low grade ore, and preserved portions of the dike (Table 2). Two non-mineralized samples were examined in order to characterize the host rock. Photomicrographs of each section were made in order to facilitate in-*situ* grain-scale analyses.

Table 2: Samples are all polished sections (mineralized/altered) containing description of pulses present, acquired depth, present minerals, Au and Ag assays and analysis conducted. All polished sections in this table were acquired from sample FC 0703

Sample	Depth (m)	Pulse Generation(s)	Mineral phases	Assay Au/Ag ppm	SEM (Y/N)	EMPA (Y/N)	LA-ICP-MS (Y/N)
47-1-2	296.8	1 & 2	Cal, Qtz, Py, Apy, Clay	0.02 / 0	Y	N	N
47-3-4	297.75	1 & 2	Plag, CPX, Py, Clay	0.21 / 0	N	Y	Y
47-5-3	298.88	1 & 3	Plag, Cal, Qtz, Py, Clay	37.5 / 3.6	N	N	N
47-5-4	299.08			37.5 / 3.6	N	N	N
48-2-1	299.82	1 & 2	Plag, Qtz, Py, Clay	37.5 / 3.6	N	N	N
48-4-4	301.34	1 & 2	Plag, Qtz, Py, Clay	0.83 / .3	N	N	N
48-4-5	301.44	1?	Plag, Py, Mo	0.83 / .3	Y	N	N
49-2-2	302.7	1 & 2	Qtz, Cal, Py, Clay	0.27 / .9	N	Y	Y
49-3-2	303.2	2 & 3	Qtz, Cal, Py	1.99 / 2.9	N	N	N
49-4-2	303.72	1 & 2	Plag, Qtz, Py, Clay	1.99 / 2.9	N	Y	Y
49-4-3	303.81	1 & 2	Qtz, Py, Clay	1.99 / 2.9	N	N	N
49-5-2	304.4	1 & 2	Qtz, Cal, Plag, Py	29.8 / 13.6	N	N	N
50-1-1	304.52	1, 2 & 3	Qtz, Cal, Py, Clay, Plag	4.88/ 213	N	Y	Y
50-1-2-1	304.72	1, 2 & 3	Plag, Cpx, Qtz, Py, Clay	4.88/ 213	N	Y	N
50-1-2-2	304.77	1, 2 & 3	Plag, Cpx, Qtz, Cal, Py, El, Clay	4.88/ 213	Y	Y	Y
50-1-3-1	304.87	1 & 3	Plag, Qtz, Cal, Py, El	4.88/ 213	Y	N	N
50-1-3-2	304.91	1, 2 & 3	Plag, Cpx, Qtz, Py, El, Clay	4.88/ 213	Y	N	N
50-4-3	306.39	1 & 2	Qtz, Cal, Py, Clay	3.66 / 5.9	N	N	N
50-5-3	307.1	1 & 2	Plag, Qtz, Py, Clay	3.66 / 5.9	N	N	N

Qtz- Quartz, Plag- plagioclase, Cpx- Clinopyroxene, Cal- Calcite, Py- Pyrite, Apy- Arsenopyrite, El- electrum

Figure 7: Core unit FC 0703 in boxes 47-50 (box numbers go from left to right and continued to image below). Yellow tags with numbers indicate the region where a polished section was acquired from. First number indicates the box number, second number (after the dash) indicates the row number, and last number(s) (after the dash) indicate petrologic note order (notes were taken in a notebook). Red numbers are zones which magnetic susceptibility was measured. Results are shown in table 3.

Figure 7: Continued

4.3 Semi-quantitative and quantitative major-element mineral chemistry

Scanning Electron Microscopy (SEM) analysis of 5 carbon-coated polished sections (Table 1) was performed at the Calit2 Nano3 facility at the University of California, San Diego using a Philips XL30 field-emission Environmental Scanning Electron Microscope equipped with an Oxford Pentafet detector (10 mm^2 window). The instrument was used to perform energy dispersive X-ray spectrometry (EDX) with

a beam energy of 20kV at a distance of 10 mm. An average of 5000 X-ray counts per second were obtained for semi-quantitative geochemical analysis. Samples for SEM were carefully chosen in order to acquire an understanding of elemental spatial relationship between pulse generations.

Quantitative mineral chemistry was performed using a Cameca SX-100 electron microprobe of the Earth Sciences Electron Microscopy, Diffraction and Micro-Analysis Laboratory, University of California, Santa Barbara. A total of six polished sections (Table 2) were analyzed and a total of seven mineral phases (electrum, calcite, quartz, sulfides, plagioclase, pyroxene and magnetite) were investigated in order to conduct a mineral-scale study of magmatic and hydrothermal processes. Five altered slides and one unaltered slide of the dike material were analyzed. Samples were chosen in order to encompass host rock mineral phases and distinctive mineral pulse phases. Mineral chemistries were determined in wave-length dispersive spectral mode using an accelerated potential of 15keV, a 10-15 nA beam current, with beam focus of 1 μm. Peak and background counting times of 20 s and standard ZAF (PAP) correction procedures were used. Plagioclase compositions were determined using a 10 nA beam current, a 5 μm beam size, and longer counting times to avoid mobilization of Na or K. Natural and synthetic standards were used for calibration. Drift was within counting error through the analytical session. Detection limits (3σ above background) were <0.03 wt.% for all elements listed.

4.4 In-situ trace-element mineral chemistry

This study reports the first laser ablation inductive coupled plasma mass spectrometry (LA-ICP-MS) analysis of both sulfide and electrum phases from any epithermal Au deposit globally. Analyses were conducted using a New Wave Research UP-213 laser ablation system coupled to a ThermoFinnigan Element 2 high-resolution sector field ICP-MS at the University of Maryland, College Park. Phases were analyzed using individual spots with a 25-55 μm diameter, a laser repetition rate of 7 Hz and a photon fluence of 2-3.5 J cm^{-2}. Th/ThO production was <0.1% for the analytical session. The ablation analysis took place in a 3 cm^3 ablation cell. The cell was flushed with a He gas flow of 1 L/min to enhance production and transport of fine aerosols, and was mixed with an Ar carrier gas flow of 0.4 L/min before reaching the torch. Background on ICP-MS sample gas were collected for ~30 s followed by 60 s of laser ablation of the sample. A pre-ablation stage was introduced (before collecting background gas) in order to eliminate detection of any surface contamination. Washout time between analyses was in excess of 2 minutes. Data were collected in time-resolved mode so that effects of inclusions, mineral zoning, and possible penetration of the laser beam to underlying phases could be evaluated for each analysis. Plots of counts per second versus time were examined for each analysis, and integration intervals for the gas background and the sample analysis were selected manually using LAM-TRACE software. Each LA-ICP-MS analysis of sulfide was normalized to Fe, measured previously by electron microprobe, used as an internal standard to account for variable ablation yield. LA-ICP-MS time-resolved patterns

show that the ablated volumes were generally homogeneous. For electrum, normalization was performed using copper. NIST 610 and JB Sulfide were used as standards for the detection of a wide range of elements (S, Ti, MnO, Fe, Co, Ni, Cu, Ga, As, Mo, Ru, Rh, Pd, Ag, Sn, W, Re, Os, Ir, Pt, Au, Pb). Samples were limited to those used in EMPA and were chosen in order to encompass distinct pulse events (Table 1). Details and development of the new LA-ICP-MS method to study sulfide and electrum in epithermal Au deposits are provided in the discussion.

EMP analysis was also performed in order to attain an internal standard for LA-ICP-MS. For both electrum and sulfide phases, iron was to be used as an internal standard. Internal standardization became an issue when ablation on electrum phases began. Iron was briefly recorded during ablation and would immediately drop below background levels. This suspicious behavior was then followed by a longer pre-ablation stage which then showed no detectible signs of iron during analysis. The behavior of iron within electrum phases appears to be a result of surface contamination and is likely due to polishing near iron-sulfide phases. Electrum grains in these samples, therefore, are comprised of Au, Ag, and only trace amounts of other chemical impurities. Consequently, iron and sulfur concentrations were removed from electrum totals (Figure 8).

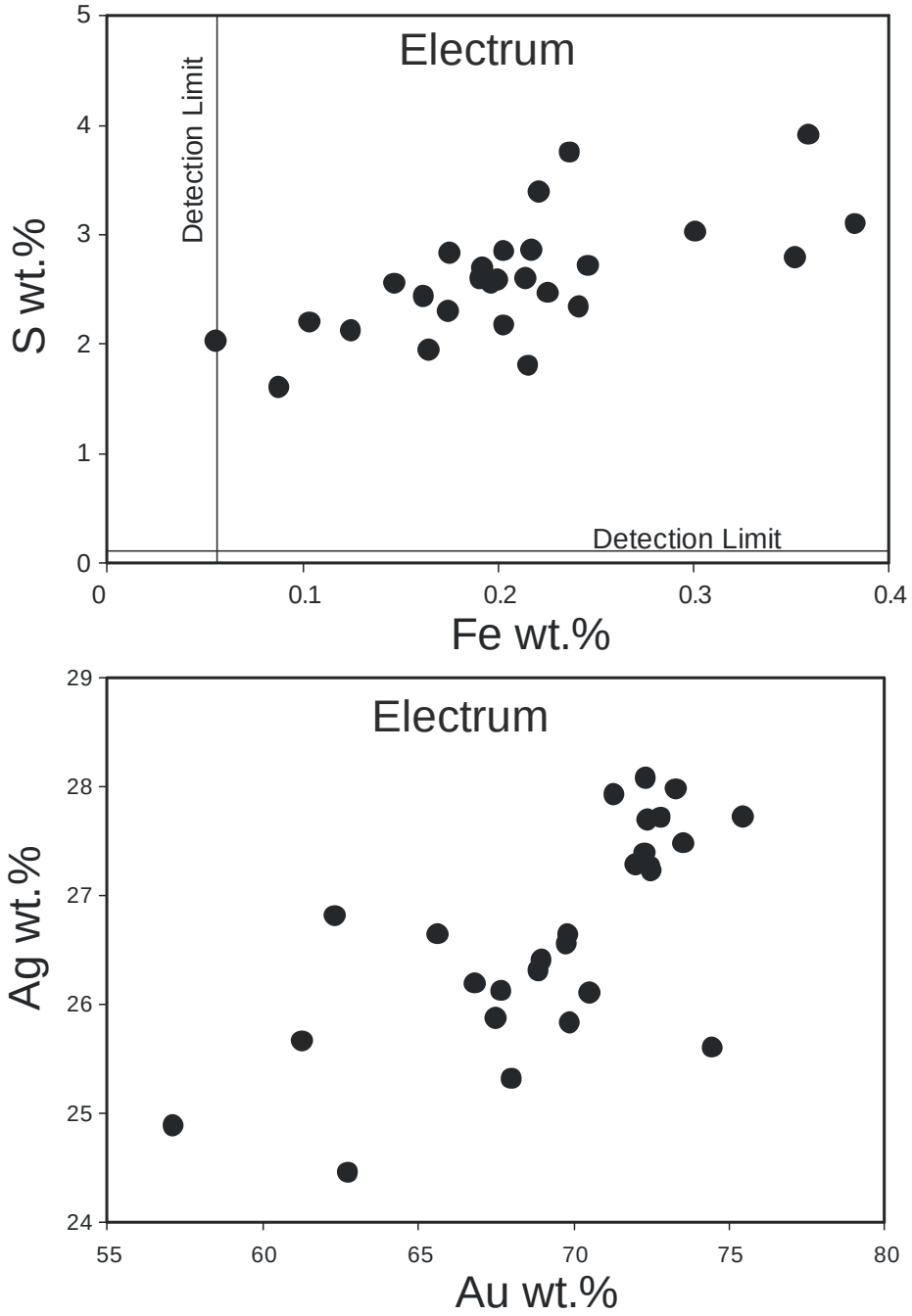

Figure 8: Au, Ag, S and Fe concentrations (data acquired from EMPA) within electrum grains displaying positive correlations. Fe and S are products of surface contamination (most likely caused by polishing).

4.5 Whole-rock geochemistry

Powders for XRF analysis were prepared at SIO. Samples were chosen in order to encompass the suite of mid-Miocene units (unaltered) at Fire Creek. All samples were crushed using a tungsten crusher. The crusher was taken apart and cleaned with deionized water and alcohol between each sample. The samples were then powdered using a tungsten shatter box. The shatter box was cleaned thoroughly using deionized water and alcohol in-between samples. In-between samples a sand cycle was also run in order to remove any leftover material. The samples were powdered until no aggregate (sample needed to be the consistency of talc) material was left over. If left over aggregate material was still present, the sample was powdered with an agate mortar and pestle, which was also cleaned with sand, deionized water and alcohol. A set of separately prepared mineralized samples were also sent to Franklin & Marshall College. These samples were cut and photographs were taken in order to record vein to host rock percentages. These cut samples were crushed and powdered using an agate mortar and pestle. All samples were then sent to Franklin & Marshall College where they were analyzed for major and trace elements, loss on ignition (LOI), and $Fe^{2+}/^{3+}$ using a PW2403 Panalytical, Inc. XRF vacuum spectrometer.

Major elements were measured by using lithium tetraborate flux and whole rock powder fused into glass discs, which were then used for X-ray fluoresence (XRF) analysis. For trace element analyses, whole-rock powder was combined with high purity Copolywax powder to make briquettes, which were then used for XRF trace-

element determinations. Working curves for all major and trace elements were determined by analyzing geochemical rock standards. For major elements, all the errors that could accrue from weighing, mixing, preparation of the fusion glass disk, and peak and background measurements yield an uncertainty of <0.1 wt.% (e.g., 0.02 wt.% for Na_2O, and 0.005 wt.% for Al_2O_3). For trace elements discussed in this study, all the errors that could accrue from preparation and instrumentation yield an uncertainty of <5% from the accepted value for geochemical standards with the exception of Ba, having >10% variation from the accepted standard value.

5. RESULTS

5.1 Magnetic susceptibility measurements

Field magnetic susceptibility averaged results are reported in Table 4. These measurements were used during core log selection and sampling to establish strong magnetism and alteration. Result show that magnetic susceptibility for individual units vary from <1 to $14x10^{-3}$ (SI). Susceptibility measurements made on FC 1102 show that susceptibility decreases as the rock becomes more altered. Generally results for FC 0703 (Table 3) show a variation in susceptibility. Quartz/calcite altered zones typically display a susceptibility below $1x10^{-3}$ (SI), pyrite veinlets display a susceptibility of $>5x10^{-3}$ (SI) and zones with little to no alteration display a susceptibility of $16x10^{-3}$-$5x10^{-3}$ (SI).

Magnetic susceptibility can be crucial in determining areas of alteration at Fire Creek. The relationship between the magnetization induced in a material M_I (in this case the rock) and an external field H (caused by the hand held device) is defined as: $M_I=x_bH$ where x_b is known as the bulk magnetic susceptibility (MS) (Tauxe, 2009). Certain mineral phases may exhibit a larger response to an external field and thus alteration and replacement mineral may result in a change in magnetic susceptibility. At Fire Creek altered zones exhibit low magnetic susceptibility. A reduction in MS might be in response to the alteration and destruction of ferromagnetic minerals (magnetite) and emplacement of diamagnetic minerals (quartz and calcite).

Conversely, high magnetic susceptibility occurred in fresh samples with high proportions of magnetite. Magnetic susceptibility proved a useful 'high-grading' tool during sampling at Fire Creek.

Table 3: Magnetic susceptibility results from core samples (FC 0703)

Sample #	*Magnetic susceptibility	Error (±)
1	5.72	3.478
2	0.14	0.120
3	5.27	1.552
4	12.23	2.913
5	4.52	1.144
6	11.48	0.991
6	6.97	2.561
7	10.70	1.433
8	1.06	0.271
9	8.23	0.609
10	0.015	0.007
11	0.017	0.001
12	0.057	0.013
13	0.012	0.003

*Average magnetic susceptibility in 10^{-3} SI units

Table 4: Magnetic susceptibility results from surface samples

Sample	Unit	*Magnetic susceptibility	Error (±)	Comments
FC 1101	Tb3	13.3	2.98	Solid fine grained unit
FC 1102	Tb3	0.1	0.03	Strongly altered zone
FC 1102	Tb3	3.5	0.1	Moderately altered zone
FC 1102	Tb3	7.5	0.3	Little to no alteration
FC 1103	Tb3	4.1	0.01	Vesicular flow top
FC 1104	Tb2	3.3	1.89	Large vesicles present
FC 1105	Tb2	2.2	0.17	Flow top
FC 1106	Tb1	9.5	0.99	Platy unit with multiple joints

*average Magnetic susceptibility in 10^{-3} SI units

5.2 Petrography

Petrographic results were conducted and will be given in the order of: (1) representative logged core observations, (2) petrographic dike observation and (3)

petrographic vein observations. This order allowed for zones of alteration and diagnostic host rock minerals to be characterized and further examined.

The petrology of FC 0703 is noted by a black to dark gray, hard aphanitic dike. Alterations consisted of brassy pyrite veins and veinlets, large quartz and calcite veins and strongly altered quartz and calcite solution breccia zones. These vein systems strongly alter the host rock marked by its strongly discolored appearance. At times pyrite veinlets propagate from a zone of coarse-grained gabbroic material. These coarse grained zones appear to be a remnant slightly altered region of the dike. A small anomalous veinlet with small discontinuous red mineral grains was also noted in the sample.

All mineralized samples acquired from Fire Creek are hosted by the dike. Unmineralized dike consists of fine grained (aphanitic to holohyaline) matrix within, euhedral to subhedral plagioclase (7-10%), subhedral clinopyroxene (1-3%) and euhedral magnetite grains (5-6 %). Magnetite is relatively equigranular and dispersed evenly throughout the slide and is never present in mineralized samples. Unaltered to slightly altered portions of the dike are found within certain strongly altered zones (FC 47-3-4, 50-1-2-2 and 50-1-3-2). These portions of remnant dike have fine-grained plagioclase and pyroxene crystals.

Detailed petrographic analyses were performed on 19 mineralized samples. Mineral phases observed vary from opaque minerals such as pyrite, arsenopyrite, electrum, and molybdenum to anisotropic minerals such as quartz, calcite and

smectite. Pervasive argillic and propylitic alteration is apparent throughout the host rock, creating zoned regions along veins. Degrees of host rock alteration are typically controlled by the pulse type. Three primary pulses were identified within the sample set (Figure 9).

Pulse 1 (P1) is a sulfide-rich pulse which varies from micro-veinlets (<2mm wide) to veinlets (>2mm wide) with occasional concentric veining. This pulse includes euhedral to anhedral sulfide-rich minerals, mostly pyrite, that appear tan to cream in reflected light. Common sulfide crystal forms include cubic, hexagonal, elongate, and irregular/smeared (Figure 10 B, C & D). The texture of sulfide phases appears to change through the interstellar medium. High concentrations of smeared, hexagonal, and/or cubic sulfide phases appear within veins. In the host rock, elongated sulfide phases are dispersed throughout in low concentrations, while other sulfide geometries are rare.

Pulse 2 (P2) consists of narrow/confined veinlets of anhedral to subhedral quartz and/or sulfide phases (Figure 9). This vein is characterized by its heterogeneous vein mineralogy and the lack/absence of calcite. P2 is not present in every sample and mineralogy tends to vary. Within certain polished sections, sulfide phases are highly concentrated near the host rock; otherwise they are evenly dispersed within the vein (e.g., 49-2-2 and 49-5-2). Sulfide grains vary from subhedral to anhedral with an irregular shape. Quartz is typically anhedral and is the most abundant mineral within P2. P1 and P2 appear to be temporally associated with one another due to the fact that

they alternately cross-cut each other in different sections; occasionally, a single vein can transition between quartz rich regions to sulfide rich micro-veinlets.

Pulse 3 (P3) varies in style of deposition from stockwork veins to solution breccias which display altered fragments of the host rock. Textural relationships are relatively homogenous within P3 but slight variations are found. Calcite is the most abundant mineral, followed by quartz (Figure 9). Quartz phases vary in P3 from euhedral to anhedral (textural variations are increased in solution breccias). Quartz was found to have a lath-like euhedral structure only when it is near the host rock (or solid substrate) (Figure 11 A). All other quartz appears to be anhedral to subhedral, hexagonal regardless of its spatial association with the host rock. Calcite is typically euhedral to subhedral and found in the center of the vein with lath-like quartz surrounding it (Figure 11 A). Bladed calcite with large euhedral quartz and small subhedral quartz is present in sample FC 47-1-2 and appears to be associated with P3. Electrum (Au-Ag alloy) was only found within P3 but is not present within every P3 vein. P3 cuts all other pulses and therefore is considered the youngest pulse in the sample set.

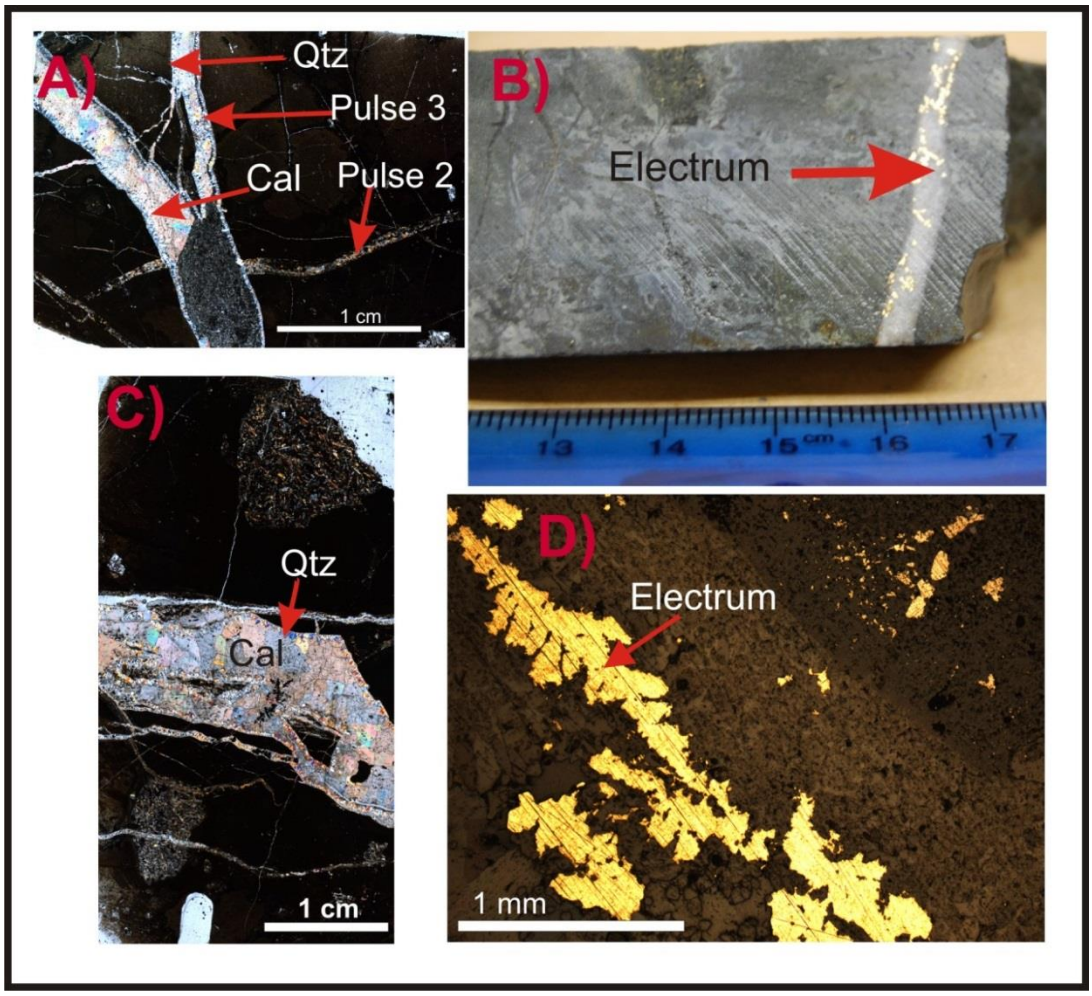

Figure 9: a) photomicrograph; xpl (from sample 50-1-1) b) Strongly altered core with a large Qtz/Cal vein hosting electrum (from core unit FC 0703, box 50, row 2) c) late stage pulse 3 composed of quartz and calcite hosting dendritic electrum; xpl (sample 50-1-2-2). Coarse grained regions appear to be remnant portions of the dike that have been slightly altered. D) Native dendritic electrum (sample 50-1-3-1). Scale bars shown in the figures.

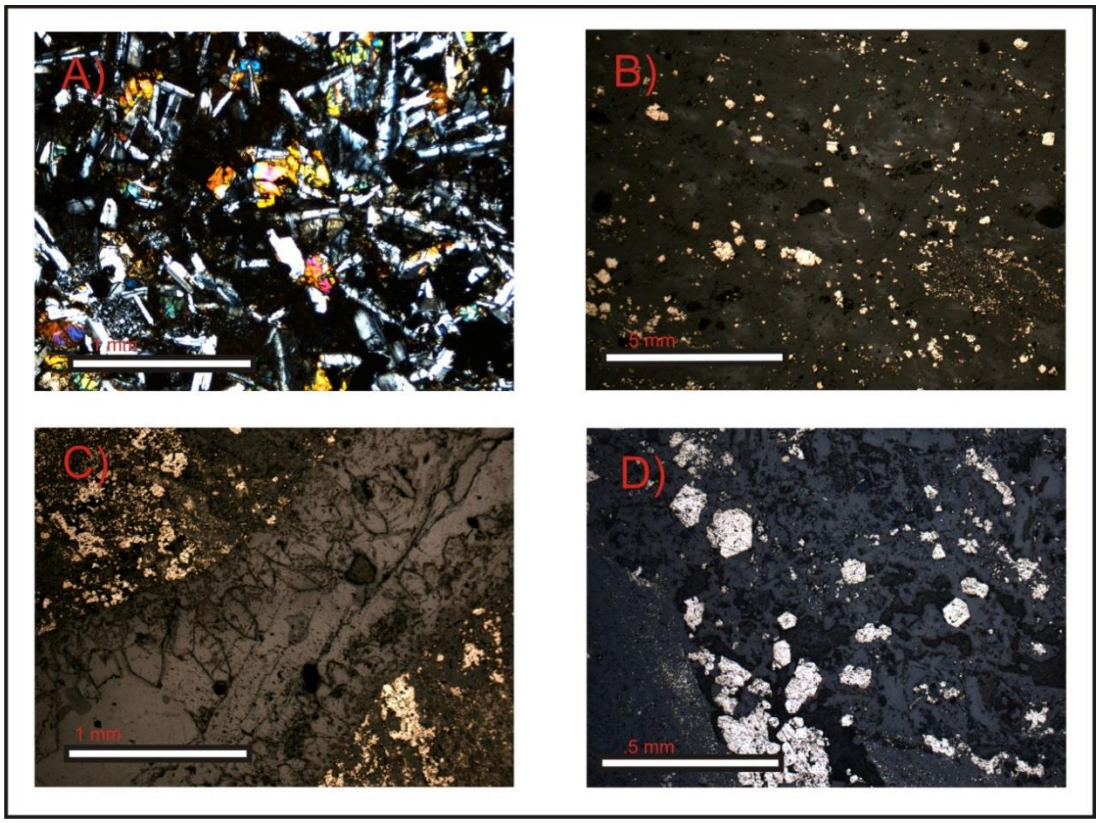

Figure 10: A) Image of preserved, slightly altered dike within a pervasively altered slide (sample 47-3-4; host rock); xpl. B) Tan, cubic to hexagonal sulfide grains in pulse 1 (sample 50-4-3; pulse 1); reflected light. C) Sulfide grains on the outer edges of pulse 3 (sample 50-1-2-1; pulse 3 in the center and possibly pulse 1 on the outer edges); xpl. D) Cream, cubic to hexagonal sulfide grains in pulse 1 (sample 49-5-2; pulse 1 or 2).

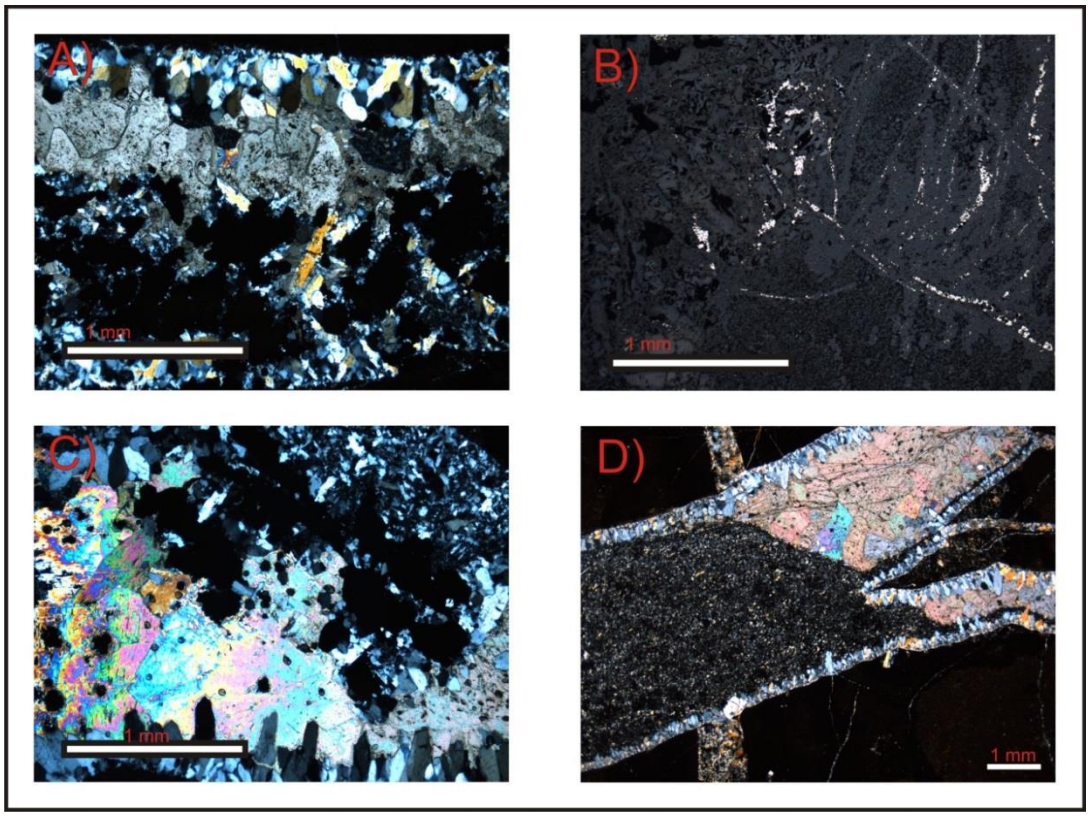

Figure 11: A) lath-like quartz, large crystalline calcite grains and electrum present in pulse 3 (50-1-3-2; pulse 3); xpl. B) Sulfide rich pulse (P1) propagating from preserved portion of the dike (sample 47-3-4; pulse 1); reflected light. C) Both lath-like and irregular quartz present with calcite and electrum in pulse 3 (sample 50-1-3-1); xpl. D) Pulse 3 with a fine grained mass, calcite and lath-like quartz cutting pulse 2 (sample 50-1-1); xpl.

Petrographic observations show pervasive hydrothermal alteration throughout the host rock. SEM images show that along with hydrothermal pulses, pervasive host rock alterations are present. Figure 12 is an SEM element map that shows elemental abundances throughout sample FC 51-2-2. The figure shows two distinct pulses cutting one another, hosted by a dominantly altered dike. The host rock shows increasing potassium nearing the vein, primarily along pulse 1. The host rock appears to also have a slightly higher concentration of aluminum near the vein and weakens away from the vein (center of host rock). Magnesium and silica slightly increase in abundances toward the center of the host rock.

SEM analysis allows for a more thorough understanding/characterization of ore phases. All visible ore within each section is made up of electrum and no native gold is present. Figure 13 shows that electrum exhibits a porous texture throughout the ore. Electrum was only found to be present when quartz/calcite veins cut sulfide-rich veins. Electrum is typically surrounded by quartz, which in turn is surrounded by calcite and is found in proximity to pyrite on rare occasions.

Electrum phases appear to exhibit distinctive elemental compositions from sample to sample. Enrichments tend to be moderately uniform throughout an electrum grain. In addition to gold and silver electrum may contain minor amounts of aluminum, manganese, potassium, titanium, iron, sulfur, sodium and/or magnesium.

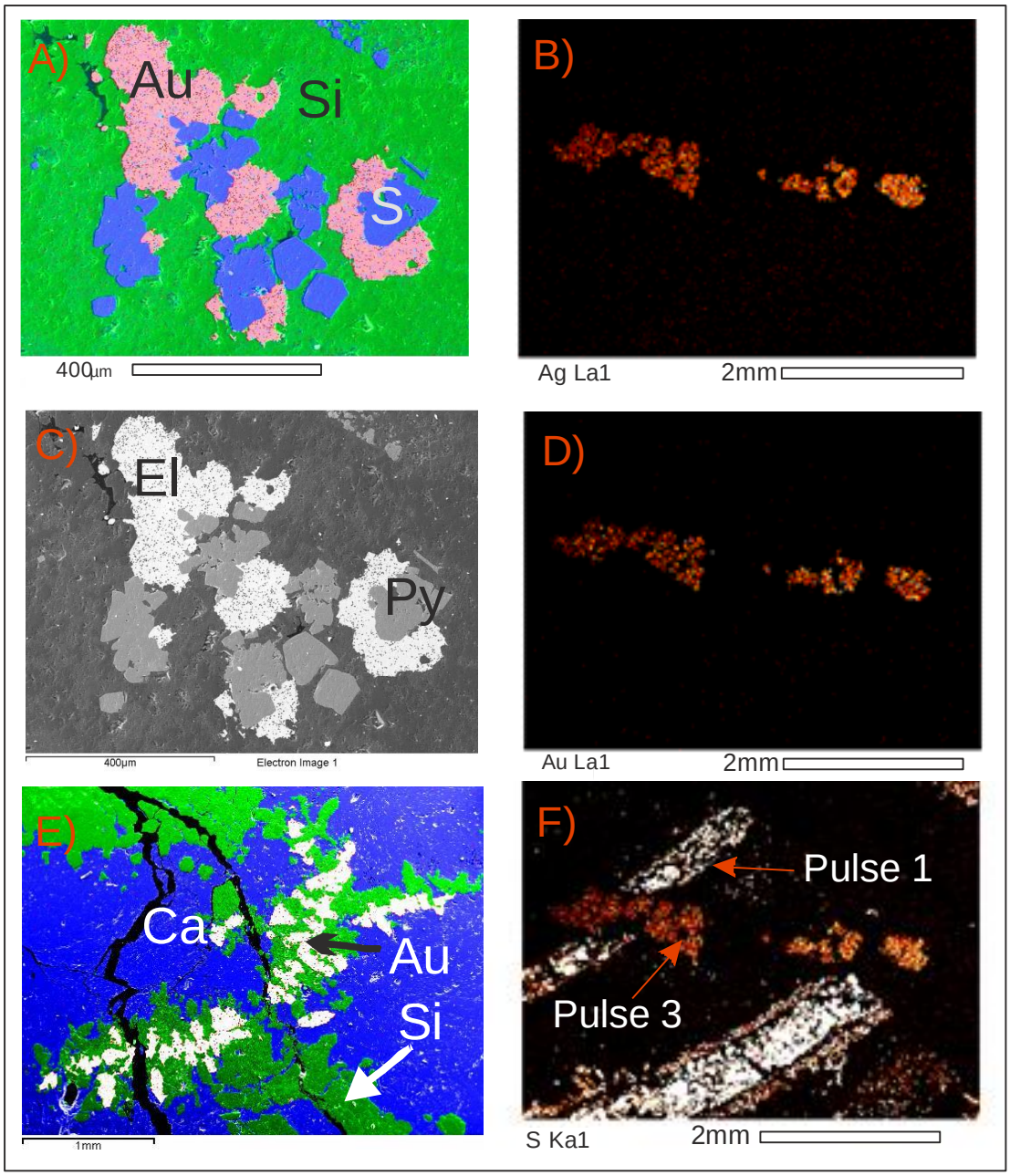

Figure 12: A) SEM mosaic with green representing silica present, blue representing sulfur and pink representing gold. B) EDS map showing Ag enrichment in pulse 3. C) SEM image of (A). D) EDS map showing Au enrichment in pulse 3. E) SEM mosaic showing dendritic enrichment of Au (white) surrounded by Si (green) surrounded by Ca (blue). F) EDS map showing sulfur enrichment in both pulse 1 and 3.

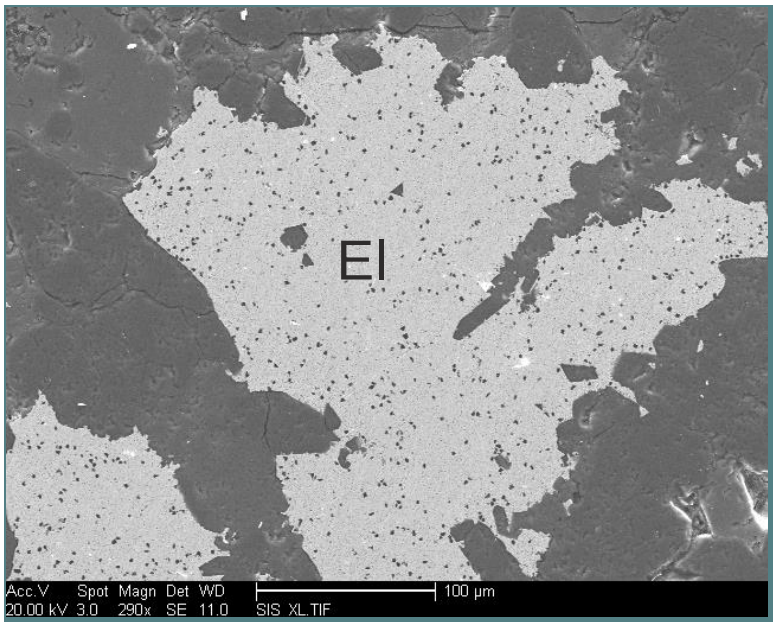

Figure 13: SEM image of porous electrum grain surrounded by quartz and calcite.

5.3 Major element mineral chemistry

Electron microprobe analysis (EMPA) was performed on both host rock and hydrothermal mineral phases (results shown in Table 5 and Table A1). Pyroxenes present are limited to clinopyroxene with wollastonite, enstatite and ferrosilite varying from 28.8-41.7, 34.0-46.6 and 17.5-24.7 % (Figure 14). All feldspars are limited to bytownite with An_{50}-An_{70} (Figure 15).

EMP analysis on electrum grains show variations in gold, silver, iron and sulfur. Gold ranges from 57.1 -75.5 wt. % and Silver ranges from 24.5 -28.1 wt. %. Iron and sulfur variation ranges from 0.05-0.38 wt. % and 0.32-0.72 wt. %. Sulfide grains displayed variation in iron, sulfur and arsenic. Sulfur and iron vary from 19.7-54.0 wt. % and 44.2-48.2 wt. %. Arsenic variations are large (0-43.8 wt. %); zones with higher values of arsenic in sulfides are accompanied by lower concentrations of

iron and sulfur and typically have low totals. Magnetite‘s from sample FC 1110 (unmineralized) have small variations in Iron and magnesium (Table A2). Mineral chemistries of quartz and calcite don’t exhibit any unusual variations (Table A2).

Table 5: Representative major element chemistry acquired from EMPA on sulfide grains and electrum (in wt. %).

Sample	49-2-2	49-2-2	49-2-2	49-2-2	49-2-2	49-2-2	49-2-2	49-2-2	49-2-2	49-4-2	49-4-2
Line no.	353	358	362	363	364	377	378	379	380	42	43
Mineral	1	1	1	1	1	1	1	1	1	1	1
Si WT%	0.02	0.07	<0.03	<0.03	0.02	0.02	0.44	<0.03	0.28	0.06	0.03
Fe WT%	46.89	46.76	47.00	47.64	47.53	47.65	44.20	48.18	44.50	37.31	35.74
Co WT%	<0.03	0.06	<0.03	<0.03	0.01	0.01	<0.03	0.02	<0.03	0.10	0.01
Ni WT%	<0.03	<0.03	<0.03	<0.03	<0.03	0.03	0.05	<0.03	<0.03	0.00	<0.03
Cu WT%	<0.03	<0.03	<0.03	<0.03	<0.03	0.07	0.08	0.03	<0.03	0.06	<0.03
Mn WT%	0.02	<0.03	0.05	0.01	<0.03	<0.03	<0.03	<0.03	<0.03	<0.03	<0.03
P WT%	<0.03	<0.03	<0.03	0.02	0.01	<0.03	0.06	<0.03	0.29	0.58	0.22
S WT%	52.69	52.43	53.63	53.15	53.10	52.87	48.85	53.12	50.05	21.47	20.82
As WT%	0.08	0.74	<0.03	<0.03	0.29	0.25	0.98	<0.03	0.42	43.80	41.12
Ag WT%	<0.03	0.10	0.05	<0.03	0.01	0.05	<0.03	<0.03	0.05	<0.03	<0.03
Au WT%	<0.03	<0.03	0.11	0.14	<0.03	0.15	<0.03	<0.03	<0.03	<0.03	0.01
TOTAL	99.36	99.80	100.77	100.91	100.68	101.10	94.52	100.58	95.47	102.82	97.82

Sample	49-4-2	50-1-2-2	50-1-2-2	50-1-2-2	50-1-2-2	50-1-2-2	50-1-2-2	50-1-2-2	50-1-2-2	50-1-2-2	50-1-2-2
Line no.	46	437	438	439	445	446	447	456	457	458	459
Mineral	1	2	2	2	2	2	2	2	2	2	2
Si WT%	0.79	-	-	-	-	-	-	-	-	-	-
Fe WT%	34.84	0.22	0.20	0.10	0.24	0.15	0.20	0.16	0.36	0.12	0.09
Co WT%	<0.03	-	-	-	-	-	-	-	-	-	-
Ni WT%	0.02	-	-	-	-	-	-	-	-	-	-
Cu WT%	<0.03	<0.03	0.06	-0.03	-0.01	0.01	0.05	0.02	<0.03	0.02	0.02
Mn WT%	<0.03	<0.03	<0.03	<0.03	<0.03	0.01	0.01	<0.03	<0.03	<0.03	<0.03
P WT%	<0.03	-	-	-	-	-	-	-	-	-	-
S WT%	20.06	0.53	0.42	0.42	0.46	0.46	0.55	0.47	0.72	0.43	0.32
As WT%	39.16	<0.03	0.01	<0.03	<0.03	<0.03	<0.03	<0.03	<0.03	<0.03	<0.03
Ag WT%	<0.03	26.81	25.31	26.19	26.55	24.45	26.64	25.87	25.65	27.38	25.60
Au WT%	<0.03	62.34	68.02	66.85	69.78	62.75	65.63	67.51	61.28	72.30	74.47
TOTAL	94.77	89.80	93.97	93.54	97.01	87.82	93.09	93.98	88.02	100.24	100.44

1= Sulfides
2=Electrum

Table 6: Representative data from plagioclase and pyroxene grains. Samples which begin with BL were acquired from Baragar et al. (1996) and are representative of the Mackenzie large igneous province.

Pyroxene					
Sample	line no.	Wo	En	Fs	Mg#
47-3-4	81	37.29673	44.73025	17.97302	71.33639
47-3-4	82	39.03394	43.43045	17.53561	71.2371
47-3-4	83	28.77367	46.57329	24.65304	65.38775
47-3-4	64	41.71225	34.00757	24.28018	58.34428
BLH6 81	-	36.34209	44.48339	19.17451	69.87882
BLH68	-	35.98103	42.16257	21.85641	65.85948
BLB6 931	-	38.67923	46.47198	14.8488	75.78505
BLB6 98	-	36.98453	40.72592	22.28955	64.62845
BL614O	-	36.59239	45.77352	17.63409	72.18931
BLB6 981	-	0	66.28642	33.71358	66.28642
Plagioclase					
Sample	line no.	An	Ab	Or	Mg#
1110	52	73.42593	25.2161	1.357961	21.74589
1110	53	76.28288	22.67208	1.045033	19.29386
1110	59	69.2024	29.22651	1.571093	9.428984
1110	61	74.00679	24.87454	1.118665	22.27762
47-4-3	76	72.36499	26.16408	1.47093	20.49436
47-4-3	77	75.21012	23.62727	1.16261	20.34435
47-4-3	78	72.32202	26.17282	1.505154	22.44742
47-4-3	79	81.64271	17.78063	0.576655	45.1347
50-1--1	87	76.15918	22.7509	1.089915	22.63747
50-1--1	88	72.26179	26.36199	1.376225	31.38863
50-1--1	89	73.17051	25.59328	1.23621	22.50283
50-1-2-2	144	75.77676	23.16625	1.056993	19.91612
50-1-2-2	145	76.15261	22.7808	1.066594	26.87947
50-1-2-2	146	79.56489	19.87687	0.558242	39.96189
50-1-2-2	147	79.47489	19.87456	0.650544	44.43103
BLH6 8	-	13.13792	79.90952	6.952561	-
BLB6 93	-	69.24961	27.68192	3.068468	-
BLB6 932	-	1.850116	97.92959	0.220293	-
BLB6 982	-	9.072495	90.7717	0.155806	-
BL616O	-	77.56088	21.49134	0.947777	-

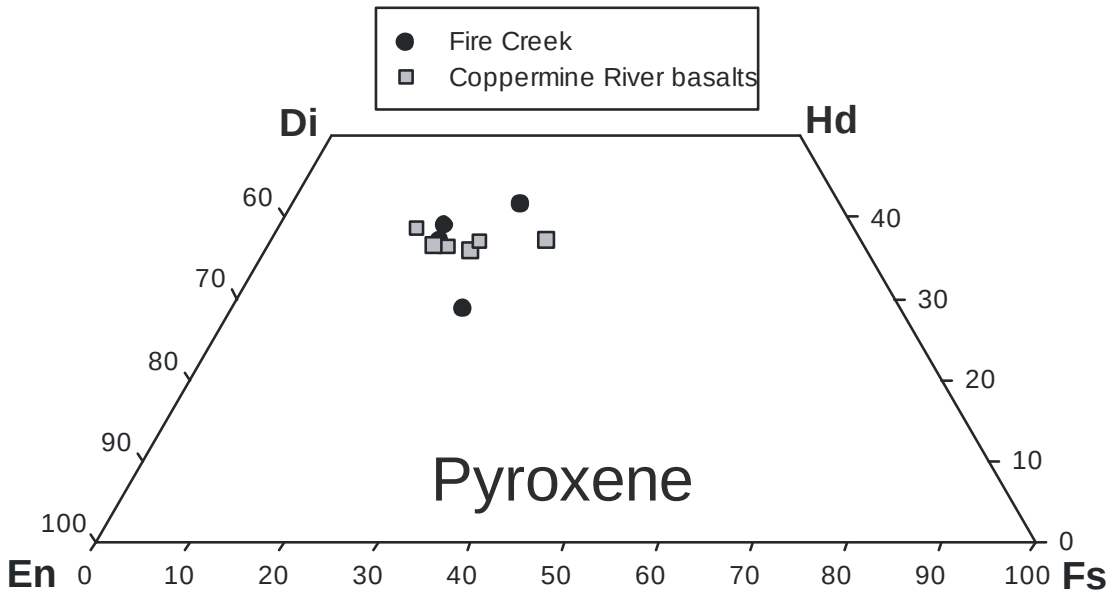

Figure 14: Ca-Mg-Fe plot of pyroxene composition in the dike. Gray points are from the Coppermine River basalts representative of the Mackenzie large igneous province (Baragar et al., 1996).

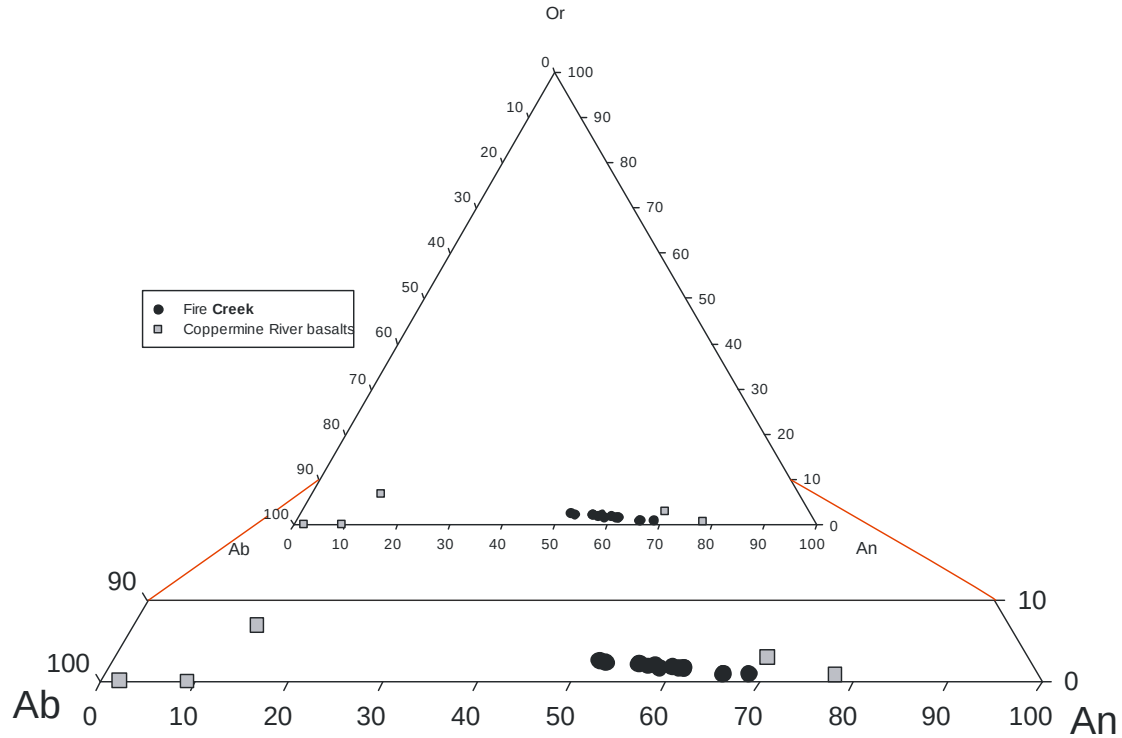

Fig. 15: classification diagram for Ab-An-Or for feldspars, showing variability for plagioclase in the dike. Gray points are from the Coppermine River basalts representative of the Mackenzie large igneous province (Baragar et al., 1996).

5.4 Trace Element Chemistry

In-*situ* LA-ICP-MS spot analysis for 65 sulfides and 20 electrum phases are given in Table 7 and 8. With the exception of Au, sulfide grains typically yielded results below detection for one or more highly siderophile elements (HSE) including Re, Au, Os, Ir, Ru, Pt and Pd, resulting in an incomplete suite of HSE data. Concentrations and trends of detectible HSE appear to be consistent throughout sulfide grains. Sulfide HSE values are typically below chondritic values and show strong fractionation patterns with an increased concentration in Pd, Rh, Os relative to Re, Pt and Ir (Figure 16). Fractionation within sulfide phases is also expressed by large Au concentrations.

HSE values for electrum grains were all within detection limits which resulted in a complete suite of data. Au was not standardized for electrum phases since values were attained from EMP analysis. HSE values for electrum phases displayed an antithetical fractionation pattern to that of sulfides (Figure 16). Re and Pt display an increased concentration relative to Pd, Rh and Ru. Ir and Os appear to have a similar partition coefficient.

For sulfide phases Ag, As, Ga, Mo, W, Pb and MnO concentrations are highly to slightly variable and typically were above detection limits. Along with Au, Ag and HSE's electrum grains appear to have detectible concentrations of Mo, Cd, Sn and W. Other elements that were standardized for electrum and/or sulfide phases were either consistently below detection or unusable due to the use of these elements as an

internal standard. Although most sulfide elemental results show consistent behavior, some slight to large variations are noted between distinct pulses and/or locations.

Within sulfide grains, specific elements may display enrichments in accordance to their corresponding pulse (Figure 17). Sulfides in P1 appear to have a few anomalously larger Au, Ru and Rh concentrations when P2 is the only other pulse present. Mo is enriched in P1 relative to P2 but has a slightly larger concentration when accompanied by only P2 in the slide. W is strongly enriched when P2-sulfides are in the presence of P3 and P1 (sample FC 50-1-1). Slight W enrichment exists when P1-sulfides are in the presence of P3 and P2. Arsenic appears to have a strong to slight enrichment when P1 sulfides are found in the presence of only P2 (slight enrichments are also displayed in P2 sulfides, in the presence of P1). Other elements measured are either not consistent within individual pulses or require observations at a finer scale.

Trace element concentrations in sulfide grains not only vary from pulse to pulse but also vary within a single pulse based on its proximity to other pulses. These spatial changes are unique to only a few elements in specific zones or regions. Elements that exhibit these slight to large spatial changes consist of Mo, Ag, W, Au and Pb (Figure 18 & 19). Both Mo decreased concentrations as P1-sulfide grains near P2 and/or P3. Au in one case displayed an increased abundance as P2-sulfides neared P3. Pb exhibited slight to large variations in two distinct veins with Pb concentrations increasing in P1-sulfides as they near P2 but decrease away from P3. Ag and W displayed two opposing trends—one in which P1-sulfides increased towards P2 and another in which Ag concentration decreased as sulfides neared P2. Elements that did

not display these spatial features showed either a random distribution throughout the section or were consistently below detection.

LA-ICP-MS analysis on sulfide grains display an average Au and Ag abundance of 27.7 ± 47.5 ppm and 46.6 ± 77.7 ppm in P1 and 6.7 ± 8.8 ppm and 33.0 ± 51.6 ppm in P2. Correlation between elements is displayed in figure 20. Positive correlations for sulfide grains are only observed when Au is plotted against Mo or W. No other trends were observed throughout the sulfide sample set. Electrum phases display a series of positive correlations when W is plotted against Sn, Cd and Mo (Mo slight trend) (Figure 21).

Table 7: Representative LA-ICP-MS data on electrum grains

Sample:		Fe15a08	Fe15a11	Fe15d10	Fe15d11	Fe15d12	Fe15d13	Fe15d14	Fe15d15
Element	**Isotopic mass**								
S	**33**	-	-	-	-	-	-	-	-
Ti	**47**	*<4.17*	*<4.47*	*<5.87*	*<6.93*	*<3.89*	*<5.06*	*<6.05*	*<6.06*
Ti	**49**	*<4.25*	*<4.03*	*<2.46*	*<6.27*	*<3.74*	*<6.08*	*<7.51*	*<4.73*
MnO	**55**	BDT	BDT	BDT	BDT	BDT	BDT	BDT	BDT
Fe	**57**	-	-	-	-	-	-	-	-
Co	**59**	*<0.51*	*<0.17*	*<0.51*	*<0.20*	*<0.30*	*<0.33*	*<0.63*	*<0.14*
Ni	**61**	-	-	-	-	-	-	-	-
Ni	**62**	-	-	-	-	-	-	-	-
Cu	**63**	-	-	-	-	-	-	-	-
Cu	**65**	-	-	-	-	-	-	-	-
Ga	**69**	*<0.25*	*<0.31*	*<0.33*	*<0.26*	*<0.69*	*<0.47*	*<0.32*	*<0.43*
As	**75**	*<150.39*	*<7.14*	*<5.81*	*<4.35*	*<5.36*	*<3.50*	*<5.06*	*<3.08*
Mo	**95**	**1.7**	**0.21**	**0.12**	**0.11**	**0.080**	**0.12**	*<0.46*	*<0.51*
Mo	**97**	**1.9**	*<0.68*	**0.14**	**0.25**	**0.16**	*<1.11*	*<0.75*	*<0.60*
Ru	**99**	**0.14**	*<0.24*	*<0.43*	*<0.33*	*<0.36*	**0.29**	*<0.87*	*<0.23*
Ru	**101**	*<0.17*	*<0.18*	*<0.19*	**0.064**	*<0.42*	*<0.19*	*<0.21*	*<0.17*
Rh	**103**	*<0.07*	*<0.03*	*<0.04*	**0.039**	*<0.04*	*<0.05*	*<0.09*	**0.032**
Pd	**105**	**0.74**	**0.74**	**0.71**	**0.62**	**0.71**	**0.83**	**0.74**	*<0.85*
Ag	**107**	*<2.58*	*<2.49*	**658629**	**637459**	**653569**	**671076**	**758889**	**668826**
Cd	**111**	**14**	**15**	**13**	**11**	**11**	**12**	**14**	**13**
Sn	**117**	**9.4**	**8.4**	**6.8**	**7.3**	**7.8**	**7.5**	**7.2**	**7.4**
Sn	**118**	**2.5**	**2.6**	**2.1**	**1.8**	**2.4**	**1.8**	**2.4**	**1.8**
W	**182**	**0.36**	**0.39**	**0.33**	**0.37**	**0.32**	**0.34**	**0.38**	**0.32**
Re	**185**	**0.15**	**0.18**	**0.17**	**0.16**	**0.11**	**0.14**	**0.18**	**0.12**
Os	**189**	**0.36**	**0.41**	**0.41**	**0.38**	**0.39**	**0.36**	**0.41**	**0.27**
Ir	**193**	**0.33**	**0.38**	**0.33**	**0.31**	**0.33**	**0.38**	**0.36**	**0.35**
Pt	**195**	**4.7**	**5.1**	**5.0**	**4.9**	**5.1**	**4.8**	**5.1**	**5.0**
Au	EMPA	697876.2	713250.1	675100.5	725132.1	754785.5	735627.5	723002.3	728186.1
Pb	**204**	**65**	**73**	**53**	**50**	**58**	**55**	**61**	**75**
Pb	**206**	*<0.36*	*<0.38*	*<0.63*	*<0.17*	*<0.61*	**0.22**	*<0.34*	*<0.33*
Pb	**207**	*<0.46*	*<0.21*	*<0.47*	*<0.37*	*<0.28*	*<0.50*	*<0.67*	**0.23**
Pb	**208**	*<0.40*	*<0.26*	*<0.31*	*<0.21*	**0.14**	*<0.24*	*<0.29*	*<0.18*

Table 8: Representative LA-ICP-MS results for sulfide grains

Sample:		Fe14a08	Fe14a09	Fe14b05	Fe14b14	Fe14c09	Fe14d07	Fe14d08	Fe15b07	Fe15b15	Fe15e05	Fe15e09
*Pulse:		1_2	1_2	1_2	2_1	1_2	2_3_1	2_3_1	1_3_2_e	1_3_2_e	1	1
Element	Isotopic mass											
S	**33**	-	-	-	-	-	-	-	-	-	-	-
Ti	**47**	-	-	-	-	-	-	-	**3111**	*<7.77*	**228**	**498**
Ti	**49**	-	-	-	-	-	-	-	**3083**	**8.6**	**247**	**514**
MnO	**55**	**0.016**	**0.002**	**0.000**	**0.006**	**0.002**	**0.015**	**0.015**	**0.005**	**0.010**	**0.053**	**0.069**
Fe	**57**	-	-	-	-	-	-	-	-	-	-	-
Co	**59**	**87.679**	**39.752**	**36.669**	**7.844**	**21.362**	**0.651**	**0.500**	**93.969**	**2.256**	**241.831**	**173.473**
Ni	**61**	-	-	-	-	-	-	-	-	-	**567.843**	**179.104**
Ni	**62**	-	-	-	-	-	-	-	-	-	*<432.80*	*<221.70*
Cu	**63**	-	-	-	-	-	-	-	-	-	-	-
Cu	**65**	-	-	-	-	-	-	-	-	-	-	-
Ga	**69**	**1.384**	**1.250**	*<0.23*	**0.928**	**1.309**	**1.041**	**1.293**	**0.375**	**0.731**	**0.354**	**0.724**
As	**75**	**426300.1**	**16537.6**	**20523.0**	**3724.3**	**24467.4**	**66.1**	**184.4**	**10821.6**	**1982.4**	*<80.75*	*<43.43*
Mo	**95**	**13.339**	**0.746**	**1.636**	**2.071**	**0.232**	**0.073**	**0.091**	**4.257**	**1.177**	**0.530**	**0.233**
Mo	**97**	**15.110**	**0.629**	**1.257**	**1.613**	**0.414**	**0.193**	**0.304**	**3.926**	**0.870**	**0.841**	**0.312**
Ru	**99**	**0.508**	**0.042**	*<0.08*	*<0.13*	*<0.06*	**0.037**	*<0.07*	*<0.15*	*<0.27*	**0.090**	*<0.09*
Ru	**101**	**0.294**	*<0.24*	**0.018**	**0.015**	**0.051**	**0.008**	*<0.03*	**0.025**	**0.027**	**0.008**	**0.010**
Rh	**103**	**0.041**	**0.028**	**0.053**	**0.006**	**0.084**	*<0.02*	*<0.01*	**0.006**	**0.002**	*<0.01*	*<0.01*
Pd	**105**	**0.301**	*<0.09*	*<0.10*	*<0.10*	**0.135**	*<0.06*	*<0.05*	*<0.04*	*<0.16*	*<0.27*	*<0.05*
Ag	**107**	**34.642**	**11.327**	**9.537**	**44.727**	**54.438**	*<0.04*	**0.106**	**25.251**	**50.017**	*<0.46*	*<0.32*
Sn	**117**	**2.219**	*<1.50*	*<0.19*	**0.691**	*<0.97*	*<0.37*	*<0.23*	*<0.31*	**0.939**	**0.623**	**0.863**
Sn	**118**	**1.725**	*<1.14*	*<0.18*	**0.676**	**0.867**	**0.295**	**0.181**	*<0.13*	*<1.19*	**0.342**	**0.899**
W	**182**	**2.116**	**0.438**	**0.025**	**0.507**	**0.252**	**45.362**	**41.932**	**0.320**	**0.293**	**0.594**	**0.630**
Re	**185**	**0.015**	**0.007**	*<0.02*	*<0.02*	**0.005**	**BDL**	*<0.02*	**0.002**	**0.015**	*<0.06*	**0.001**
Os	**189**	**0.021**	**BDL**	**0.004**	**BDL**	**0.003**	*<0.03*	*<0.04*	*<0.03*	**0.014**	*<0.12*	**0.002**
Ir	**193**	**BDL**	**BDL**	**0.001**	**BDL**	**BDL**	*<0.01*	**0.000**	*<0.01*	**BDL**	**0.002**	**BDL**
Pt	**195**	*<0.28*	*<0.06*	**0.003**	**BDL**	*<0.04*	*<0.02*	**0.004**	*<0.02*	**0.005**	**BDL**	**<0.05**
Au	**197**	**157.379**	**20.917**	**17.028**	**0.797**	**36.739**	**2.508**	**4.748**	**33.057**	**9.801**	**<0.58**	**<0.26**
Pb	**204**	**152.761**	**70.586**	**55.722**	**62.080**	**54.703**	**61.886**	**778.701**	**58.647**	*<40.85*	**49.622**	**30.326**
Pb	**206**	**67.670**	**74.750**	**59.681**	**67.620**	**59.337**	**0.334**	**0.287**	**60.945**	**38.439**	**30.168**	**13.372**
Pb	**207**	**58.939**	**61.344**	**54.798**	**65.582**	**54.407**	**0.242**	**0.235**	**54.098**	**37.577**	**26.753**	**11.790**
Pb	**208**	**56.287**	**64.859**	**54.556**	**63.193**	**56.386**	**0.318**	**0.269**	**57.720**	**36.091**	**27.735**	**12.371**
Cd	**111**	-	-	-	-	-	-	-	*<0.25*	**0.126**	*<0.36*	**0.391**

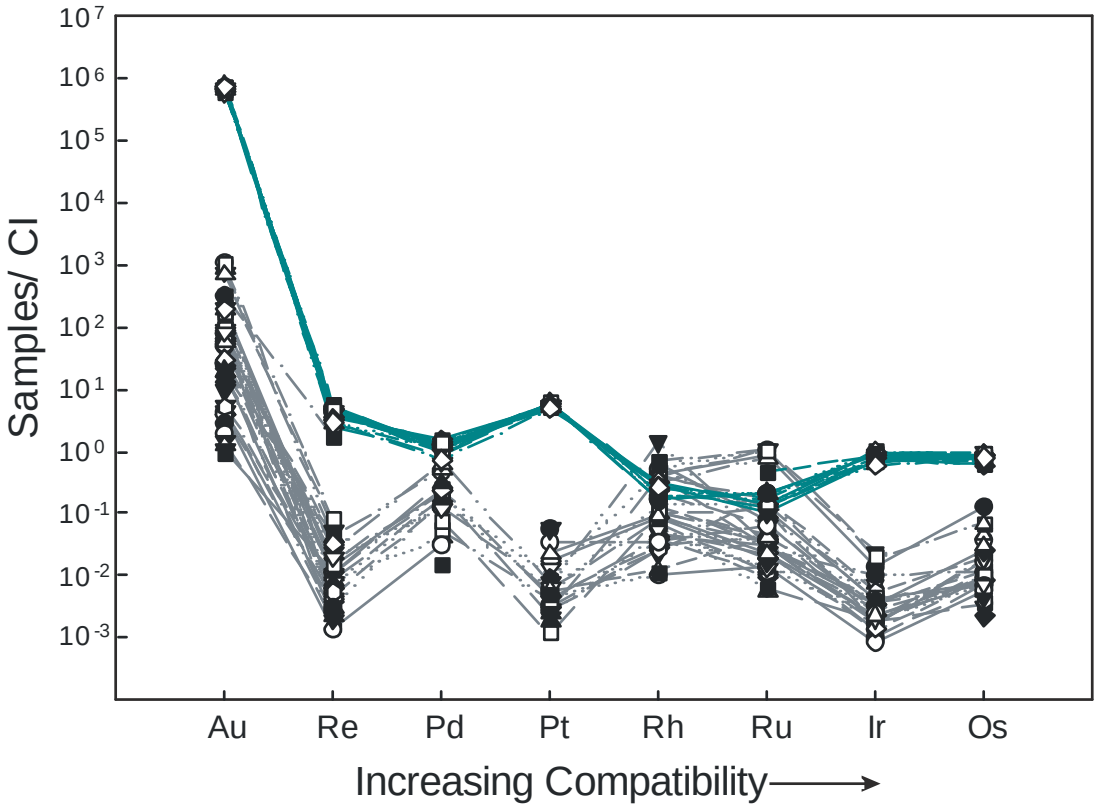

Figure 16: HSE patterns for electrum (blue) and sulfides (gray). Trends observed define relative compatibilities observed. Samples were normalized to chondritic values (Day, 2013)

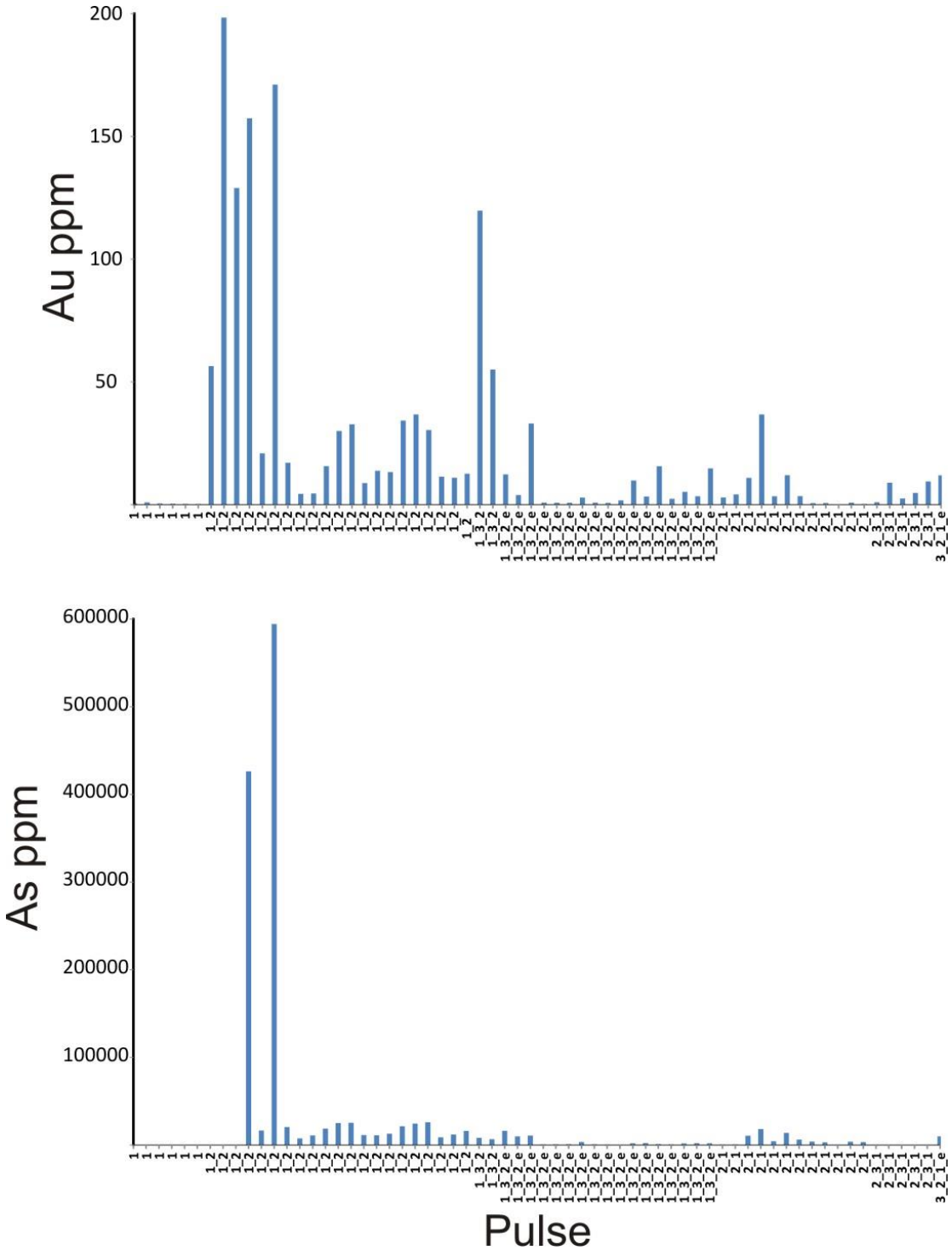

Figure 17: Histogram element concentration (LA-ICP-MS) vs. pulse of associated sulfide. For example; 1_3_2_e refers to a sulfide measured in pulse 1 with pulse 2, 3 and electrum present within the same section.

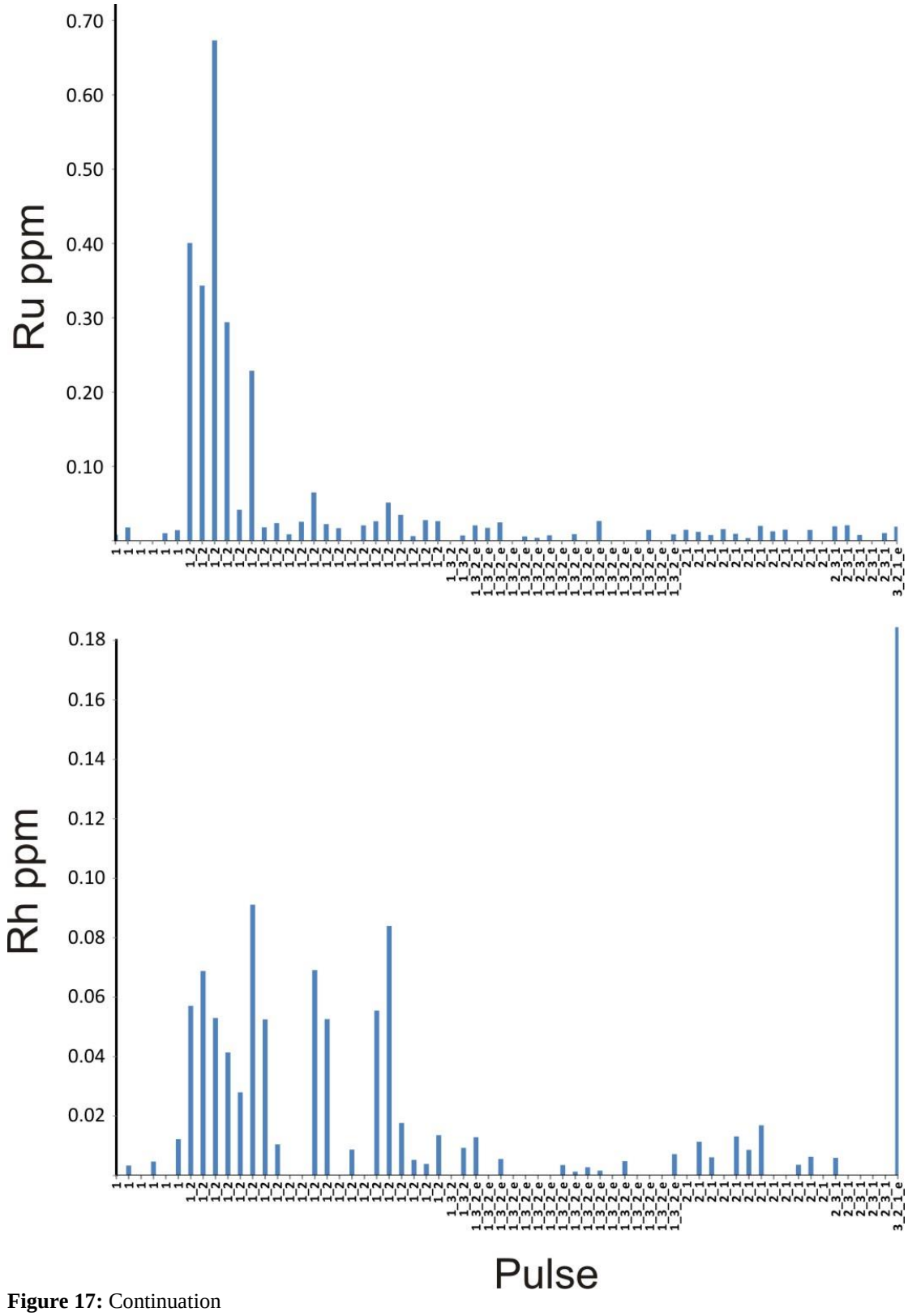

Figure 17: Continuation

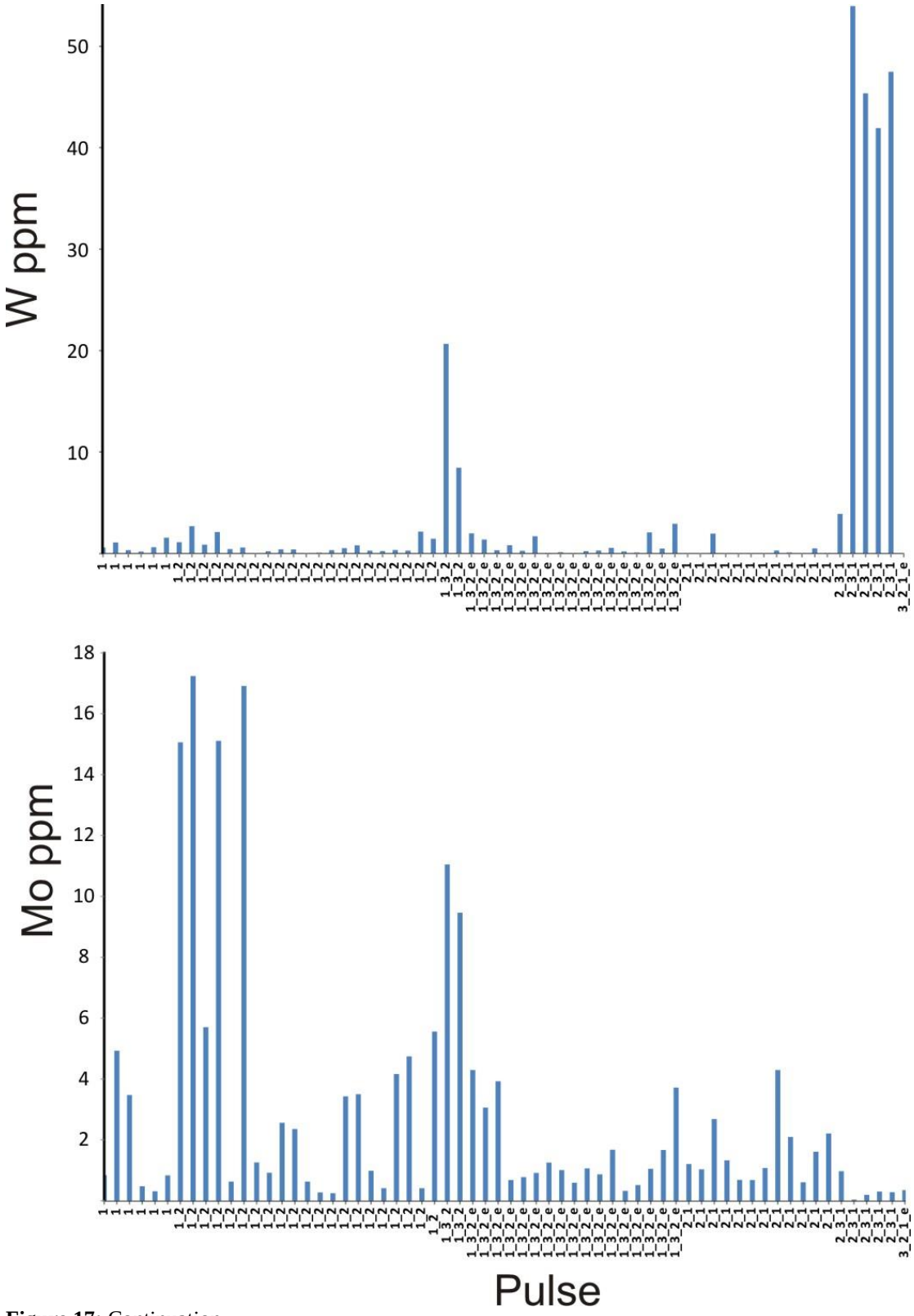

Figure 17: Continuation

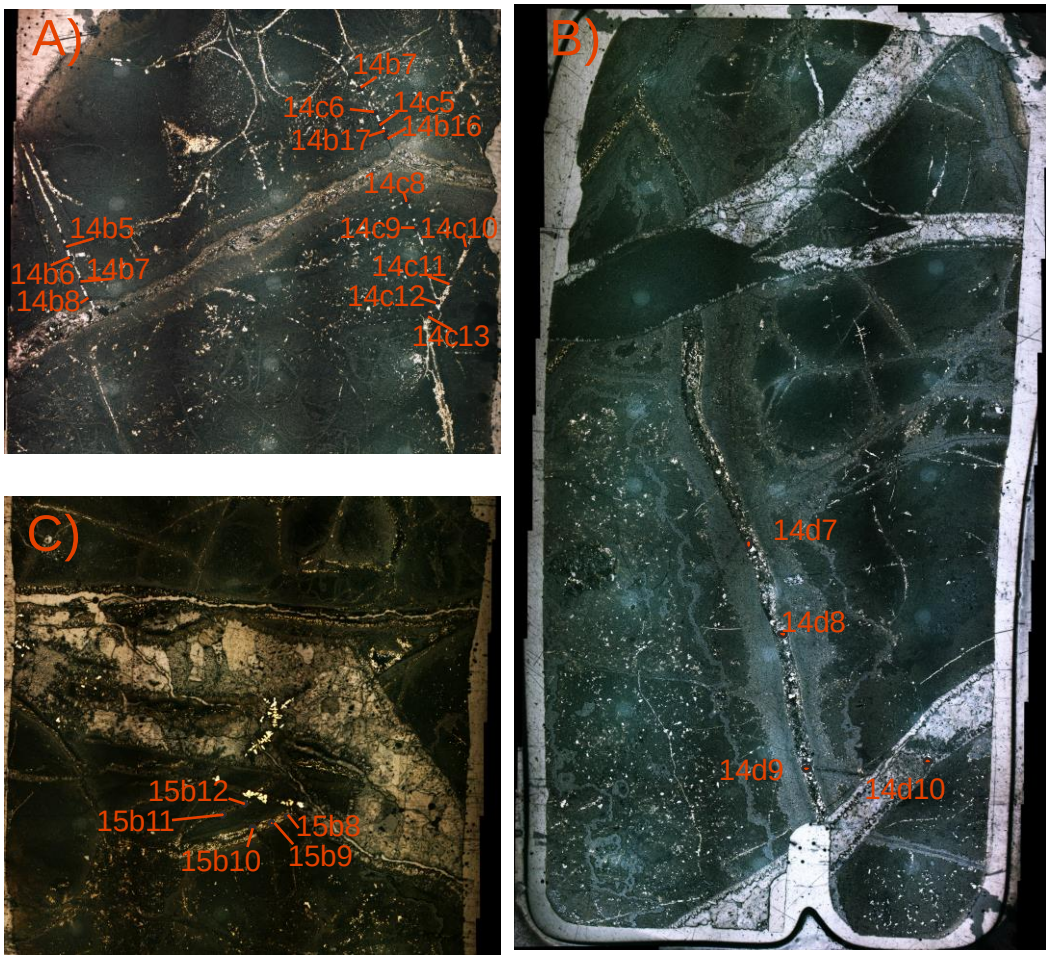

Figure 18: Photomicrographs with LA-ICP-MS spots analysis for sulfide phases (A-C; xpl). Spot analysis display trends shown in Figure 19. Image A contains pulse 2 (left to right) cutting pulse 1. Image B contains pulse 3 cutting pulse 2. Image C contains pulse 3 cutting pulse 1.

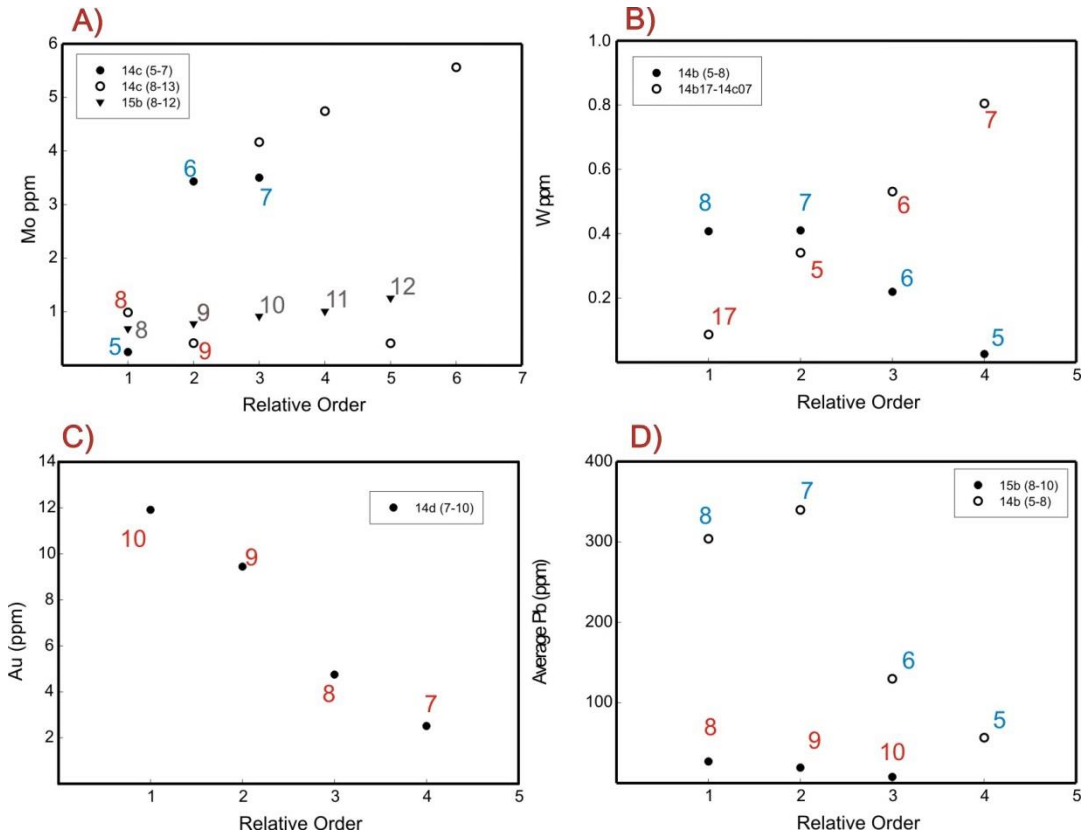

Figure 19: Graphs A-D display trends from spot analysis in Figure 18. The X axis represents the relative order of the sulfide from the corresponding vein (1 being the closes to the vein)**.** Numbers correspond to individual spot analysis.

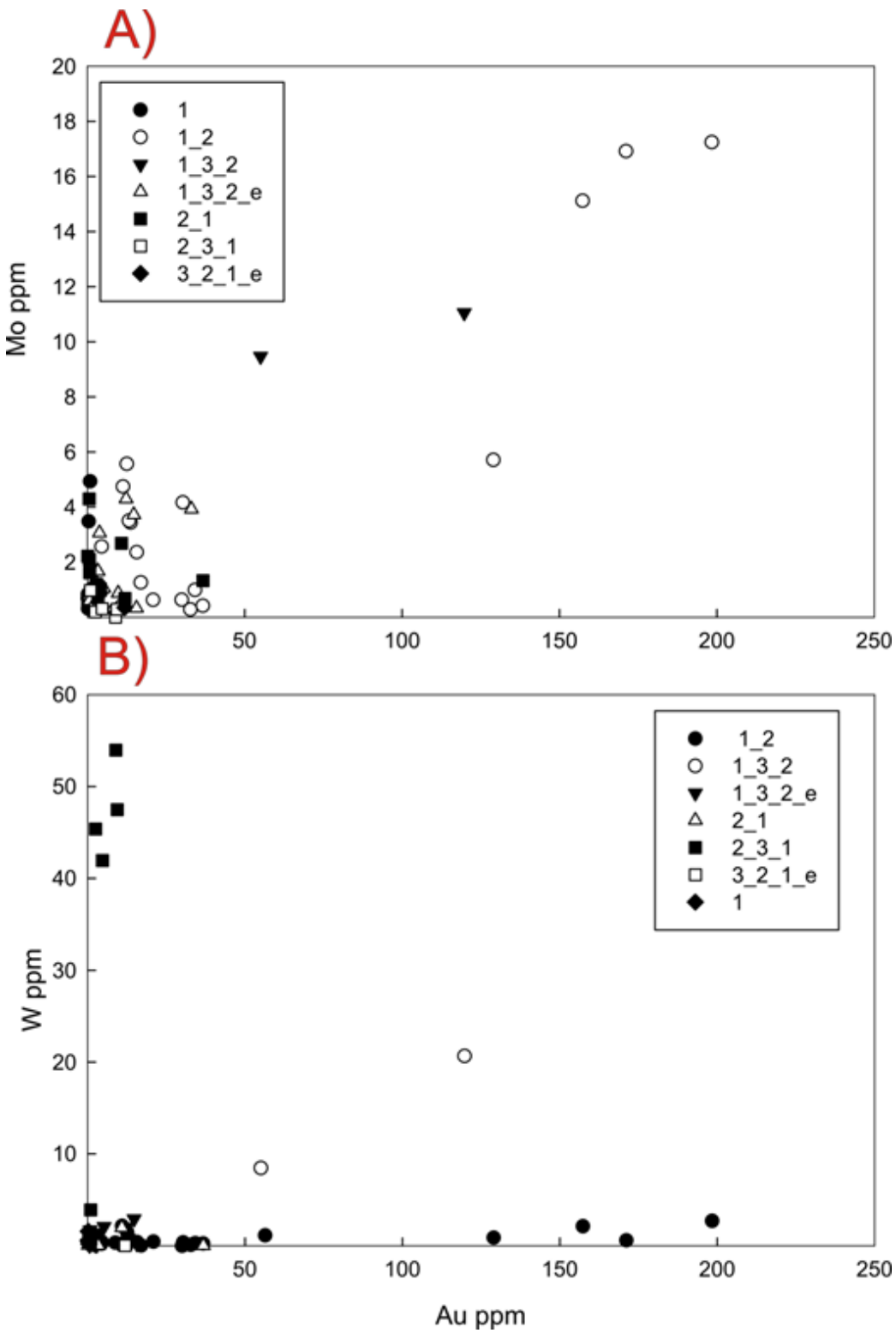

Figure 20: Plots of Au concentration versus (A) Mo and (B) W for sulfide grains (results acquired from laser ablation ICP-MS). Mo displays a single trend while W displays three distinct trends. Symbols represent different pulses and pulse associations.

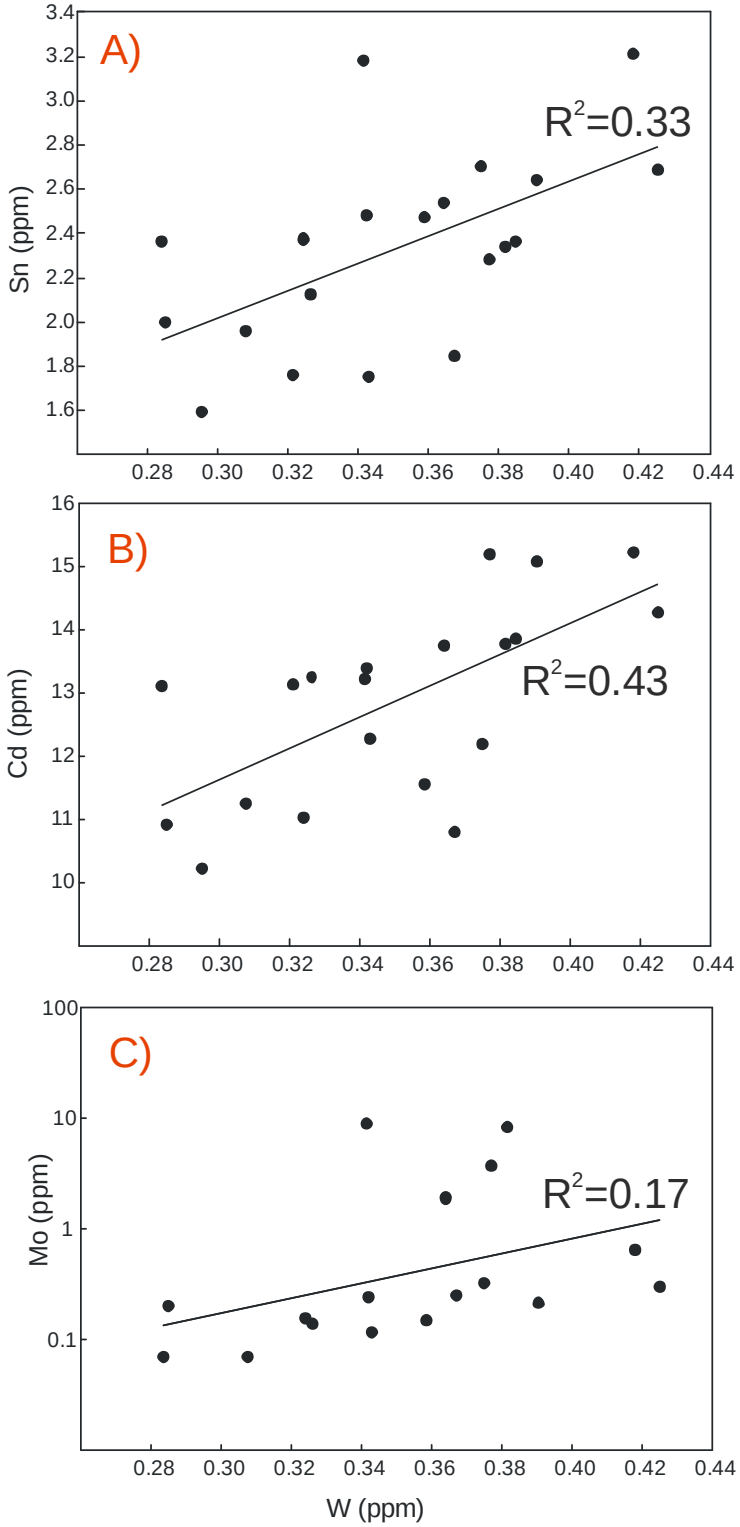

Figure 21: Plots of W versus (A) Sn, (B) Cd and (C) Mo for electrum grains. R^2 values represent the coefficient of determination.

5.5 Geochemistry

Volcanic Rocks comprising Fire Creek are a co-genetic suite of bimodal transitional sub-alkalic rocks and consist of basalts, basaltic-andesites, andesites and a unique trachydacitic unit (Figure 22 &23). Major element composition of Fire Creek rocks are variable with SiO_2 ranging from 64.7-53.9 wt. %; Al_2O_3 from 19.7-14.1 wt. %; MgO from 7.14- 0.68 wt. %; CaO ranges from 12.1-3.0 wt. %; K_2O ranges from 0.24-4.4 wt. %; Na_2O ranges from 4.41-1.98 wt. % ; $Fe_2O_3^T$ ranges from 14.45-8.39 wt. %. Tb1 is a trachydacitic unit which postdates mineralization. The MgO versus FeO plot (Figure 24) shows a positive trending slope with an inflection point occurring at 3.5 MgO wt. %. Both CaO and Al_2O_3 have a positive trending slope when plotted against MgO (Figure 24); with Tb1 (youngest unit) plotting at the end of the trend.

Table 9: Whole-rock major (wt. %) and trace (ppm) element data.

Unit	Tb1	Tb2	Tb3	Tbeq	Tbma	T&B	T&B	T&B	T&B	T&B	T&B	Dike	Dike	Dike	Dike	LAT	LAT
Sample	1106	1104	1109	702-3	427-2	427-3	427-4	427-5	427-6	427-8	427-10	1110	427-7	427-9	702-2	1108	427-1
SiO_2	64.66	60.79	61.69	54.27	60.77	53.94	55.75	57.34	54.41	57.14	54.99	57.42	59.17	50.73	60.44	76.31	54.25
TiO_2	0.91	1.63	1.74	1.35	1.57	1.36	1.99	1.65	0.95	1.55	1.30	1.71	1.73	1.46	2.08	2.00	1.11
Al_2O_3	14.14	14.08	16.71	15.25	18.24	15.85	18.92	16.14	19.69	15.07	15.71	14.20	14.87	17.59	16.83	20.98	19.08
$Fe_2O_3^T$	8.40	11.35	12.93	12.47	13.70	11.88	14.46	12.76	10.53	11.85	12.27	12.02	12.42	15.27	14.37	16.34	10.41
MnO	0.14	0.18	0.18	0.20	0.17	0.19	0.13	0.18	0.14	0.19	0.18	0.22	0.20	0.24	0.18	0.17	0.17
MgO	0.68	2.47	3.80	6.32	7.15	4.82	5.51	4.15	8.03	4.47	6.47	3.41	4.30	7.04	4.17	5.89	7.01
CaO	3.01	6.07	6.97	10.67	8.00	10.69	8.39	8.79	10.96	8.19	10.12	6.73	6.82	9.42	6.47	4.80	12.07
Na_2O	3.87	2.98	3.02	2.35	1.99	3.09	3.51	3.02	2.21	2.47	2.31	3.32	2.62	2.25	2.85	0.69	2.92
K_2O	4.41	2.50	1.02	0.87	0.83	0.77	0.78	1.13	0.25	2.03	0.87	2.22	1.79	1.95	0.97	0.53	0.41
P_2O_5	0.25	0.51	0.64	0.42	0.41	0.44	0.59	0.49	0.25	0.55	0.40	0.67	0.70	0.48	0.88	0.66	0.30
SO_3	0.05	0.06	0.12	0.37	0.82	0.85	0.11	0.28	0.19	0.14	0.22	0.09	0.21	2.44	0.21	0.23	0.24
LOI	0.53	2.58	8.12	4.32	11.94	3.73	9.13	5.57	7.10	3.54	4.63	1.99	4.62	8.11	8.58	22.12	7.38
Total - LOI	99.92	97.98	92.16	95.30	87.46	96.36	90.08	94.11	93.24	96.67	95.52	98.22	95.62	91.49	90.90	77.36	92.40
Na+K	8.29	5.48	4.04	3.22	2.82	3.86	4.29	4.14	2.46	4.50	3.18	5.54	4.41	4.20	3.82	1.22	3.33
%FeO	5.32	5.98	4.48	6.35	4.06	6.01	2.33	6.1	4.91	6.65	5.72	7.42	5.84	3.91	5.2	3.01	0.49
$\%Fe_2O_3$	2.48	4.47	6.94	4.82	7.47	4.77	10.44	5.23	4.36	4.07	5.36	3.56	5.39	9.62	7.28	6.27	12.1
$\%SO_3$	0.12	0.14	0.18	0.36	1.64	2.09	3.35	3.11	0.2	0.31	0.51	0.13	0.44	4.92	1.8	0.79	0.48
Rb	117.3	56.0	20.8	13.6	22.7	17.8	4.5	20.2	2.7	28.0	10.6	46.1	31.0	22.1	21.3	7.4	2.7
Sr	252	320	388	313	449	362	443	381	338	387	332	364	396	277	463	201	381
Y	61.8	39.4	45.8	36.6	39.0	36.4	41.8	37.1	29.6	37.7	36.3	39.0	41.3	37.5	45.5	25.7	32.8
Zr	452	213	177	118	116	130	159	148	65	172	110	197	187	105	211	141	84
V	26	281	293	286	284	249	342	270	190	293	290	281	289	272	333	205	260
Ni	4	4	9	24	15	16	11	10	37	5	25	3	4	15	3	9	35
Cr	23	22	52	113	130	106	112	78	132	35	95	31	25	88	18	48	133
Nb	32.3	12.9	12.7	7.2	7.8	7.8	10.0	9.2	3.9	11.5	6.7	13.1	13.1	7.9	14.3	11.1	5.5
Ga	23.6	18.3	18.2	16.2	16.5	16.5	19.0	17.4	16.3	17.6	16.1	18.9	18.2	16.3	19.5	16.5	16.6
Cu	8	17	15	56	36	31	37	29	34	15	48	11	13	29	15	25	51
Zn	98	115	159	96	123	110	182	119	87	115	100	100	124	104	134	121	99
Co	18	36	55	43	42	46	45	38	43	38	42	37	38	38	35	43	47
Ba	1724	628	465	263	507	444	491	615	149	612	274	742	663	635	567	235	306
La	65	29	28	19	17	19	18	16	15	22	17	28	24	14	23	21	13
Ce	168	61	60	37	50	38	44	46	27	59	45	66	62	43	65	47	33
U	3.5	2.0	1.8	0.5	0.6	0.5	1.4	1.8	1.0	2.2	0.5	1.7	0.5	1.1	3.6	0.5	1.1
Th	14.7	4.9	5.6	0.5	1.7	3.7	5.6	5.7	0.5	8.3	0.5	7.8	7.1	2.6	14.9	12.4	0.5
Sc	12	26	34	32	39	33	45	34	29	32	35	26	31	33	32	37	37
Pb	24	8	16	8	1	12	5	8	1	4	1	12	6	1	5	14	1

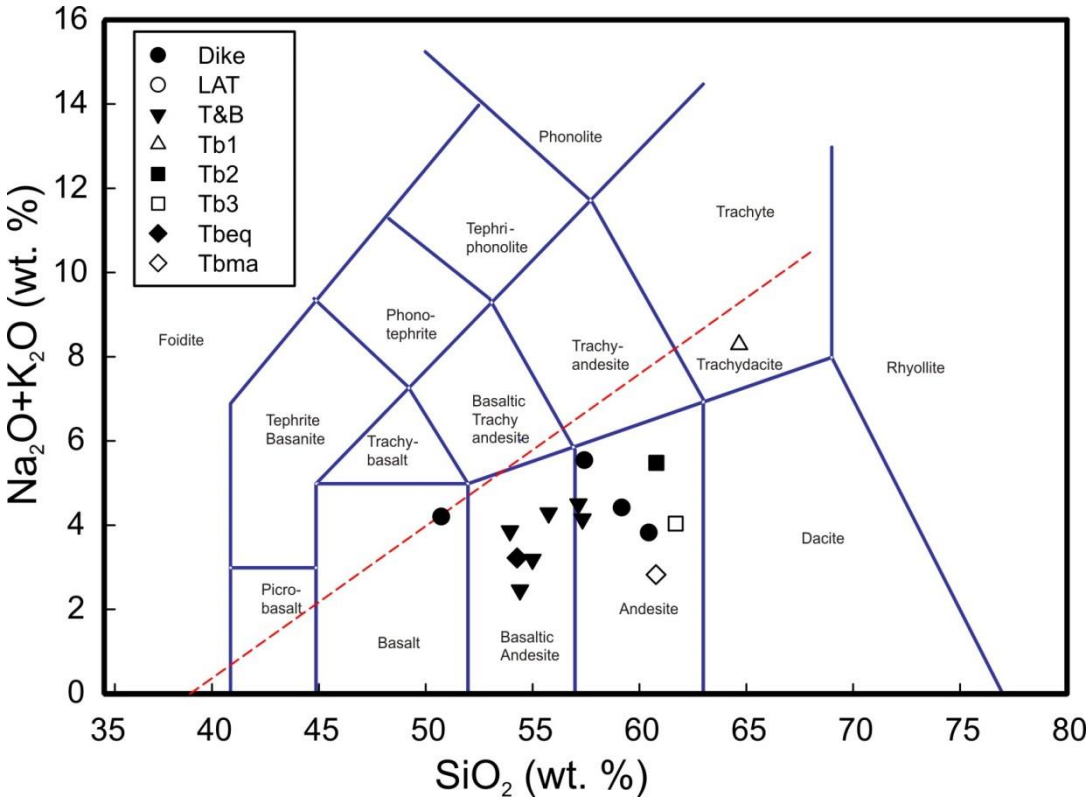

Figure 22: TAS plot showing range of volcanic compositions in Fire Creek. The red line is used as a subdivide for alkalic and sub-alkalic rocks.

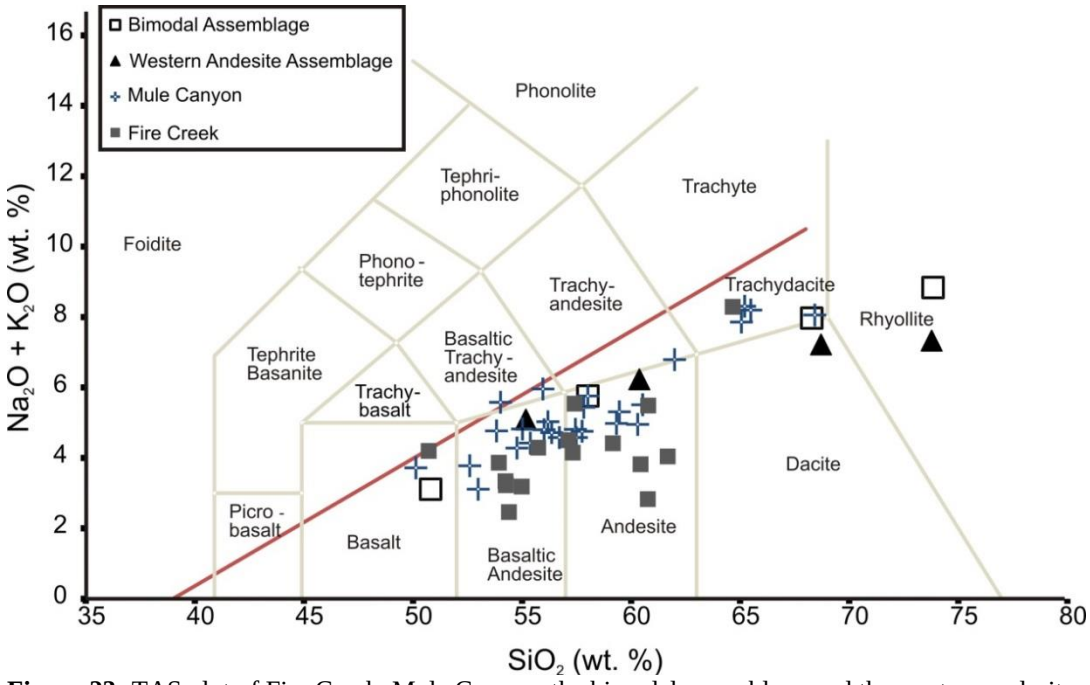

Figure 23: TAS plot of Fire Creek, Mule Canyon, the bimodal assemblage and the western andesite assemblage (John, 2001).

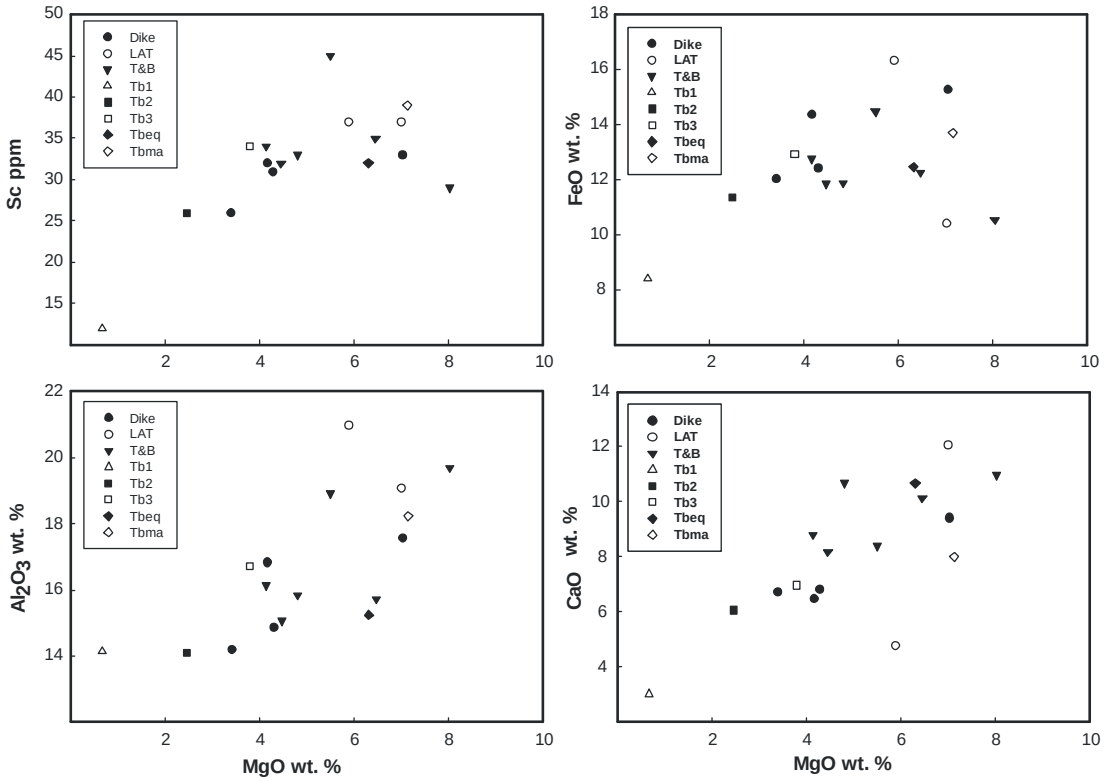

Figure 24: Plots showing MgO versus various major elements oxides and trace elements. In general, Compatible trends are observed in all plots

6. DISCUSSION

6.1 Lithology of Fire Creek

Fire Creek is host to a co-genetic basalt to trachy-dacite suite of rocks which exhibit strong similarities to units at Mule Canyon (Fire Creek possess lower Na_2O+K_2O which is possibly due to alteration; Figure 22 & 23). Fire Creek possesses compositions of lithologies which vary systematically with the relative stratigraphy (Figure 22). Compatible element depletions indicate plagioclase and pyroxene crystallization and segregation, making residual melts depleted in these elements, while the inflection at ~4.5 wt. % MgO of TiO_2 and FeO indicates the onset of magnetite crystallization. Trends observed in the trace elements are consistent with those seen in Harker plots (Figure 20).

Units at Fire Creek typically tend to become more fractionated up the general section but a large variation in dike composition implies multiple diking events (Figure 22). Mafic and andesitic dikes are both present at Fire Creek; geochemically the andesitic dike appears to have been emplaced before Tb2 and contemporaneously with Tb3. The mafic dike, on the other hand, was possibly emplaced sooner than the andesitic dikes leading to a more primitive composition.

6.2 Pulse Characterization and Interaction

At least three discrete magmatic and/or hydrothermal pulse events (P1, P2 and P3) are recognized after the emplacement of Tb2 and are numbered in relative

chronological order. These pulses all contain nominally high concentrations of Au and Ag which are present in two distinct forms: (1) disseminated in sulfide grains in P1 and P2 or; (2) as native electrum and minor sulfide in P3. P1 and P2 sulfides contain detectible Au and Ag concentrations from LA-ICP-MS, but exhibit differences in petrography, degree of alteration and geochemical composition. Petrographically these pulses both contain sulfides but P2 tends to be dominated by quartz in discontinuous veins. Wall rock alterations vary but stronger zoned regions of alteration are displayed in P2. Geochemically, P1 contains an average Au and Ag abundance of 28.3 and 46.6 ppm whereas P2 contains significantly lower average Au (6.7 ppm) but broadly similar Ag concentrations (33 ppm; concentrations present in Table A3).

Neither P1 nor P2 sulfides display coherent behavior which allows an individual pulse suite to be geochemically classified. This inconsistency may be due to more sulfide pulses than are obvious from petrographic scrutinization or from the complex interplay of sulfide remobilization from later pulses. For example, Au concentrations on average were higher in P1 than P2 but sample 47-3-4 (spot analysis 15e05-10; Table A3) results show low concentrations of Au (0.2-0.9 ppm) for P1.

Although dominated by sulfide grains, P1 may include several distinct pulses which can only be distinguished through textural observations and geochemical data. For example, sample FC 49-4-2 (LA-ICP-MS: 14a05-10) shows an anomalously large concentration in As, Mo and Au relative to other P1-sulfides. Texturally sample FC 49-4-2 is different than other P1-sulfides in that it consists of cream/white, subhedral

sulfides in a narrow veinlet with random sulfides dispersed at the rim of wall rock altered zones. These textural and geochemical differences indicate that P1 contains several geochemically and texturally distinct sulfide generations but were all categorized as pulse 1 (P1).

Spatially P1-sulfides also display slight chemical change with respect to P2 and P3. Gold and Mo both have spatial-chemical changes in response to the surrounding pulses. The interaction between pulses can cause variability in the data set and make it difficult to chemically classify an individual pulse.

Geochemical and textural observations show that P2-sulfides appear to have been emplaced previous to P2. Geochemical results for P2-sulfides manifest a relatively lower Au and Ag abundance (than P1), increased W and petrographically display an erratic distribution. Clusters of sulfides tend to be on the outer edges of P2 (near or on the host rock) with randomly oriented sulfides throughout the vein. P2 also has slightly finer grained sulfides (than P1) which typically display an irregular shape. P2 sulfides possibly are associated with a previous pulse and became entrained during the P2 event. This entrainment would lead to a metamorphic recrystallization (Wagner et al., 2007) and would explain the consistent irregular shapes, the distribution of sulfides and the Au, Ag and W anomalies. P2 could have also exploited P1 as a zone of weakness; therefore explaining why some pulses show a transition between P2 and P1.

P3 is the only pulse where sulfide grains are rare and electrum is present. P3 is characterized by the presence of euhedral calcite and lath-like quartz. The presence of electrum is rare but is only present when P3 cuts a pre-existing sulfide rich vein (either P1 or P2). Petrographically P3 is the most unique pulse present and yields the highest concentration of Au and Ag (electrum average: 69.5 wt. % Au and 26.6 wt. % Ag; Table A1). P3 also displays a lower Ag/Au ratio than P1 and P2-sulfides (Ag/Au: P3-electrum 0.4, P2-sulfides 5.3 and P1-sulfides 16.2). These Ag/Au ratios play an important role in determining which type of metal complex dominated the system and at which conditions these metals existed (Cole and Drummond, 1986; Yilmaz et al. 2013).

The capacity of Au and Ag to be transported and concentrated within a vein is dependent on the activity and availability of its corresponding ligand (Pirajno, 2009). The transportation of Ag and Au in a hydrothermal system can be primarily credited to two ligands, HS^- and Cl^- (Cole and Drummond, 1986; Rickard and Luther, 2006; Pirajno, 2009). Other ligands (e.g., NH_3, SO_4^{2-}, F^- and HCO_3^-) can also contribute to the mobilization of metals but are thought to be less common (Pirajno, 2009). The transportation of metals by HS^- is typically dominant in low temperature, neutral pH environment and Cl^- transportation tends to dominant in high temperature, acidic environments. Fire Creek exhibits an average Ag/Au ratio of 0.4 in P3-electrum, 16.2 in P2-sulfides and 5.3 in P1-sulfides. These ratios likely indicate that $Au(HS)_2^-$ complexes dominated the system in a low temperature (200-250°C), moderate to high

ΣH_2S and pH environment for P3 and $AuCl_2^-$ complexes dominated at low ΣH_2S, low to moderate pH for both P1 and P2-sulfides (Cole and Drummond, 1986).

6.3 Trace Element Trends

Sulfide grains display compatibility of Au when plotted against Mo and W (Figure 16). This single trend suggests that Mo generally precipitated simultaneously with Au. Figure 16B shows three distinct trends all pertaining to different pulses or pulse associations. The steepest trend shows a large increase in W with a slight increase in Au. Pulse 1_3_2 is consistent with both Au and W precipitating simultaneously. Slope 1_2 exhibits the gentlest slope showing a large increase in Au but a slight and inconsistent increase in W concentration. These trends indicate different fluid chemistries precipitating sulfide grains in the pulses, consistent with ligand transport discussed above.

All W trends pertain to a chemically and possibly temporally distinct pulses. The steepest slope (2_3_1; Figure 16) is possibly associated with P1-sulfides which were entrained and altered by P2. This action would have dissociated Au in sulfide phases and made relative W concentrations large. Additionally, slope 2_3_1 is associated with varying Au concentrations relative to P3 (Figure 15C). This suggests that P3 might have also had an effect on Au concentrations which would result in a shifted trend.

Within electrum grains, Cd, Sn and W appear to be coupled (Mo also appears to be slightly coupled; Figure 17). Correlation coefficients (R^2) are low but compatible

trends suggest that these elements must follow the same chemical behavior. Gold concentrations (from electrum grains) were not collected from LA-ICP-MS but EMP gold results did not yield any trace element trends.

6.4 Comparison to other deposits

Fire Creek is an epithermal low-sulfidation Au-Ag deposit, spatially and temporally associated with mid-Miocene bimodal basalt magmatism. This makes Fire Creek distinct from rhyolite-hosted low-sulfidation Au-Ag deposits such as Sleeper (e.g., Saunders et al., 2008), and most similar in character to basalt-hosted deposits such as Mule Canyon and Buckhorn (John and Wallace, 2000; John et al., 2003A). In this discussion, I will draw heavily on work on the Mule Canyon deposit by John et al. (2003A), rather than for Buckhorn, where no systematic geological and geochemical studies have yet been performed.

Mule Canyon is an inactive mine just north of Fire Creek (Figure 1), geochemical and structural studies were conducted by John et al. (2003A). At both Mule Canyon and Fire Creek Au-Ag ores are present along steeply dipping, north-northwest and north-north-east-striking faults (John et al., 2003A; Raven et al., 2011). These ores are typically confined at Mule Canyon by narrow silica-adularia and adularia-smectite altered zones that are stratigraphically controlled and tend to extend outward. Like Fire Creek, Mule canyon hosts several periods of Au-Ag deposition which are hosted by distinct phases and styles of mineralization.

Despite similarities in hosting lithology, Mule Canyon shows many distinct features of mineralization to Fire Creek, that are perhaps more akin to more evolved rhyolitic-hosted low sulfidation epithermal Au-Ag deposits in the NNR. For example, while Mule Canyon and Fire Creek both display an early stage pyrite and arsenopyrite pulse event, occasionally containing elevated concentrations of Au and Ag (Serenko, 1995; John et al., 2003A), Mule Canyon has a second pulse consisting of euhedral arsenopyrite whereas at Fire Creek's second pulse consist of subhedral quartz and anhedral pyrite. Mule Canyon has a late stage pulse consisting of chalcedony-opal ± adularia ± carbonate veins and hydrothermal breccias containing marcasite and/or pyrite, electrum, minor selinide and silver sulfides. In this context, another major distinction between Fire Creek and Mule Canyon is the abject lack of adularia in Fire Creek mineral veins, making indirect dating of the Fire Creek deposit by Ar-Ar or K-Ar challenging at best. A late stage pulse at Fire Creek results in euhedral calcite with lath-like quartz (on the outer edges) and/or subhedral to euhedral quartz and electrum, hosted within veins and breccias. Electron microprobe data shows that Ag concentration in electrum grains are higher at Mule Canyon (30-35 wt. %) than at Fire Creek (24-28 wt. %).

Generally high grade ores are hosted in late stage pulses within veins and breccias at both Fire Creek (P3) and Mule Canyon. Given the evidence for a change in ligand chemistry, I suggest that sub-boiling became an increasingly important mechanism for the deposition and pre-concentration of gold and silver, as also suggested by John et al. (2003A) for Mule Canyon. Although similar to one another,

late stage pulse events at Fire Creek and Mule Canyon exhibit slight mineralogical differences. At Fire Creek the late stage pulse is typically very consistent, only possessing calcite, quartz and occasionally electrum whereas Mule Canyon's mineralogy tends to vary dramatically. This large discrepancy may be due to the degree of boiling or a distinct fluid source.

Adularia is a potassium feldspar which occurs in hydrothermal environments through the replacement of andesine phenocrysts and groundmass (Steiner, 1970). Adularia was significant mineral used for dating mineralization at Mule Canyon and was generally present in most of the ore types. Fire Creek does not appear to have any adularia present and therefore a date of mineralization was not possible. The absence of adularia might be caused by high Fe and low silica wall rock concentrations which do not allow for adularia to efficiently be produced (John et al., 2003A).

6.5 Paragenetic Model

Kamenov et al. (2007) used Pb isotopes to chemically link mid-Miocene bimodal basalt-rhyolite hosted ores and the earliest emergence of the Yellowstone Hotspot plume (Hames et al., 2009). Hames et al. (2009) then established a model which depicted magma chambers of basalt overlain by rhyolite which fed bimodal volcanism associated with the emergence of the Yellowstone Hotspot. In this model, Fire Creek and Mule Canyon were fed by a deeper basalt magma chamber whereas locations like Sleeper, Buckskin, Midas, National and DeLamar were fed by a shallow rhyolite magma chamber. The heat from these chambers allowed for shallow

geothermal systems to proceed and then ores were deposited as magma chambers evolved to episodically release ore rich fluids.

Hofstra and Creaser (2009) confirmed the relationship of the Sleeper deposit ores to the Columbian River basalts by comparing Re-Os isotopes. This study was accompanied by very low concentrations of both Re and Os, and only one out of the three studied locations (Sleeper, Round Mountain and Seven Troughs) were able to yield useful Re-Os isotope data (concentrations were at lower than ppt levels in some instances, suggesting very low absolute analyte). However, at Fire Creek Re, Os and other HSE's tend to display large concentrations (ppm) within sulfide and electrum grains. Concentration differences between Hofstra and Creaser (2009) and this study are conceivably due to the nature of the of the corresponding magma chamber (basaltic vs. rhyolitic) that fed the area. Magmas with higher MgO contain higher abundances of the compatible HSE prior to extensive fractional crystallization and sulfide saturation (Day, 2013), which allows locations like Fire Creek (basaltic) to acquire a larger HSE concentration and Sleeper (rhyolitic) to acquire lower HSE concentrations. If concentrations of HSE are dependent on magma source, then Au, being an HSE, must have been episodically exsolved from the magma and not leached from the surrounding units as implied by John et al. (2003A). This genetic model supports the concept of Kamenov et al. (2007) and Hames et al. (2009), which states that mid-Miocene ores must be associated to a primitive magmatic source chemically linked to the Columbian River basalts.

Understanding the origin of gold at Fire Creek, and elsewhere in the NNR, requires resolution of whether inter-element fractionations of the HSE reflect derivation from S-segregation and/or alloy formation direct from a magmatic source, or fractionation from a crustal source. Figure 25 shows HSE concentrations in ocean island basalts (OIB) (i.e., mantle magmatic source), continental crust (crustal source) and Fire Creek electrum. Continental crust displays the lowest HSE values from the data set and has shown high Rh and low Os and Ir. Conceivably, fractionation of S prior to electrum alloy formation could explain the elevated Pt in Fire Creek electrum, but a crustal source is a very poor fit for the elevated Os and Ir concentrations and low Ru and Rh in Fire Creek electrum. Combined with the sulfide data, there is strong evidence to suggest sulfide/alloy fractionation of a mantle-derived magma source that became increasingly enriched in Au due to ligand transport.

A potential cause of concern is that this study is the first ever of native electrum by LA-ICP-MS. It is remotely possible that interferences from high Au and Ag yields could cause artificial concentrations of the other HSE. There are two main reasons to contend that this is not the case. First, there are no direct or argide interferences consistent with the masses measured for HSE in the study; a prerequisite for interferences during LA-ICP-MS. Second, large concentrations of HSE's do not appear to have been a cause of analytical error from a previous study of gold coins. Dussubieux and Van Zelst (2004) determined that LA-ICP-MS was a suitable method to determine trace element abundances in gold coins because of a lack of potential interferences. It is notable that the HSE patterns obtained from the gold coins

measured in the Dussubieux and Van Zelst (2004) study show similar fractionations of the HSE to the electrum from Fire Creek, and at higher absolute concentrations (Figure 26). LA-ICP-MS of both native gold and electrum as well as ancient coins may offer a powerful method for provenancing and tracing precious metals in the future.

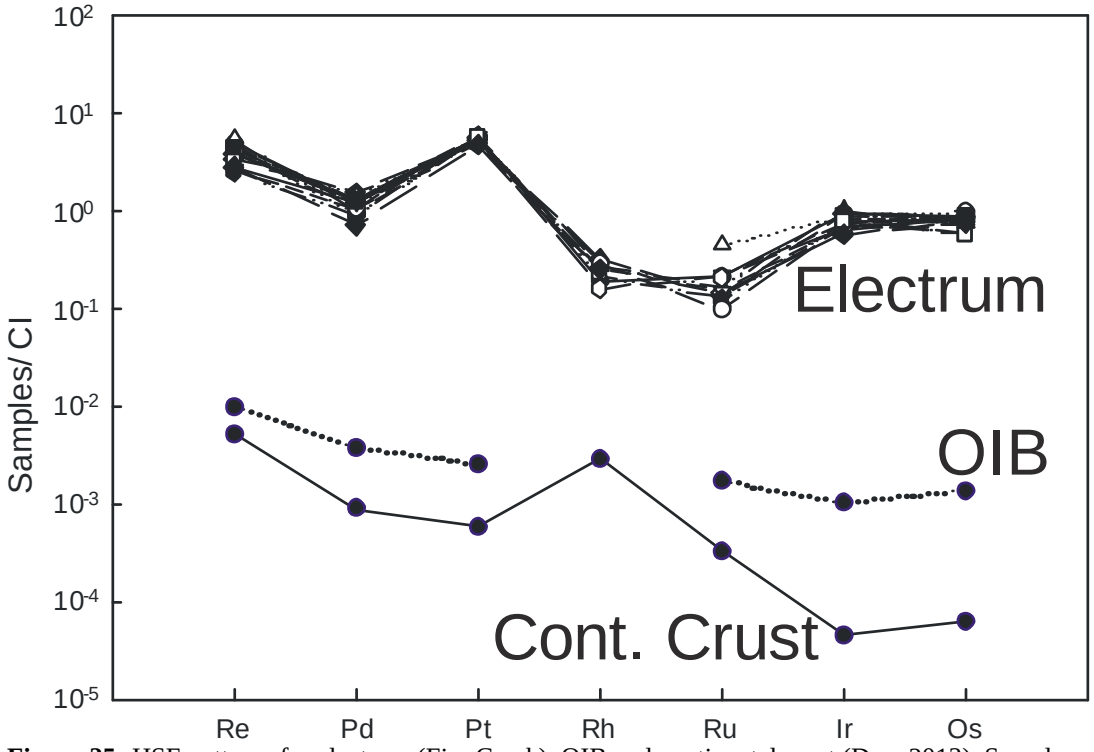

Figure 25: HSE patterns for electrum (Fire Creek), OIB and continental crust (Day, 2013). Samples were all normalized to CI Chondritic values (Day, 2013).

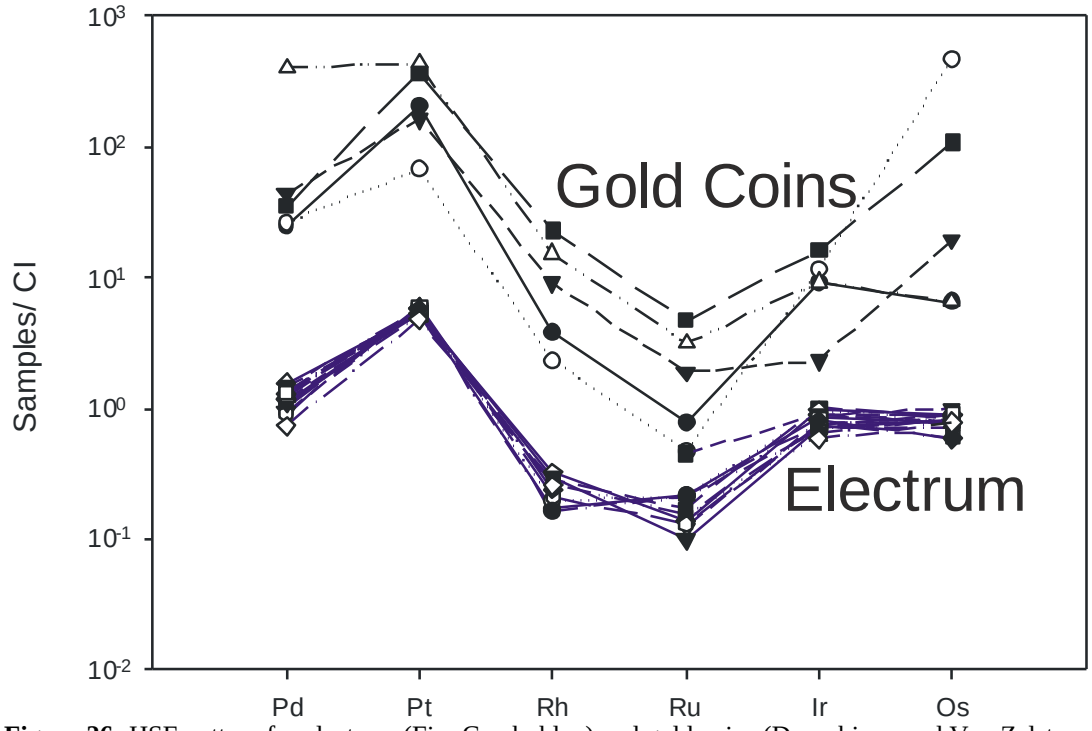

Figure 26: HSE pattern for electrum (Fire Creek; blue) and gold coins (Dussubieux and Van Zelst, 2004). Concentrations were normalized to CI chondritic values (Day, 2013)

6.6 Implications for gold deposition

As discussed above, HSE concentrations and petrographic observations suggest that Au and Ag are present in two distinct forms and were exsolved from a relatively less evolved, primitive magma source (Kamenov et al., 2007; Saunders et al., 2008). Therefore, Fire Creek must have evolved directly from a basalt rich magma source which was episodically altered by magmatic and hydrothermal pulses (present in three forms; P1, P2 and P3). Sulfide pulses (P1 and P2; Figure 27) at Fire Creek appear to be the earliest pulse events present and typically consist of detectible Au and Ag concentrations. These early stage fluids were not boiling and precipitated metals as the fluids cooled and reacted with the iron rich wall rock. Sulfide rich pulses also appear to be coeval with silica rich pulses (P2) which typically display sulfide grains

with lower Au and Ag concentrations and larger degrees of wall rock alteration. A late stage pulse, rich in silica and calcite, produced the largest Au-Ag concentrations at Fire Creek (Figure 27). This pulse contains the only electrum present throughout the deposit and the presence of sulfides is rare. Pulse 3 precipitated after the boiling and cooling of moderate temperature fluids which allowed for electrum to become the dominate Au-Ag phase. Electrum is typically found in the presence of P3 only when it cuts a sulfide rich vein. This implies that something within P1 or P2 was working as a catalyst which allowed Au and Ag to precipitate in these regions.

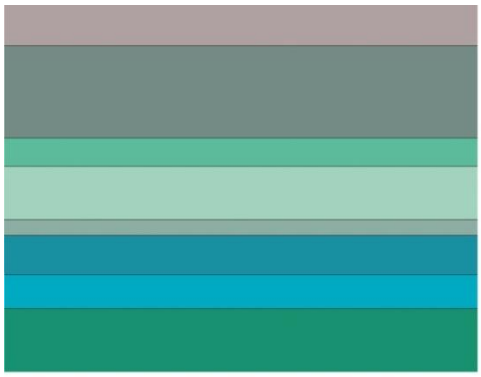

Stage 1
1. Units through Tb2 are emplaced

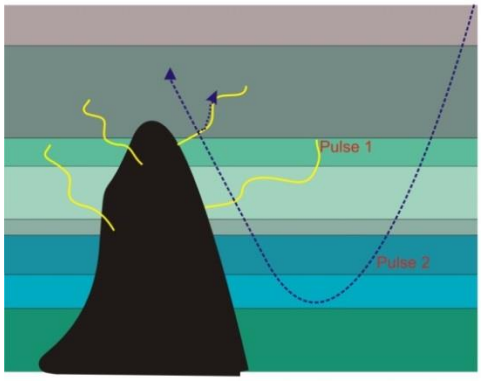

Stage 2
1.Dike cuts though units
2. Pulse 1 with low grade ore is emplaced
3. Pulse 2 is emplaced

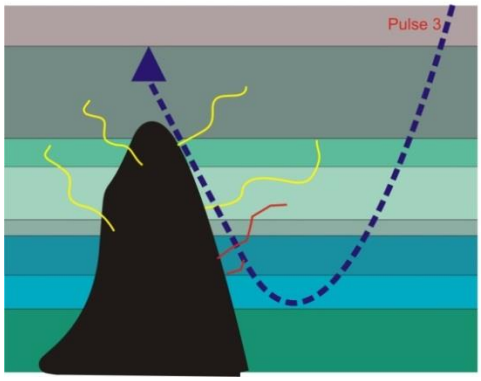

Stage 3
1. Hydrothermal fluids rich in Si and C intermix w/ magmatic fluids
2. Boiling of P3 causes de-sulfidation and Au-Ag are emplaced

Figure 27: Model depicting the emplacement of units and pulses. Stage 1: shows the emplacement of units through Tb2. Stage 2: shows an early stage sulfide pulse event which precipitated as it reacted to the iron-rich wall rock. This sulfide rich pulse was then preceded by a silica rich pulse dominantly meteoritic) which cut the sulfide rich pulse and used it as a zone of weakness. Stage 3: this depicts pulse 3 which is a dominantly meteoric pulse, rich in silica and carbon that intermixed with ore rich magmatic fluids. Pulse 3 precipitated after a boiling and cooling event which precipitated Au-Ag into electrum phases.

Although northern Nevada mid-Miocene low sulfidation epithermal ore deposits all appear to be derived from a common source (John, 2001), HSE concentrations may vary from deposit to deposit. Studies by Hofstra and Creaser

(2009) show low concentrations of Re and Os for rhyolite hosted ores, whereas this study shows large concentrations of both Re and Os for Fire Creek. This implies that it is best to conduct a high precision study on Re-Os isotopes on ores which are hosted directly by basalts (like Fire Creek and Mule Canyon).

This suggests that in order for Fire Creek to attain its ores it must have had (1) volcanism associated to the Yellowstone hotspot, (2) episodic magma pulses (rich in HSE) and (3) hydrothermal fluids concentrating Au and Ag into narrow and confined zones (P3). The absence of any of these events would have possibly led to a region with no economical value.

6.7 Future Work

Whole rock measurements were done by XRF but do not provide the sensitivity to yield high precision trace element concentrations. It is possible that trace elements trends would yield better results for processes occurring in the magma chamber feeding Fire Creek. These magmatic conditions could also determine the state of the magma chamber before the release of metal ores which would allow for a better constraint on a mechanism for ore deposition. In order to achieve these trace element values a high-precision solution-based ICP-MS will need to be considered.

No direct age constraints of Au-Ag ore have ever been established for northern Nevada mid-Miocene deposits. Instead, $^{40}Ar/^{39}Ar$ ages from adularia ($KAlSi_3O_8$) have been used to indicate a relative age of mineralization. Dating adularia allows for a date to be established for the gauge mineral but its presence does not always indicate the

presence of Au and Ag. Comparably, the Re-Os isotope system serves as an important tool for the studying the age and origin of ore forming systems. Large Os isotope composition differences between the crust and the mantle make discerning the origin of Os ideal (Shirey & Walker, 1998). Gold is a mono-isotopic element and is not produced as a result of radioactive decay, making direct genetic tracing via stable isotopes impossible (Shirey & Walker, 1998). However, both Au and Os are noble metals and share some chemical similarities, making the Re-Os isotope system an ideal candidate for the tracing and direct dating of Au mineralization (Walker et al., 1989; Hart & Kinloch, 1989; Shirey & Walker, 1998). Fire Creek possessing large concentrations of both Re and Os should allow this isotope system to yield a precise age for Au-Ag deposition.

Pressure, temperature and fluid (gauge) origin were not directly analyzed in this study. Therefore, the next obvious step would be to conduct a fluid inclusion and stable isotope analysis. Silica rich zones might contain small fluid inclusions which would help to discern the temperature of the fluids and whether or not boiling occurred (John et al., 2003A). Oxygen, carbon and sulfur isotopes would be acquired from silicate, carbonate and sulfide phases. This data would help characterize the hydrothermal fluids involved, determine the source of the fluids and constrain the temperature of the formation.

7. CONCLUSIONS

Fire Creek is a low sulfidation epithermal Au-Ag deposit spatially and temporally associated with bimodal basalt-rhyolite volcanism. Fire Creek possesses no less than three pulse events which host Au and Ag in two distinct forms. Au-Ag bearing sulfide phases are present in pulse 1 and 2. Late stage carbonate and silica pulse (P3) host Au-Ag phases as electrum and is host to the highest ore grades. Electrum, although occasionally present, appears to only exist when carbonate-silica pulses cut sulfide rich pulses and is typically found in dendritic form. P1-sulfides generally possess larger Au concentrations than P2-sulfides.

Whole rock data and HSE concentrations suggest that Au and Ag were transported by mid-Miocene magmas and episodically exsolved to form low sulfidation deposits at Fire Creek. The initial pulse (P1) was a sulfur rich pulse which cooled and reacted with the iron rich wall rock and led to the precipitation of Au and sulfidation (John et al., 2003A). P2 was then exsolved and used P1 veins as zones of weakness to become mobile. This pulse most likely had a lower pH which led to a larger degree of alteration. The highest grade hosting pulse (P3) was precipitated through the boiling and cooling of magmatic and meteoric fluids.

APPENDIX

Table A1: Major element chemistry acquired from EMPA (in wt. %).

Sample	49-2-2	49-2-2	49-2-2	49-2-2	49-2-2	49-2-2	49-2-2	49-2-2	49-2-2	49-2-2
Line no.	348	349	350	351	352	353	354	355	356	357
Mineral	1	1	1	1	1	1	1	1	1	1
Si WT%	0.04	0.05	<0.03	0.04	0.02	0.02	0.01	0.04	1.20	0.01
Fe WT%	46.11	47.23	47.11	47.37	46.07	46.89	47.30	47.53	44.26	47.11
Co WT%	0.02	0.09	<0.03	<0.03	<0.03	<0.03	0.11	0.08	<0.03	<0.03
Ni WT%	0.01	0.01	0.02	0.05	0.02	<0.03	0.01	0.04	<0.03	0.06
Cu WT%	0.07	<0.03	<0.03	<0.03	<0.03	<0.03	<0.03	<0.03	0.06	0.07
Mn WT%	0.01	0.02	<0.03	0.01	<0.03	0.02	<0.03	<0.03	0.01	<0.03
P WT%	<0.03	0.01	<0.03	<0.03	<0.03	<0.03	<0.03	0.06	<0.03	0.09
S WT%	50.67	53.48	52.88	53.44	51.38	52.69	52.61	52.86	49.96	52.99
As WT%	1.49	0.03	1.42	0.13	0.40	0.08	0.30	0.48	0.63	0.62
Ag WT%	<0.03	<0.03	0.04	<0.03	0.05	<0.03	<0.03	<0.03	<0.03	0.01
Au WT%	0.21	0.12	0.43	0.70	0.05	<0.03	<0.03	<0.03	0.36	0.18
TOTAL	98.53	101.00	101.91	101.57	97.98	99.36	100.08	100.52	96.37	101.10

Sample	50-1-2-2	47-3-4	47-3-4	47-3-4	47-3-4	47-3-4	47-3-4	47-3-4	47-3-4	47-3-4
Line no.	434	462	463	464	465	466	467	468	469	470
Mineral	1	1	1	1	1	1	1	1	1	1
Si WT%	0.31	<0.03	0.01	0.12	0.01	0.65	0.68	0.06	0.01	1.90
Fe WT%	43.90	47.37	47.64	46.50	47.45	41.20	45.52	47.13	46.67	44.55
Co WT%	0.08	<0.03	0.07	0.13	<0.03	0.02	0.03	0.09	0.02	0.07
Ni WT%	<0.03	<0.03	0.04	0.02	0.05	0.03	0.02	<0.03	<0.03	<0.03
Cu WT%	<0.03	<0.03	0.09	0.03	0.05	<0.03	<0.03	<0.03	<0.03	0.06
Mn WT%	0.01	0.02	<0.03	0.02	<0.03	0.02	0.03	<0.03	0.02	0.05
P WT%	0.08	<0.03	<0.03	<0.03	<0.03	0.96	0.02	<0.03	<0.03	<0.03
S WT%	48.87	53.86	52.46	50.93	53.41	45.33	50.48	52.66	52.19	50.08
As WT%	1.67	<0.03	<0.03	<0.03	<0.03	0.06	0.01	<0.03	<0.03	<0.03
Ag WT%	<0.03	<0.03	0.02	0.03	<0.03	<0.03	0.05	<0.03	0.06	0.05
Au WT%	0.21	0.13	0.04	0.14	0.05	0.20	<0.03	0.21	<0.03	0.36
TOTAL	95.13	101.15	100.33	97.92	100.92	88.39	96.34	100.04	98.77	97.11

1= Sulfides
2=Electrum

Table A1: Continued

Sample	49-2-2	49-2-2	49-2-2	49-2-2	49-2-2	49-2-2	49-2-2	49-2-2	49-2-2	49-2-2
Line no.	358	359	360	361	362	363	364	365	366	367
Mineral	1	1	1	1	1	1	1	1	1	1
Si WT%	0.07	0.01	0.05	0.19	<0.03	<0.03	0.02	<0.03	0.04	0.29
Fe WT%	46.76	47.01	46.82	47.20	47.00	47.64	47.53	47.27	47.63	46.25
Co WT%	0.06	<0.03	<0.03	<0.03	<0.03	<0.03	0.01	<0.03	<0.03	0.04
Ni WT%	<0.03	<0.03	0.03	0.01	<0.03	<0.03	<0.03	0.05	<0.03	0.02
Cu WT%	<0.03	0.01	0.05	0.02	<0.03	<0.03	<0.03	0.06	<0.03	0.03
Mn WT%	<0.03	0.02	<0.03	<0.03	0.05	0.01	<0.03	<0.03	<0.03	<0.03
P WT%	<0.03	<0.03	0.01	<0.03	<0.03	0.02	0.01	0.01	<0.03	0.01
S WT%	52.43	53.22	52.88	53.05	53.63	53.15	53.10	53.43	53.12	50.70
As WT%	0.74	<0.03	0.29	0.10	<0.03	<0.03	0.29	<0.03	<0.03	0.27
Ag WT%	0.10	0.07	0.02	<0.03	0.05	<0.03	0.01	0.07	<0.03	0.02
Au WT%	<0.03	<0.03	0.06	0.01	0.11	0.14	<0.03	<0.03	<0.03	<0.03
TOTAL	99.80	99.98	100.19	100.58	100.77	100.91	100.68	100.65	100.28	97.36

Sample	47-3-4	47-3-4	47-3-4	47-3-4	47-3-4	47-3-4	47-3-4	47-3-4	47-3-4	47-3-4
Line no.	471	472	473	474	475	476	477	478	479	480
Mineral	1	1	1	1	1	1	1	1	1	1
Si WT%	0.08	0.02	0.75	0.01	0.30	<0.03	0.01	0.26	0.51	1.12
Fe WT%	45.87	46.97	45.23	47.28	41.54	47.41	47.49	44.33	44.58	45.75
Co WT%	0.05	<0.03	0.05	0.04	<0.03	0.11	0.06	0.03	<0.03	<0.03
Ni WT%	0.04	0.04	0.02	<0.03	<0.03	<0.03	<0.03	<0.03	<0.03	0.01
Cu WT%	0.05	0.04	<0.03	0.07	0.03	<0.03	<0.03	0.06	0.02	0.05
Mn WT%	0.32	<0.03	<0.03	<0.03	0.20	0.03	<0.03	0.15	0.06	0.06
P WT%	<0.03	<0.03	0.01	<0.03	<0.03	<0.03	0.01	0.03	0.04	<0.03
S WT%	52.42	53.06	50.87	52.66	47.55	53.58	52.93	50.60	48.98	51.03
As WT%	<0.03	<0.03	<0.03	<0.03	0.02	<0.03	<0.03	0.01	<0.03	0.02
Ag WT%	<0.03	0.05	0.05	0.05	0.03	<0.03	<0.03	<0.03	<0.03	<0.03
Au WT%	0.21	<0.03	0.07	<0.03	0.48	0.85	0.17	0.18	<0.03	0.02
TOTAL	99.03	99.92	97.04	99.50	90.07	101.91	100.47	95.59	94.12	98.00

1= Sulfides
2=Electrum

Table A1: Continued

Sample	49-2-2	49-2-2	49-2-2	49-2-2	49-2-2	49-2-2	49-2-2	49-2-2	49-2-2	49-2-2
Line no.	368	369	370	371	372	373	374	375	376	377
Mineral	1	1	1	1	1	1	1	1	1	1
Si WT%	0.05	0.28	<0.03	0.11	0.01	<0.03	<0.03	0.06	<0.03	0.02
Fe WT%	47.25	46.80	47.01	46.22	46.93	47.86	47.36	47.46	47.39	47.65
Co WT%	0.06	0.06	<0.03	0.06	<0.03	<0.03	0.10	<0.03	<0.03	0.01
Ni WT%	0.02	0.03	0.04	<0.03	0.03	<0.03	0.03	<0.03	<0.03	0.03
Cu WT%	0.02	<0.03	0.25	<0.03	<0.03	<0.03	0.18	<0.03	<0.03	0.07
Mn WT%	<0.03	0.03	0.03	0.03	0.04	0.02	0.04	<0.03	<0.03	<0.03
P WT%	<0.03	<0.03	<0.03	0.02	<0.03	<0.03	<0.03	<0.03	<0.03	<0.03
S WT%	52.88	52.89	53.92	52.73	52.86	53.82	51.70	53.12	51.58	52.87
As WT%	<0.03	<0.03	<0.03	<0.03	<0.03	<0.03	1.18	<0.03	1.92	0.25
Ag WT%	<0.03	<0.03	0.08	<0.03	0.11	<0.03	0.04	<0.03	0.05	0.05
Au WT%	0.43	<0.03	<0.03	0.15	0.16	0.51	0.16	<0.03	<0.03	0.15
TOTAL	100.69	100.01	101.27	99.18	100.08	102.14	100.80	100.43	100.76	101.10

Sample	47-3-4	47-3-4	47-3-4	49-4-2	49-4-2	49-4-2	49-4-2	49-4-2	49-4-2	49-4-2
Line no.	481	482	483	42	43	44	46	48	49	50
Mineral	1	1	1	1	1	1	1	1	1	1
Si WT%	0.26	0.02	3.05	0.06	0.03	1.65	0.79	0.05	0.09	0.24
Fe WT%	46.68	47.26	42.94	37.31	35.74	32.40	34.84	45.69	41.67	46.29
Co WT%	<0.03	<0.03	0.08	0.10	0.01	0.02	<0.03	<0.03	<0.03	0.06
Ni WT%	0.04	0.03	<0.03	<0.03	<0.03	<0.03	0.02	0.03	0.01	<0.03
Cu WT%	<0.03	<0.03	0.01	0.06	<0.03	0.07	<0.03	0.08	<0.03	<0.03
Mn WT%	0.16	<0.03	<0.03	<0.03	<0.03	<0.03	<0.03	0.01	0.02	0.02
P WT%	<0.03	<0.03	0.07	0.58	0.22	<0.03	0.01	<0.03	0.02	<0.03
S WT%	51.79	52.70	48.61	21.47	20.82	19.70	20.06	51.65	46.51	52.41
As WT%	<0.03	<0.03	0.04	43.80	41.12	36.82	39.16	<0.03	0.04	0.03
Ag WT%	0.07	0.05	0.04	<0.03	<0.03	<0.03	<0.03	0.06	<0.03	0.02
Au WT%	<0.03	0.34	<0.03	<0.03	0.01	0.14	<0.03	<0.03	0.56	0.34
TOTAL	98.91	100.38	94.82	102.82	97.82	90.76	94.77	97.43	88.83	99.35

1= Sulfides
2=Electrum

Table A1: Continued

Sample	49-2-2	49-2-2	49-2-2	49-2-2	49-2-2	49-2-2	49-2-2	49-2-2	49-2-2	49-2-2
Line no.	378	379	380	381	382	383	384	385	386	387
Mineral	1	1	1	1	1	1	1	1	1	1
Si WT%	0.44	<0.03	0.28	0.08	0.15	0.10	0.04	0.04	0.59	0.04
Fe WT%	44.20	48.18	44.50	46.75	46.10	46.15	46.52	47.02	45.84	47.69
Co WT%	<0.03	0.02	<0.03	0.09	<0.03	0.01	0.10	0.09	<0.03	<0.03
Ni WT%	0.05	<0.03	<0.03	0.02	<0.03	0.01	<0.03	<0.03	<0.03	0.04
Cu WT%	0.08	0.03	<0.03	0.02	0.01	0.04	0.10	<0.03	0.02	<0.03
Mn WT%	<0.03	<0.03	<0.03	<0.03	0.02	<0.03	<0.03	<0.03	<0.03	<0.03
P WT%	0.06	<0.03	0.29	<0.03	0.02	<0.03	<0.03	0.03	0.10	0.02
S WT%	48.85	53.12	50.05	51.66	51.23	50.02	51.00	51.66	51.38	52.41
As WT%	0.98	<0.03	0.42	0.72	0.58	1.20	2.41	0.26	0.24	0.26
Ag WT%	<0.03	<0.03	0.05	<0.03	<0.03	0.02	<0.03	<0.03	<0.03	<0.03
Au WT%	<0.03	<0.03	<0.03	<0.03	0.42	<0.03	<0.03	<0.03	0.15	<0.03
TOTAL	94.52	100.58	95.47	99.26	98.48	96.93	99.65	98.35	98.25	100.15

Sample	49-4-2	49-4-2	49-4-2	49-4-2	49-4-2	50-1-1	50-1-1	50-1-1	50-1-1	50-1-1
Line no.	51	52	53	54	55	57	58	59	60	61
Mineral	1	1	1	1	1	1	1	1	1	1
Si WT%	0.87	0.74	0.16	0.02	<0.03	<0.03	<0.03	0.01	<0.03	0.05
Fe WT%	45.51	45.24	46.73	47.37	47.47	47.96	46.99	46.94	47.59	47.00
Co WT%	0.05	<0.03	<0.03	<0.03	<0.03	<0.03	0.02	0.11	<0.03	0.04
Ni WT%	<0.03	0.02	<0.03	<0.03	0.04	<0.03	<0.03	0.03	0.01	0.04
Cu WT%	0.03	0.02	0.06	<0.03	<0.03	0.04	<0.03	<0.03	<0.03	<0.03
Mn WT%	0.09	0.02	0.04	<0.03	<0.03	<0.03	0.04	<0.03	<0.03	0.01
P WT%	0.02	0.14	0.03	0.03	<0.03	<0.03	<0.03	<0.03	0.01	0.13
S WT%	51.62	49.02	51.44	52.45	53.38	53.77	52.54	52.93	53.14	51.93
As WT%	0.07	0.49	0.35	0.28	<0.03	<0.03	<0.03	<0.03	<0.03	0.27
Ag WT%	0.08	0.05	0.02	0.08	0.06	0.03	<0.03	<0.03	<0.03	0.02
Au WT%	<0.03	0.07	0.19	<0.03	<0.03	0.02	<0.03	<0.03	<0.03	<0.03
TOTAL	98.05	95.76	98.94	100.07	100.82	101.80	99.38	99.48	100.18	99.34

1= Sulfides
2=Electrum

Table A1: Continued

Sample	49-2-2	49-2-2	49-2-2	49-2-2	49-2-2	49-2-2	49-2-2	49-2-2	49-2-2	49-2-2
Line no.	388	389	390	391	393	395	396	397	398	399
Mineral	1	1	1	1	1	1	1	1	1	1
Si WT%	0.02	0.04	<0.03	0.14	0.51	0.01	<0.03	0.73	0.53	0.22
Fe WT%	46.04	47.11	46.88	47.01	44.47	47.23	47.21	45.29	45.39	46.76
Co WT%	0.02	0.03	<0.03	<0.03	0.08	0.04	<0.03	<0.03	0.02	<0.03
Ni WT%	<0.03	0.03	0.01	0.02	0.05	0.03	0.02	<0.03	0.02	0.08
Cu WT%	0.03	0.18	0.06	0.02	0.08	<0.03	<0.03	<0.03	0.02	<0.03
Mn WT%	<0.03	<0.03	<0.03	<0.03	<0.03	<0.03	<0.03	<0.03	0.01	<0.03
P WT%	<0.03	0.02	<0.03	<0.03	0.34	0.10	0.03	<0.03	0.07	0.05
S WT%	49.80	51.36	51.14	52.47	49.30	53.03	51.31	50.26	50.10	51.53
As WT%	2.46	0.83	2.96	0.32	1.10	0.11	2.69	1.19	1.35	0.93
Ag WT%	0.03	0.09	<0.03	<0.03	<0.03	<0.03	0.02	0.06	<0.03	<0.03
Au WT%	0.47	0.32	0.17	0.37	<0.03	0.36	<0.03	<0.03	0.22	0.23
TOTAL	98.83	100.00	101.18	100.30	95.78	100.91	101.11	97.52	97.73	99.72

Sample	50-1-1	50-1-1	50-1-1	50-1-2-1	50-1-2-1	50-1-2-1	50-1-2-1	50-1-2-1	50-1-2-1	50-1-2-1
Line no.	62	63	64	66	67	68	69	70	71	72
Mineral	1	1	1	1	1	1	1	1	1	1
Si WT%	0.03	0.02	<0.03	0.21	0.08	<0.03	<0.03	<0.03	<0.03	0.15
Fe WT%	46.97	47.79	47.54	46.18	47.08	47.22	46.65	47.82	47.93	45.88
Co WT%	0.08	<0.03	0.03	0.01	0.13	0.06	0.06	0.08	0.07	0.05
Ni WT%	<0.03	0.03	0.04	0.02	<0.03	<0.03	<0.03	<0.03	0.03	<0.03
Cu WT%	<0.03	0.06	<0.03	<0.03	<0.03	<0.03	<0.03	<0.03	0.01	0.05
Mn WT%	<0.03	0.01	0.01	0.07	<0.03	0.01	0.05	0.04	0.11	0.01
P WT%	0.15	<0.03	<0.03	<0.03	<0.03	<0.03	<0.03	<0.03	<0.03	<0.03
S WT%	51.93	53.04	53.02	52.73	52.40	52.99	52.71	52.87	53.98	52.01
As WT%	0.53	0.11	0.02	<0.03	<0.03	<0.03	<0.03	<0.03	<0.03	<0.03
Ag WT%	0.14	0.02	0.05	<0.03	<0.03	0.07	<0.03	<0.03	0.02	<0.03
Au WT%	0.25	<0.03	0.25	<0.03	<0.03	0.41	<0.03	<0.03	0.10	0.15
TOTAL	100.04	101.01	100.96	98.85	99.51	100.74	98.93	100.66	102.25	98.28

1= Sulfides
2=Electrum

Table A1: Continued

Sample	50-1-2-2	50-1-2-2	50-1-2-2	50-1-2-2	50-1-2-2	50-1-2-2	50-1-2-2	50-1-2-2	50-1-2-2	50-1-2-2
Line no.	410	411	412	413	414	415	416	417	418	421
Mineral	1	1	1	1	1	1	1	1	1	1
Si WT%	0.09	0.09	0.09	0.09	0.09	0.19	0.28	0.55	0.07	0.09
Fe WT%	45.05	44.88	44.66	44.97	44.61	44.46	44.36	46.75	45.14	44.28
Co WT%	0.03	0.08	<0.03	0.05	0.05	<0.03	0.02	0.09	<0.03	0.04
Ni WT%	<0.03	<0.03	0.03	<0.03	0.03	0.05	<0.03	0.04	0.03	<0.03
Cu WT%	<0.03	0.01	<0.03	<0.03	<0.03	<0.03	0.05	0.04	0.02	<0.03
Mn WT%	<0.03	<0.03	<0.03	<0.03	0.01	0.12	0.12	0.08	<0.03	0.03
P WT%	<0.03	<0.03	<0.03	0.02	<0.03	<0.03	0.01	<0.03	<0.03	<0.03
S WT%	51.30	50.90	51.84	51.37	51.38	51.02	50.88	51.94	51.77	51.26
As WT%	<0.03	0.34	<0.03	<0.03	<0.03	0.02	<0.03	<0.03	<0.03	<0.03
Ag WT%	<0.03	0.06	0.01	<0.03	0.08	0.08	0.11	<0.03	<0.03	<0.03
Au WT%	<0.03	<0.03	0.21	0.15	<0.03	0.78	<0.03	0.11	0.10	0.37
TOTAL	96.14	96.26	96.82	96.56	96.08	96.70	95.61	99.49	97.11	96.03

Sample	50-1-2-2	50-1-2-2	50-1-2-2	50-1-2-2	50-1-2-2	50-1-2-2	50-1-2-2	50-1-2-2	50-1-2-2	50-1-2-2
Line no.	442	443	444	445	446	447	448	449	450	451
Mineral	2	2	2	2	2	2	2	2	2	2
Si WT%	-	-	-	-	-	-	-	-	-	-
Fe WT%	0.20	0.24	0.38	0.24	0.15	0.20	0.21	0.25	0.20	0.19
Co WT%	-	-	-	-	-	-	-	-	-	-
Ni WT%	-	-	-	-	-	-	-	-	-	-
Cu WT%	0.00	<0.03	0.09	<0.03	0.01	0.05	0.02	0.01	<0.03	0.01
Mn WT%	<0.03	<0.03	<0.03	<0.03	0.01	0.01	<0.03	<0.03	0.04	<0.03
P WT%	-	-	-	-	-	-	-	-	-	-
S WT%	0.50	0.65	0.65	0.46	0.46	0.55	0.52	0.57	0.53	0.52
As WT%	<0.03	<0.03	0.01	0.01	0.01	0.01	<0.03	<0.03	<0.03	<0.03
Ag WT%	26.11	24.88	27.69	26.55	24.45	26.64	26.63	27.97	27.26	26.10
Au WT%	67.69	57.13	72.38	69.78	62.75	65.63	69.83	73.32	72.48	70.53
TOTAL	94.52	82.79	101.17	97.01	87.82	93.09	97.20	102.10	100.47	97.30

1= Sulfides
2=Electrum

Table A1: Continued

Sample	50-1-2-2	50-1-2-2	50-1-2-2	50-1-2-2	50-1-2-2	50-1-2-2	50-1-2-2	50-1-2-2	50-1-2-2	50-1-2-2
Line no.	422	423	424	426	427	428	429	430	431	432
Mineral	1	1	1	1	1	1	1	1	1	1
Si WT%	0.11	0.11	2.90	0.13	0.10	0.21	0.12	0.47	0.07	0.08
Fe WT%	44.11	44.72	40.17	44.83	45.01	45.06	47.67	46.30	44.85	44.66
Co WT%	<0.03	0.11	<0.03	<0.03	0.02	0.03	0.05	0.02	0.03	<0.03
Ni WT%	<0.03	0.02	0.03	<0.03	<0.03	<0.03	<0.03	<0.03	<0.03	<0.03
Cu WT%	0.05	<0.03	<0.03	0.01	<0.03	0.04	<0.03	0.03	<0.03	<0.03
Mn WT%	0.02	0.03	0.01	0.05	0.01	<0.03	0.01	0.11	<0.03	0.01
P WT%	<0.03	<0.03	0.02	0.09	<0.03	<0.03	<0.03	<0.03	<0.03	<0.03
S WT%	51.10	51.03	46.31	50.31	50.77	50.86	52.09	51.70	51.08	50.58
As WT%	0.20	0.05	<0.03	<0.03	0.01	<0.03	<0.03	<0.03	0.08	0.47
Ag WT%	<0.03	<0.03	<0.03	<0.03	<0.03	0.05	0.02	0.18	<0.03	<0.03
Au WT%	0.01	0.14	0.37	0.27	0.39	<0.03	<0.03	0.50	0.51	0.21
TOTAL	95.56	96.20	89.73	95.64	96.28	96.05	99.78	99.30	96.54	95.95

Sample	50-1-2-2	50-1-2-2	50-1-2-2	50-1-2-2	50-1-2-2	50-1-2-2	50-1-2-2	50-1-2-2	50-1-2-2	50-1-2-2
Line no.	452	453	454	455	456	457	458	459	460	461
Mineral	2	2	2	2	2	2	2	2	2	2
Si WT%	-	-	-	-	-	-	-	-	-	-
Fe WT%	0.17	0.22	0.18	0.19	0.16	0.36	0.12	0.09	0.06	0.16
Co WT%	-	-	-	-	-	-	-	-	-	-
Ni WT%	-	-	-	-	-	-	-	-	-	-
Cu WT%	<0.03	<0.03	<0.03	<0.03	0.02	0.01	0.02	0.02	-0.01	<0.03
Mn WT%	<0.03	<0.03	<0.03	<0.03	<0.03	0.01	<0.03	<0.03	0.00	<0.03
P WT%	-	-	-	-	-	-	-	-	-	-
S WT%	0.45	0.71	0.60	0.55	0.47	0.72	0.43	0.32	0.39	0.40
As WT%	0.02	<0.03	<0.03	<0.03	<0.03	<0.03	<0.03	<0.03	<0.03	<0.03
Ag WT%	25.82	27.47	27.71	27.22	25.87	25.65	27.38	25.60	26.30	27.71
Au WT%	69.89	73.56	75.47	72.51	67.51	61.28	72.30	74.47	68.88	72.81
TOTAL	96.28	101.93	103.91	100.46	93.98	88.02	100.24	100.44	95.62	101.08

1= Sulfides
2=Electrum

Table A2: Major element chemistry acquired from EMPA on pyroxene, plagioclase, magnetite, calcite and quartz (in wt. %).

Sample_mineral	LINE	SiO2 WT%	TiO2 WT%	Al2O3 WT%	Cr2O3 WT%	FeO WT%	MgO WT%	CaO WT%	Na2O WT%	K2O WT%	O WT%	TOTAL	-
1110_plagioclase	52	52.7167	0.052818	29.3119	0.031508	0.79512	0.123999	11.7537	4.46112	0.365125	0.000004	99.612	-
1110_plagioclase	53	51.7858	0.05144	30.0451	<0.03	0.745318	0.099993	12.3422	4.05413	0.284004	0.000004	99.4051	-
1110_plagioclase	54	23.8332	9.75033	9.80229	0.026436	50.7422	0.300768	1.63668	2.64717	1.88601	<0.03	100.625	-
1110_plagioclase	55	97.4574	0.190061	1.5195	0.010937	0.104439	0.007141	0.04415	0.156855	0.058923	0.000004	99.5494	-
1110_plagioclase	56	69.3945	0.198019	17.5949	0.01578	0.490904	0.014015	0.576002	4.00082	7.55773	<0.03	99.8427	-
1110_plagioclase	57	35.2668	0.53765	12.318	0.04018	16.6941	4.74492	4.3572	2.07066	1.74949	<0.03	77.7789	-
1110_plagioclase	58	51.2999	0.546724	5.87186	0.037066	12.7899	11.4621	14.6865	1.04654	0.128543	0.000004	97.869	-
1110_plagioclase	59	53.7484	0.051317	28.5721	<0.03	0.970218	0.056684	10.7002	4.99446	0.408039	<0.03	99.4975	-
1110_plagioclase	60	69.4882	0.653344	17.0751	0.016674	2.06056	0.031631	0.919085	3.77817	6.68582	<0.03	100.709	-
1110_plagioclase	61	52.533	0.063143	29.1889	<0.03	0.789052	0.126924	11.7359	4.35954	0.297971	0.000008	99.0807	-
Sample_mineral	LINE	SiO2 WT%	TiO2 WT%	Al2O3 WT%	Cr2O3 WT%	FeO WT%	MnO WT%	MgO WT%	CaO WT%	Na2O WT%	K2O WT%	O WT%	TOTAL
1110_pyroxene	62	71.5372	0.277349	15.9451	<0.03	0.562061	0.01311	0.011344	0.751565	3.07524	6.47491	<0.03	98.642
1110_pyroxene	63	29.5229	0.693221	10.4838	0.030304	21.8702	0.336268	6.17987	6.25461	0.588138	0.653346	<0.03	76.6126
1110_pyroxene	64	52.1587	0.447472	11.4921	0.018147	10.1111	0.268788	7.94763	13.5584	2.18047	0.236099	<0.03	98.4189
1110_pyroxene	65	50.1698	<0.03	1.01087	0.008845	23.2613	0.015851	4.20737	1.20255	0.073694	0.725553	0.000004	80.6491
1110_pyroxene	66	69.2611	0.619259	17.2009	<0.03	1.70273	0.04747	0.051358	1.21934	2.94582	5.63567	0.000008	98.6672
1110_pyroxene	67	52.577	0.061774	28.3356	0.001974	0.798697	0.016343	0.117571	12.0963	4.36685	0.330363	<0.03	98.7024
Sample_mineral	LINE	TiO2 WT%	Al2O3 WT%	Cr2O3 WT%	Fe2O3 WT%	NiO WT%	MnO WT%	MgO WT%	O WT%	TOTAL	-	-	-
1110_magnetite	70	21.5512	3.81882	0.073723	74.5827	0.025595	1.89509	0.050067	0.000004	101.997	-	-	-
1110_magnetite	71	24.1382	1.45464	0.054131	76.6932	<0.03	0.652798	0.188911	<0.03	103.181	-	-	-
1110_magnetite	72	22.5751	1.6319	0.055128	78.8141	<0.03	0.314513	0.299998	<0.03	103.662	-	-	-
1110_magnetite	73	27.7854	1.55343	0.016161	71.4739	0.024007	0.392675	0.29355	<0.03	101.539	-	-	-
1110_magnetite	74	21.8438	1.39106	0.061462	77.723	<0.03	2.05037	0.093395	<0.03	103.155	-	-	-
Sample_mineral	LINE	SiO2 WT%	TiO2 WT%	Al2O3 WT%	Cr2O3 WT%	FeO WT%	MgO WT%	CaO WT%	Na2O WT%	K2O WT%	O WT%	TOTAL	-
47_3_4_plagioclase	75	53.746	0.09016	20.3505	<0.03	6.43363	2.95911	2.17509	0.70937	7.45008	0.000004	93.909	-
47_3_4_plagioclase	76	52.7441	0.06026	28.8863	<0.03	0.675703	0.097748	11.2032	4.47672	0.382503	<0.03	98.5198	-
47_3_4_plagioclase	77	52.1776	0.086702	29.6424	0.000986	0.821199	0.117704	12.0228	4.1743	0.312171	<0.03	99.3558	-
47_3_4_plagioclase	78	50.9491	0.119109	32.2827	0.011846	0.912888	0.148287	10.5244	4.20938	0.367906	<0.03	99.5256	-
47_3_4_plagioclase	79	49.4683	0.058569	31.3113	0.015719	0.431227	0.199083	13.6649	3.2891	0.162119	0.000004	98.6004	-
47_3_4_plagioclase	80	96.7903	<0.03	0.81478	0.028681	0.093189	<0.03	0.061352	0.027428	0.02434	0.000011	97.8311	-

Table A2: Continued

Sample_mineral	LINE	SiO2 WT%	TiO2 WT%	Al2O3 WT%	Cr2O3 WT%	FeO WT%	MnO WT%	MgO WT%	CaO WT%	Na2O WT%	K2O WT%	O WT%	TOTAL
47_3_4_pyroxene	81	51.4124	0.785805	2.02792	0.191513	11.0246	0.27521	15.3978	17.8571	0.2448	0.001025	<0.03	99.2182
47_3_4_pyroxene	82	50.8731	0.873207	1.99251	0.147139	10.771	0.27166	14.9708	18.7144	0.238347	<0.03	0.000004	98.8519
47_3_4_pyroxene	83	50.7235	0.480018	2.24667	0.035576	14.7028	0.387394	15.5877	13.3944	0.185177	0.015349	<0.03	97.7585
Sample_mineral	LINE	SiO2 WT%	TiO2 WT%	Al2O3 WT%	Cr2O3 WT%	FeO WT%	MgO WT%	CaO WT%	Na2O WT%	K2O WT%	O WT%	TOTAL	-
50_1_1_plagioclase	87	52.0671	0.076187	29.7664	<0.03	0.813038	0.133513	12.2569	4.04667	0.294632	<0.03	99.4478	-
50_1_1_plagioclase	88	53.4585	0.098186	29.0123	0.014761	0.511017	0.131198	11.3024	4.55702	0.36156	<0.03	99.4468	-
50_1_1_plagioclase	89	52.8233	0.084756	28.9287	<0.03	0.772307	0.125851	11.4054	4.40901	0.323665	0.000004	98.821	-
Sample_mineral	LINE	FeO WT%	CoO WT%	MnO WT%	MgO WT%	CaO WT%	SrO WT%	SO3 WT%	As2O3 WT%	CO2 WT%	O WT%	TOTAL	-
50_1_1_calcite	90	0.269821	0.043007	0.644387	0.081255	56.017	0.008661	0.010597	0.005648	43.1004	<0.03	100.181	-
50_1_1_calcite	91	0.402654	<0.03	0.675195	0.162312	53.8857	0.02654	<0.03	<0.03	43.5335	<0.03	98.6712	-
50_1_1_calcite	92	0.101987	0.011718	0.418401	0.057312	55.9294	0.026381	<0.03	<0.03	43.2442	<0.03	99.7495	-
50_1_1_calcite	93	0.07519	0.059771	0.692263	0.046042	55.0807	<0.03	0.011539	0.012014	43.3565	0.000004	99.33	-
50_1_1_calcite	94	0.497369	<0.03	0.902277	0.251138	53.9995	0.039203	0.044527	<0.03	43.4294	0.000004	99.0803	-
50_1_1_calcite	95	0.163202	<0.03	0.413481	0.049071	54.7042	0.054509	<0.03	0.014696	43.5093	<0.03	98.8353	-
50_1_1_calcite	96	0.053847	0.034236	0.520203	0.041509	54.6187	<0.03	<0.03	<0.03	43.5325	<0.03	98.7815	-
50_1_1_calcite	97	0.065582	<0.03	0.472842	0.066524	52.9794	<0.03	0.008089	<0.03	43.9612	0.000004	97.4741	-
50_1_1_calcite	98	0.138532	0.003216	0.862325	0.095692	53.8965	<0.03	<0.03	<0.03	43.5723	<0.03	98.5457	-
50_1_1_calcite	99	0.128299	0.003077	0.470975	0.108629	54.8548	0.017083	<0.03	0.009254	43.459	<0.03	99.0361	-
50_1_1_calcite	100	0.046935	<0.03	0.462863	0.049179	55.5871	<0.03	0.010673	<0.03	43.347	0.000004	99.475	-
50_1_1_calcite	101	0.080538	0.027593	0.43542	0.049007	54.3745	<0.03	<0.03	<0.03	43.6182	<0.03	98.5138	-
50_1_1_calcite	102	0.080913	0.02418	0.658876	0.075096	55.3507	0.000928	<0.03	<0.03	43.3122	<0.03	99.4884	-
50_1_1_calcite	103	0.16757	<0.03	0.658597	0.067257	55.0267	<0.03	<0.03	<0.03	43.3649	<0.03	99.2194	-
50_1_1_calcite	104	0.082587	0.10649	0.667307	0.050627	54.7465	0.022609	0.000812	<0.03	43.4221	0.000004	99.0718	-
50_1_1_calcite	105	0.193017	<0.03	0.775607	0.077912	55.3243	0.01641	0.036769	<0.03	43.2958	<0.03	99.5887	-
Sample_mineral	LINE	SiO2 WT%	TiO2 WT%	Al2O3 WT%	Cr2O3 WT%	FeO WT%	MnO WT%	MgO WT%	CaO WT%	Na2O WT%	K2O WT%	O WT%	TOTAL
50_1_1_quartz	106	90.6629	0.009448	5.82625	0.018208	0.201493	0.031755	0.257605	0.168466	0.043523	0.812014	0.000004	98.0317
50_1_1_quartz	107	91.166	0.00722	3.28804	<0.03	0.957788	0.000008	0.353746	0.121674	0.038232	0.096577	0.000008	96.0293
50_1_1_quartz	108	98.9185	<0.03	0.219663	0.000977	0.000684	0.013781	0.000067	0.012961	0.007304	<0.03	<0.03	99.1556
50_1_1_quartz	109	97.1261	0.013031	1.00222	0.000977	0.04679	0.009711	0.031732	0.066308	0.035628	0.0387	0.000008	98.3712
50_1_1_quartz	110	98.5713	<0.03	0.491564	<0.03	<0.03	<0.03	<0.03	0.070146	0.03292	0.021668	<0.03	99.1513
50_1_1_quartz	111	97.1985	0.015954	0.727645	<0.03	0.011299	0.005664	0.005158	0.080161	0.029304	0.036603	<0.03	98.0956
50_1_1_quartz	112	98.4664	<0.03	0.728266	0.009765	<0.03	0.008886	0.003601	0.006857	0.018433	0.022155	<0.03	99.2279
50_1_1_quartz	113	98.6879	0.021696	0.554777	<0.03	0.00462	<0.03	0.00162	0.081462	0.032193	0.035111	<0.03	99.3914
50_1_1_quartz	114	99.2868	<0.03	0.440365	<0.03	0.003433	<0.03	0.00075	0.019843	<0.03	<0.03	<0.03	99.6827
50_1_1_quartz	115	98.6518	0.026064	0.482822	<0.03	<0.03	0.014596	<0.03	0.003049	0.001538	0.021823	0.000004	99.181
50_1_1_quartz	116	97.9405	0.001447	0.610324	<0.03	0.029986	0.009719	<0.03	0.018288	0.014057	0.011266	<0.03	98.6157
50_1_1_quartz	117	98.1827	0.015923	0.587192	<0.03	0.016761	<0.03	<0.03	<0.03	<0.03	0.007145	<0.03	98.7735

Table A2: Continued

Sample_mineral	LINE	SiO2 WT%	TiO2 WT%	Al2O3 WT%	Cr2O3 WT%	FeO WT%	MnO WT%	MgO WT%	CaO WT%	Na2O WT%	K2O WT%	O WT%	TOTAL
50_1_2_2_quartz	118	99.4567	<0.03	0.426278	0.004892	0.016287	0.001612	<0.03	0.000001	0.000709	<0.03	<0.03	99.8896
50_1_2_2_quartz	119	98.1834	<0.03	0.548965	<0.03	0.022547	<0.03	<0.03	0.01754	0.022452	0.011726	0.000004	98.7592
50_1_2_2_quartz	120	91.3964	<0.03	4.61293	0.007808	0.018315	0.029155	0.021442	0.061108	0.065795	3.13047	0.000015	99.3391
50_1_2_2_quartz	121	97.8088	<0.03	0.596567	<0.03	<0.03	<0.03	0.000458	0.01983	0.012992	0.00172	0.000008	98.3901
50_1_2_2_quartz	122	98.1965	<0.03	0.467579	<0.03	<0.03	<0.03	<0.03	0.04189	<0.03	<0.03	<0.03	98.6643
50_1_2_2_quartz	123	99.8726	<0.03	0.753805	<0.03	0.003877	0.016208	<0.03	0.03733	0.00083	0.006828	0.000008	100.647
50_1_2_2_quartz	124	95.2067	0.014469	2.13298	0.005858	0.085739	<0.03	0.019013	0.134801	0.01341	0.033356	<0.03	97.6309
50_1_2_2_quartz	125	96.2667	0.017313	1.38834	0.008763	0.023244	0.014566	0.011411	0.07291	0.014386	0.020642	<0.03	97.8382
50_1_2_2_quartz	126	96.9885	<0.03	1.3698	0.000976	0.026819	<0.03	0.00737	0.072319	0.031407	0.014183	0.000004	98.4867
50_1_2_2_quartz	127	97.4198	<0.03	0.482316	0.024466	0.002737	<0.03	0.00524	0.019847	0.007579	<0.03	<0.03	97.923
50_1_2_2_quartz	128	97.9955	<0.03	0.487996	0.012703	0.013277	0.018645	<0.03	0.057934	0.024034	0.034808	0.000008	98.6072
50_1_2_2_quartz	129	97.3814	0.011576	0.83685	0.005859	0.009788	0.011368	0.011353	0.081501	0.03928	0.035139	<0.03	98.4241
50_1_2_2_quartz	130	98.197	0.010168	0.614924	<0.03	0.020743	0.013026	<0.03	0.096338	0.041105	0.026212	<0.03	99.0042
Sample_mineral	LINE	FeO WT%	CoO WT%	MnO WT%	MgO WT%	CaO WT%	SrO WT%	SO3 WT%	As2O3 WT%	CO2 WT%	O WT%	TOTAL	-
50_1_2_2_Calcite	131	0.445832	<0.03	0.54864	0.369556	55.1698	0.03115	0.019462	0.019301	43.2541	<0.03	99.8171	-
50_1_2_2_Calcite	132	0.32785	<0.03	1.04395	0.146071	54.2606	0.00932	<0.03	<0.03	43.3641	0.000004	99.1186	-
50_1_2_2_Calcite	133	0.105598	<0.03	0.597482	0.086039	54.282	0.015883	0.043379	0.008628	43.5815	<0.03	98.6906	-
50_1_2_2_Calcite	134	0.156213	<0.03	0.704593	0.160363	53.7426	0.002319	<0.03	0.03269	43.6543	<0.03	98.381	-
50_1_2_2_Calcite	135	0.201201	0.019384	0.602802	0.183754	53.7772	<0.03	0.039407	0.0062	43.654	<0.03	98.4706	-
50_1_2_2_Calcite	136	0.525777	0.030898	0.883161	0.182117	53.2843	0.006066	<0.03	<0.03	43.57	0.000004	98.4667	-
50_1_2_2_Calcite	137	0.408072	0.083562	0.660052	0.129415	53.5625	0.016069	0.0069	0.011143	43.5904	<0.03	98.4681	-
50_1_2_2_Calcite	138	0.215335	0.025651	1.05649	0.2871	53.3322	<0.03	0.040515	0.011638	43.6033	<0.03	98.5544	-
50_1_2_2_Calcite	139	0.132817	<0.03	0.55256	0.08011	53.6954	0.021627	0.003631	<0.03	43.732	<0.03	98.1472	-
50_1_2_2_Calcite	140	0.18931	0.010796	0.79653	0.227411	54.4783	0.008565	0.01475	<0.03	43.4286	<0.03	99.1424	-
50_1_2_2_Calcite	141	0.51148	<0.03	1.29295	0.249891	52.1845	0.01933	0.02594	<0.03	43.7225	<0.03	97.9573	-
50_1_2_2_Calcite	142	0.331602	0.125731	0.640934	0.109155	53.9313	0.030764	<0.03	<0.03	43.5188	0.000004	98.6158	-
50_1_2_2_Calcite	143	0.107478	<0.03	0.521972	0.064641	54.5232	0.012843	0.018678	<0.03	43.5501	<0.03	98.766	-
Sample_mineral	LINE	SiO2 WT%	TiO2 WT%	Al2O3 WT%	Cr2O3 WT%	FeO WT%	MgO WT%	CaO WT%	Na2O WT%	K2O WT%	O WT%	TOTAL	-
50_1_2_2_plagioclas	144	51.721	0.089301	29.5756	<0.03	0.809561	0.112986	12.1098	4.09164	0.283728	0.000004	98.7886	-
50_1_2_2_plagioclas	145	51.8433	0.032209	29.885	<0.03	0.668375	0.137885	12.2116	4.03736	0.287287	0.000004	99.0972	-
50_1_2_2_plagioclas	146	50.7319	0.030758	30.3536	0.011792	0.619276	0.231323	13.02	3.59483	0.153441	0.000008	98.7469	-
50_1_2_2_plagioclas	147	50.9016	0.064535	30.5901	<0.03	0.436336	0.19579	13.203	3.64906	0.18153	<0.03	99.2081	-

Table A3: LA-ICP-MS data on electrum grains (ppm)

Element:	S	Ti	Ti	MnO	Fe	Co	Ni	Ni	Cu
Isotopic mass:	33	47	49	55	57	59	61	62	63
Fe15a05	-	*<4.26*	*<3.76*	*BDL*	-	*<0.22*	-	-	-
Fe15a06	-	**13**	**13**	**0.0004**	-	*0.17*	-	-	-
Fe15a07	-	*<2.51*	*<3.11*	*BDL*	-	*<0.37*	-	-	-
Fe15a08	-	*<4.17*	*<4.25*	*BDL*	-	*<0.51*	-	-	-
Fe15a09	-	*<3.73*	**2.1**	*BDL*	-	*<0.24*	-	-	-
Fe15a10	-	*<5.58*	*<4.70*	**0.0278**	-	*<0.35*	-	-	-
Fe15a11	-	*<4.47*	*<4.03*	*BDL*	-	*<0.17*	-	-	-
Fe15a12	-	*<4.83*	*<7.71*	*BDL*	-	*<0.21*	-	-	-
Fe15d05	-	*<7.47*	*<5.33*	*BDL*	-	*<0.35*	-	-	-
Fe15d06	-	*<9.46*	*<4.86*	*BDL*	-	*<0.83*	-	-	-
Fe15d07	-	*<5.56*	*<5.25*	*BDL*	-	*<0.38*	-	-	-
Fe15d08	-	*<8.57*	*<7.80*	*BDL*	-	*<0.39*	-	-	-
Fe15d09	-	*<6.25*	*<4.38*	*BDL*	-	*<0.22*	-	-	-
Fe15d10	-	*<5.87*	*<2.46*	*BDL*	-	*<0.51*	-	-	-
Fe15d11	-	*<6.93*	*<6.27*	*BDL*	-	*<0.20*	-	-	-
Fe15d12	-	*<3.89*	*<3.74*	*BDL*	-	*<0.30*	-	-	-
Fe15d13	-	*<5.06*	*<6.08*	*BDL*	-	*<0.33*	-	-	-
Fe15d14	-	*<6.05*	*<7.51*	*BDL*	-	*<0.63*	-	-	-
Fe15d15	-	*<6.06*	*<4.73*	*BDL*	-	*<0.14*	-	-	-
Fe15d16	-	*<5.44*	*<7.64*	*BDL*	-	*<0.19*	-	-	-

Table A3: Continued

Element:	Cu	Ga	As	Mo	Mo	Ru	Ru	Rh	Pd
Isotopic mass:	65	69	75	95	97	99	101	103	105
Fe15a05	-	*<0.47*	*<127.10*	*<0.62*	**0.30**	*<0.40*	**0.14**	**0.022**	**0.65**
Fe15a06	-	**15**	*<63.98*	**8.7**	**8.3**	*<0.17*	**0.14**	**0.026**	**0.71**
Fe15a07	-	*<0.38*	*<109.32*	**3.3**	**3.7**	*<0.31*	*<0.14*	*<0.03*	**0.54**
Fe15a08	-	*<0.25*	*<150.39*	**1.7**	**1.9**	**0.14**	*<0.17*	*<0.07*	**0.74**
Fe15a09	-	*<0.29*	*<119.04*	*<0.34*	**0.65**	**0.17**	**0.11**	**0.037**	**0.58**
Fe15a10	-	*<0.27*	*<139.15*	**8.8**	**9.0**	*<0.45*	*<0.30*	*<0.04*	**0.75**
Fe15a11	-	*<0.31*	*<7.14*	**0.21**	*<0.68*	*<0.24*	*<0.18*	*<0.03*	**0.74**
Fe15a12	-	*<0.42*	*<6.85*	*<0.54*	**0.24**	*<0.43*	**0.087**	**0.042**	**0.89**
Fe15d05	-	*<0.45*	*<4.84*	**0.13**	**0.071**	**0.14**	**0.094**	*<0.03*	**0.74**
Fe15d06	-	*<0.62*	*<4.02*	**0.071**	*<0.74*	*<0.63*	**0.079**	*<0.11*	**0.67**
Fe15d07	-	*<0.41*	*<5.17*	**0.14**	**0.15**	*<0.52*	**0.098**	**0.035**	**0.62**
Fe15d08	-	*<0.45*	*<4.70*	**0.45**	**0.20**	*<0.36*	**0.083**	**0.028**	**0.52**
Fe15d09	-	*<0.50*	*<4.29*	*<0.44*	**0.33**	*<0.28*	**0.14**	**0.021**	**0.76**
Fe15d10	-	*<0.33*	*<5.81*	**0.12**	**0.14**	*<0.43*	*<0.19*	*<0.04*	**0.71**
Fe15d11	-	*<0.26*	*<4.35*	**0.11**	**0.25**	*<0.33*	**0.064**	**0.039**	**0.62**
Fe15d12	-	*<0.69*	*<5.36*	**0.080**	**0.16**	*<0.36*	*<0.42*	*<0.04*	**0.71**
Fe15d13	-	*<0.47*	*<3.50*	**0.12**	*<1.11*	**0.29**	*<0.19*	*<0.05*	**0.83**
Fe15d14	-	*<0.32*	*<5.06*	*<0.46*	*<0.75*	*<0.87*	*<0.21*	*<0.09*	**0.74**
Fe15d15	-	*<0.43*	*<3.08*	*<0.51*	*<0.60*	*<0.23*	*<0.17*	**0.032**	*<0.85*
Fe15d16	-	*<0.50*	*<3.60*	*<1.16*	*<1.18*	*<0.61*	*<0.24*	**0.034**	**0.42**

Table A3: Continued

Element:	Ag	Cd	Sn	Sn	W	Re	Os	Ir	Pt
Isotopic mass:	107	111	117	118	182	185	189	193	195
Fe15a05	*<0.12*	14	9.2	2.7	0.43	0.19	0.37	0.37	4.9
Fe15a06	*<0.38*	14	8.9	2.3	0.38	0.19	0.40	0.41	4.9
Fe15a07	*<2.90*	15	7.8	2.3	0.38	0.17	0.46	0.38	4.9
Fe15a08	*<2.58*	14	9.4	2.5	0.36	0.15	0.36	0.33	4.7
Fe15a09	*<3.33*	15	9.1	3.2	0.42	0.21	0.39	0.44	4.8
Fe15a10	*<3.44*	13	9.2	3.2	0.34	0.15	0.28	0.33	4.6
Fe15a11	*<2.49*	15	8.4	2.6	0.39	0.18	0.41	0.38	5.1
Fe15a12	*<4.13*	13	8.1	2.5	0.34	0.13	0.41	0.41	4.7
Fe15d05	*<0.78*	13	7.0	2.4	0.28	0.15	*<0.27*	0.27	5.0
Fe15d06	*<1.93*	11	7.8	2.0	0.31	0.15	0.35	0.33	4.7
Fe15d07	593274	12	7.2	2.5	0.36	0.099	0.33	0.30	4.4
Fe15d08	612386	11	6.7	2.0	0.29	0.099	0.36	0.31	5.1
Fe15d09	645249	12	7.9	2.7	0.37	0.17	0.38	0.28	4.9
Fe15d10	658629	13	6.8	2.1	0.33	0.17	0.41	0.33	5.0
Fe15d11	637459	11	7.3	1.8	0.37	0.16	0.38	0.31	4.9
Fe15d12	653569	11	7.8	2.4	0.32	0.11	0.39	0.33	5.1
Fe15d13	671076	12	7.5	1.8	0.34	0.14	0.36	0.38	4.8
Fe15d14	758889	14	7.2	2.4	0.38	0.18	0.41	0.36	5.1
Fe15d15	668826	13	7.4	1.8	0.32	0.12	0.27	0.35	5.0
Fe15d16	542423	10	6.2	1.6	0.30	0.11	0.36	0.25	4.2

Table A3: Continued

Element:	Au	Pb	Pb	Pb	Pb
Isotopic mass:	EMPA	204	206	207	208
Fe15a05	733215.8	**73**	*<0.45*	*<0.56*	*<0.16*
Fe15a06	698379.1	**111**	*<0.36*	**0.26**	**0.13**
Fe15a07	656363.4	**72**	**0.32**	**0.24**	*<0.24*
Fe15a08	697876.2	**65**	*<0.36*	*<0.46*	*<0.40*
Fe15a09	627540.1	**61**	*<0.31*	*<0.17*	*<0.19*
Fe15a10	680229.1	**69**	*<0.32*	**0.27**	*<0.34*
Fe15a11	713250.1	**73**	*<0.38*	*<0.21*	*<0.26*
Fe15a12	723909.6	**46**	**0.23**	**0.26**	*<0.23*
Fe15d05	676937.4	**62**	*<0.24*	*<0.45*	*<0.24*
Fe15d06	571339.8	**55**	*<0.67*	*<0.22*	*<0.28*
Fe15d07	668516	**68**	*<0.17*	*<0.40*	*<0.22*
Fe15d08	689961.5	**69**	*<0.30*	**0.18**	*<0.22*
Fe15d09	688812.9	**61**	*<0.66*	**0.22**	*<0.23*
Fe15d10	675100.5	**53**	*<0.63*	*<0.47*	*<0.31*
Fe15d11	725132.1	**50**	*<0.17*	*<0.37*	*<0.21*
Fe15d12	754785.5	**58**	*<0.61*	*<0.28*	**0.14**
Fe15d13	735627.5	**55**	**0.22**	*<0.50*	*<0.24*
Fe15d14	723002.3	**61**	*<0.34*	*<0.67*	*<0.29*
Fe15d15	728186.1	**75**	*<0.33*	**0.23**	*<0.18*
Fe15d16	744768.5	**42**	*<0.45*	**0.21**	*<0.21*

Table A4: LA-ICP-MS resutls for sulfide grains (ppm)

Filter = <3 X LLD	*Pulse	S	Ti	Ti	MnO	Fe	Co	Ni
Isotopic mass		33	47	49	55	57	59	61
Fe14a05	1_2	-	-	-	0.004	-	3.027	-
Fe14a06	1_2	-	-	-	0.006	-	304.130	-
Fe14a07	1_2	-	-	-	0.006	-	26.793	-
Fe14a08	1_2	-	-	-	0.016	-	87.679	-
Fe14a09	1_2	-	-	-	0.002	-	39.752	-
Fe14a10	1_2	-	-	-	0.012	-	38.589	-
Fe14a11	2_1	-	-	-	0.019	-	41.698	-
Fe14a12	2_1	-	-	-	0.036	-	4.148	-
Fe14a13	2_1	-	-	-	0.016	-	30.804	-
Fe14a14	2_1	-	-	-	0.000	-	17.943	-
Fe14a15	2_1	-	-	-	0.000	-	0.417	-
Fe14b05	1_2	-	-	-	0.000	-	36.669	-
Fe14b06	1_2	-	-	-	0.001	-	143.973	-
Fe14b07	1_2	-	-	-	0.006	-	36.244	-
Fe14b08	1_2	-	-	-	0.001	-	12.339	-
Fe14b09	2_1	-	-	-	0.006	-	0.465	-
Fe14b10	2_1	-	-	-	0.000	-	15.932	-
Fe14b11	2_1	-	-	-	0.003	-	8.913	-
Fe14b12	2_1	-	-	-	0.048	-	5.863	-
Fe14b13	2_1	-	-	-	*<0.01*	-	2.038	-
Fe14b14	2_1	-	-	-	0.006	-	7.844	-
Fe14b15	2_1	-	-	-	0.002	-	11.698	-
Fe14b16	1_2	-	-	-	0.000	-	24.024	-
Fe14b17	1_2	-	-	-	0.001	-	32.973	-
Fe14c05	1_2	-	-	-	0.001	-	19.476	-
Fe14c06	1_2	-	-	-	0.008	-	79.691	-
Fe14c07	1_2	-	-	-	0.003	-	64.459	-
Fe14c08	1_2	-	-	-	0.002	-	13.059	-
Fe14c09	1_2	-	-	-	0.002	-	21.362	-
Fe14c10	1_2	-	-	-	0.002	-	18.675	-
Fe14c11	1_2	-	-	-	0.002	-	59.218	-
Fe14c12	1_2	-	-	-	0.033	-	22.025	-
Fe14c13	1_2	-	-	-	0.009	-	117.832	-
Fe14d05	2_3_1	-	-	-	0.051	-	0.341	-
Fe14d06	2_3_1	-	-	-	0.020	-	0.700	-
Fe14d07	2_3_1	-	-	-	0.015	-	0.651	-
Fe14d08	2_3_1	-	-	-	0.015	-	0.500	-
Fe14d09	2_3_1	-	-	-	0.017	-	1.267	-
Fe14d10	3_2_1_e	-	-	-	0.000	-	0.358	-
Fe14d11	1_3_2	-	-	-	0.026	-	49.266	-
Fe14d12	1_3_2	-	-	-	0.028	-	66.418	-
Fe15b05	1_3_2_e	-	1931	1883	0.010	-	298.782	-
Fe15b06	1_3_2_e	-	1301	1338	0.016	-	27.833	-
Fe15b07	1_3_2_e	-	3111	3083	0.005	-	93.969	-

Table A4: Continued

Filter = <3 X LLD	Ni	Cu	Cu	Ga	As	Mo	Mo
Isotopic mass	62	63	65	69	75	95	97
Fe14a05	-	-	-	4.304	*<4.84*	15.121	15.063
Fe14a06	-	-	-	6.541	*<16.41*	17.109	17.239
Fe14a07	-	-	-	3.629	*<40.43*	4.870	5.703
Fe14a08	-	-	-	1.384	426300.1	13.339	15.110
Fe14a09	-	-	-	1.250	16537.6	0.746	0.629
Fe14a10	-	-	-	9.518	594423.3	18.836	16.914
Fe14a11	-	-	-	0.340	433.7	1.116	1.207
Fe14a12	-	-	-	3.083	568.4	0.725	1.032
Fe14a13	-	-	-	8.363	10616.1	1.979	2.686
Fe14a14	-	-	-	*<0.20*	18196.3	1.216	1.329
Fe14a15	-	-	-	2.639	4326.5	0.541	0.684
Fe14b05	-	-	-	*<0.23*	20523.0	1.636	1.257
Fe14b06	-	-	-	*0.224*	7645.1	0.730	0.918
Fe14b07	-	-	-	0.612	10881.1	2.268	2.563
Fe14b08	-	-	-	0.623	18748.0	2.123	2.359
Fe14b09	-	-	-	0.520	13884.2	0.555	0.680
Fe14b10	-	-	-	*<0.09*	6243.4	0.408	1.075
Fe14b11	-	-	-	6.307	3985.5	3.316	4.295
Fe14b12	-	-	-	1.530	3068.4	2.183	2.095
Fe14b13	-	-	-	*<0.26*	217.0	0.674	0.608
Fe14b14	-	-	-	0.928	3724.3	2.071	1.613
Fe14b15	-	-	-	5.318	3320.7	1.712	2.212
Fe14b16	-	-	-	*<0.16*	25044.1	0.219	0.629
Fe14b17	-	-	-	0.177	25443.9	0.057	0.274
Fe14c05	-	-	-	0.508	11399.9	0.096	0.248
Fe14c06	-	-	-	2.035	11122.2	3.355	3.431
Fe14c07	-	-	-	4.952	12924.2	2.675	3.501
Fe14c08	-	-	-	0.736	21377.9	0.917	0.986
Fe14c09	-	-	-	1.309	24467.4	0.232	0.414
Fe14c10	-	-	-	0.716	25994.3	4.305	4.164
Fe14c11	-	-	-	1.438	8751.7	4.439	4.743
Fe14c12	-	-	-	42.558	11950.2	<0.29	0.412
Fe14c13	-	-	-	16.562	16091.4	4.936	5.561
Fe14d05	-	-	-	0.583	248.7	0.665	0.971
Fe14d06	-	-	-	1.784	45.8	0.038	*<0.50*
Fe14d07	-	-	-	1.041	66.1	0.073	0.193
Fe14d08	-	-	-	1.293	184.4	0.091	0.304
Fe14d09	-	-	-	0.611	194.2	0.031	0.282
Fe14d10	-	-	-	0.186	9838.0	*<0.07*	0.352
Fe14d11	-	-	-	14.727	8190.2	10.463	11.051
Fe14d12	-	-	-	10.341	6648.7	9.015	9.467
Fe15b05	-	-	-	1.937	16212.4	4.191	4.294
Fe15b06	-	-	-	2.943	9912.3	2.774	3.060
Fe15b07	-	-	-	0.375	10821.6	4.257	3.926

Table A4: Continued

Filter = <3 X LLD	Ru	Ru	Rh	Pd	Ag	Sn	Sn	W
Isotopic mass	99	101	103	105	107	117	118	182
Fe14a05	0.537	0.401	0.057	*<0.29*	8.683	1.933	2.428	1.126
Fe14a06	0.674	0.343	0.069	0.266	9.785	2.299	1.767	2.696
Fe14a07	0.673	*<1.71*	0.053	*<0.42*	5.464	2.661	1.732	0.878
Fe14a08	0.508	0.294	0.041	0.301	34.642	2.219	1.725	2.116
Fe14a09	0.042	*<0.24*	0.028	*<0.09*	11.327	*<1.50*	*<1.14*	0.438
Fe14a10	0.654	0.229	0.091	*<0.35*	20.346	1.307	1.184	0.600
Fe14a11	*<0.06*	0.015	*<0.02*	*<0.05*	122.766	*<0.38*	0.394	0.011
Fe14a12	*<0.17*	0.012	0.011	*<0.07*	189.114	1.837	1.367	*<0.11*
Fe14a13	*<0.14*	0.008	0.006	*<0.13*	12.355	3.027	3.052	1.968
Fe14a14	0.043	0.016	BDL	*<0.06*	14.070	*<0.82*	*<0.61*	0.012
Fe14a15	0.031	0.009	0.013	*<0.06*	21.145	*<0.32*	*<0.19*	0.028
Fe14b05	*<0.08*	0.018	0.053	*<0.10*	9.537	*<0.19*	*<0.18*	0.025
Fe14b06	*<0.07*	0.024	0.010	*<0.21*	18.939	*<0.56*	0.188	0.219
Fe14b07	*<0.19*	0.009	*<0.40*	0.074	21.026	*<0.59*	*<0.27*	0.410
Fe14b08	0.073	0.026	*<0.01*	*<0.07*	21.542	0.539	0.726	0.407
Fe14b09	*<0.09*	0.004	0.009	0.023	14.197	*<0.38*	*<0.15*	0.027
Fe14b10	*<0.07*	0.020	0.017	0.009	7.491	*<0.34*	*<0.29*	0.002
Fe14b11	*<0.16*	0.013	*<0.01*	0.031	9.726	0.513	*<0.37*	0.301
Fe14b12	0.054	0.015	*<0.02*	*<0.06*	11.807	0.316	*<0.30*	0.104
Fe14b13	*<0.12*	BDL	0.004	*<0.07*	4.417	*<0.68*	*<0.46*	0.003
Fe14b14	*<0.13*	0.015	0.006	*<0.10*	44.727	0.691	0.676	0.507
Fe14b15	*<0.10*	BDL	*<0.01*	*<0.08*	5.708	*<0.78*	0.420	0.068
Fe14b16	0.065	*<0.07*	0.069	0.099	46.906	*<0.46*	*<0.40*	BDL
Fe14b17	0.108	0.022	0.053	0.099	39.205	0.264	*<0.37*	0.086
Fe14c05	*<0.08*	0.017	*<0.01*	*<0.07*	11.109	0.866	0.680	0.340
Fe14c06	*<0.08*	*<0.09*	0.009	0.071	66.951	1.497	1.421	0.531
Fe14c07	*<0.12*	0.021	*<0.02*	0.116	71.802	1.504	1.501	0.805
Fe14c08	0.086	0.026	0.055	0.166	94.653	0.525	0.658	0.291
Fe14c09	*<0.06*	0.051	0.084	0.135	54.438	*<0.97*	0.867	0.252
Fe14c10	0.103	0.035	0.018	0.091	64.464	0.548	0.347	0.355
Fe14c11	*<0.18*	0.006	0.005	0.086	39.631	*<0.25*	0.239	0.286
Fe14c12	*<0.09*	0.028	0.004	0.138	16.684	3.385	2.632	2.160
Fe14c13	*<0.13*	0.026	0.014	0.175	50.561	0.417	0.418	1.463
Fe14d05	0.019	*<0.10*	0.006	*<0.10*	18.375	*<0.61*	0.321	3.902
Fe14d06	*<0.12*	0.021	*<0.01*	*<0.08*	*<0.03*	*<0.34*	*<0.23*	53.962
Fe14d07	0.037	0.008	*<0.02*	*<0.06*	*<0.04*	*<0.37*	0.295	45.362
Fe14d08	*<0.07*	*<0.03*	*<0.01*	*<0.05*	0.106	*<0.23*	0.181	41.932
Fe14d09	0.014	0.010	*<0.01*	*<0.06*	1.463	*<0.56*	*<0.16*	47.485
Fe14d10	*<0.11*	0.019	0.184	0.392	57.698	0.632	0.624	0.003
Fe14d11	*<0.15*	BDL	*<0.02*	0.350	361.534	6.752	6.433	20.668
Fe14d12	*<0.37*	0.007	0.009	*<0.18*	310.281	2.813	2.724	8.461
Fe15b05	0.072	0.021	0.013	0.042	276.169	0.483	0.465	1.989
Fe15b06	*<0.04*	0.017	*<0.01*	*<0.06*	46.302	*<0.30*	0.277	1.374
Fe15b07	*<0.15*	0.025	0.006	*<0.04*	25.251	*<0.31*	*<0.13*	0.320

Table A4: Continued

Filter = <3 X LLD	Re	Os	Ir	Pt	Au	Pb	Pb	Pb
Isotopic mass	185	189	193	195	197	204	206	207
Fe14a05	*<0.04*	0.061	0.006	*<0.16*	56.449	107.176	23.060	19.437
Fe14a06	*<0.05*	0.017	*<0.03*	*<0.09*	198.429	95.798	33.082	25.811
Fe14a07	0.020	*<0.14*	0.010	*<0.09*	129.023	83.273	21.278	19.779
Fe14a08	0.015	0.021	BDL	*<0.28*	157.379	152.761	67.670	58.939
Fe14a09	0.007	BDL	BDL	*<0.06*	20.917	70.586	74.750	61.344
Fe14a10	0.029	0.032	0.008	*<0.12*	171.156	86.104	29.301	26.808
Fe14a11	0.002	BDL	*<0.02*	*<0.02*	2.921	53.645	52.045	45.597
Fe14a12	*<0.03*	BDL	BDL	0.015	4.180	140.976	65.785	54.656
Fe14a13	0.001	*<0.06*	0.003	0.002	10.883	48.739	53.180	47.147
Fe14a14	0.002	0.004	0.001	*<0.05*	36.775	20.887	22.424	20.517
Fe14a15	0.001	0.005	0.001	*<0.04*	3.440	55.650	57.931	52.802
Fe14b05	*<0.02*	0.004	0.001	0.003	17.028	55.722	59.681	54.798
Fe14b06	0.004	*<0.04*	*<0.02*	0.005	4.396	118.457	142.619	122.120
Fe14b07	BDL	BDL	BDL	0.005	4.570	309.494	355.965	324.090
Fe14b08	*<0.01*	0.003	0.002	0.002	15.707	286.245	322.244	293.144
Fe14b09	0.003	BDL	*<0.01*	*<0.08*	11.998	238.954	280.230	251.987
Fe14b10	BDL	0.006	0.001	*<0.04*	3.446	496.919	555.435	499.937
Fe14b11	BDL	BDL	0.001	0.004	0.617	71.096	83.289	77.551
Fe14b12	0.001	BDL	BDL	0.003	0.664	54.387	65.533	55.987
Fe14b13	0.007	0.004	0.001	0.003	*<0.09*	18.964	22.899	21.445
Fe14b14	*<0.02*	BDL	BDL	BDL	0.797	62.080	67.620	65.582
Fe14b15	0.004	BDL	0.003	0.012	0.184	24.557	24.383	23.572
Fe14b16	0.003	BDL	0.001	0.008	30.023	52.617	59.191	52.442
Fe14b17	0.003	0.009	0.002	*<0.05*	32.757	46.209	55.920	48.226
Fe14c05	0.001	0.005	0.004	*<0.02*	8.803	17.572	20.476	18.404
Fe14c06	BDL	0.008	0.001	*<0.02*	13.784	168.134	184.023	164.175
Fe14c07	0.007	0.008	0.001	0.002	13.297	103.735	113.783	104.546
Fe14c08	BDL	0.003	*<0.01*	*<0.05*	34.243	115.542	119.501	104.248
Fe14c09	0.005	0.003	BDL	*<0.04*	36.739	54.703	59.337	54.407
Fe14c10	0.001	0.003	0.002	0.005	30.379	71.330	85.199	74.464
Fe14c11	0.002	BDL	BDL	*<0.02*	11.370	181.386	203.587	175.704
Fe14c12	0.004	*<0.05*	0.001	0.004	10.964	30.981	34.595	30.001
Fe14c13	0.004	BDL	BDL	*<0.05*	12.582	69.501	79.728	71.238
Fe14d05	0.003	0.009	0.001	*<0.03*	0.971	13.586	6.718	4.983
Fe14d06	0.001	0.004	*<0.01*	0.005	8.973	405.669	0.118	0.123
Fe14d07	BDL	*<0.03*	*<0.01*	*<0.02*	2.508	61.886	0.334	0.242
Fe14d08	*<0.02*	*<0.04*	0.000	0.004	4.748	778.701	0.287	0.235
Fe14d09	0.002	0.004	0.001	0.003	9.442	526.808	0.915	0.644
Fe14d10	0.009	0.003	0.002	0.007	11.912	39.875	46.468	42.420
Fe14d11	*<0.03*	0.031	BDL	*<0.09*	119.790	98.767	49.747	43.342
Fe14d12	0.666	BDL	BDL	*<0.11*	55.062	76.544	50.512	49.585
Fe15b05	*<0.02*	0.004	0.001	0.001	12.341	191.031	203.809	184.162
Fe15b06	*<0.01*	0.012	0.001	*<0.05*	3.886	80.953	94.601	81.986
Fe15b07	0.002	*<0.03*	*<0.01*	*<0.02*	33.057	58.647	60.945	54.098

Table A4: Continued

Filter = <3 X LLD	*Pulse	S	Ti	Ti	MnO	Fe	Co	Ni
Isotopic mass		33	47	49	55	57	59	61
Fe15b08	1_3_2_e	-	9.3	17	0.066	-	0.285	-
Fe15b09	1_3_2_e	-	12	19	0.061	-	0.391	-
Fe15b10	1_3_2_e	-	4.4	12	0.009	-	4.637	-
Fe15b11	1_3_2_e	-	71	99	0.019	-	7.495	-
Fe15b12	1_3_2_e	-	*<1.44*	7.7	0.002	-	3.389	-
Fe15b13	1_3_2_e	-	*<1.67*	7.9	0.092	-	4.853	-
Fe15b14	1_3_2_e	-	47	53	0.004	-	4.520	-
Fe15b15	1_3_2_e	-	*<7.77*	8.6	0.010	-	2.256	-
Fe15b16	1_3_2_e	-	12	26	0.013	-	2.270	-
Fe15C05	1_3_2_e	-	1.7	8.8	0.013	-	0.925	-
Fe15C06	1_3_2_e	-	12	14	0.002	-	1.298	-
Fe15C07	1_3_2_e	-	2680	2661	0.022	-	37.235	-
Fe15C08	1_3_2_e	-	983	928	0.007	-	23.871	-
Fe15C09	1_3_2_e	-	6892	6776	0.015	-	82.411	-
Fe15e05	1	-	228	247	0.053	-	241.831	567.843
Fe15e06	1	-	5272	5237	0.024	-	71.341	*<144.95*
Fe15e07	1	-	408	422	0.080	-	519.894	845.006
Fe15e08	1	-	100	100	0.062	-	117.047	283.438
Fe15e09	1	-	498	514	0.069	-	173.473	179.104
Fe15e10	1	-	294	321	0.005	-	91.044	*<45.31*
Fe15e11	NONE	-	3807	3902	0.016	-	11.425	*<30.23*

Table A4: Continued

Filter = <3 X LLD	Ni	Cu	Cu	Ga	As	Mo	Mo
Isotopic mass	62	63	65	69	75	95	97
Fe15b08	-	-	-	4.855	651.6	0.643	0.681
Fe15b09	-	-	-	5.495	705.8	0.451	0.776
Fe15b10	-	-	-	0.740	848.0	0.516	0.917
Fe15b11	-	-	-	2.507	3403.1	0.717	1.255
Fe15b12	-	-	-	0.160	748.4	0.727	1.007
Fe15b13	-	-	-	0.703	395.5	0.495	0.595
Fe15b14	-	-	-	0.359	298.5	0.828	1.063
Fe15b15	-	-	-	0.731	1982.4	1.177	0.870
Fe15b16	-	-	-	<0.41	2332.3	1.708	1.676
Fe15C05	-	-	-	0.353	984.3	0.102	0.327
Fe15C06	-	-	-	0.189	662.6	0.421	0.516
Fe15C07	-	-	-	30.759	1778.6	0.831	1.051
Fe15C08	-	-	-	9.830	2139.3	1.677	1.666
Fe15C09	-	-	-	22.738	1897.4	3.818	3.716
Fe15e05	*<432.80*	-	-	0.354	*<80.75*	0.530	0.841
Fe15e06	*<678.01*	-	-	0.588	*<124.34*	3.577	4.930
Fe15e07	*<508.51*	-	-	4.909	165.1	2.846	3.476
Fe15e08	*<275.51*	-	-	2.520	91.6	0.169	0.476
Fe15e09	*<221.70*	-	-	0.724	*<43.43*	0.233	0.312
Fe15e10	*<216.83*	-	-	2.501	98.7	0.789	0.832
Fe15e11	*<156.10*	-	-	33.914	*<26.60*	0.502	0.682

Table A4: Continued

Filter = <3 X LLD	Ru	Ru	Rh	Pd	Ag	Sn	Sn	W
Isotopic mass	99	101	103	105	107	117	118	182
Fe15b08	*<0.05*	*<0.12*	*<0.01*	*<0.06*	**18.323**	**0.411**	**0.526**	**0.822**
Fe15b09	*<0.10*	**0.006**	*<0.02*	*<0.08*	**19.550**	*<0.57*	**0.438**	**0.277**
Fe15b10	*<0.09*	**0.004**	*<0.13*	*<0.09*	**2.482**	*<0.29*	**0.262**	**1.706**
Fe15b11	*<0.20*	**0.007**	*<0.02*	*<0.11*	**20.012**	**0.854**	**0.541**	**0.059**
Fe15b12	*<0.15*	*<0.05*	**0.004**	*<0.14*	**4.946**	**0.460**	**0.429**	**0.134**
Fe15b13	*<0.08*	**0.009**	**0.001**	**0.017**	**10.180**	*<0.55*	**0.261**	**0.042**
Fe15b14	*<0.07*	*<0.04*	**0.003**	*<0.02*	**12.016**	**0.215**	**0.322**	**0.236**
Fe15b15	*<0.27*	**0.027**	**0.002**	*<0.16*	**50.017**	**0.939**	*<1.19*	**0.293**
Fe15b16	*<0.90*	*<0.21*	*<0.04*	*<0.34*	**10.817**	*<1.21*	*<1.50*	**0.555**
Fe15C05	*<0.15*	*<0.05*	**0.005**	*<0.06*	**14.396**	*<0.34*	**0.301**	**0.212**
Fe15C06	*<0.04*	*<0.05*	*<0.00*	*<0.04*	**16.143**	*<0.38*	**0.339**	**0.106**
Fe15C07	*<0.18*	**0.015**	*<0.04*	*<0.26*	**21.387**	*<0.97*	**0.792**	**2.084**
Fe15C08	*<0.07*	*<0.05*	*<0.03*	*<0.04*	**26.727**	**0.594**	**0.803**	**0.498**
Fe15C09	*<0.08*	**0.009**	**0.007**	**0.067**	**76.842**	**2.021**	**1.906**	**2.931**
Fe15e05	**0.090**	**0.008**	*<0.01*	*<0.27*	*<0.46*	**0.623**	**0.342**	**0.594**
Fe15e06	**0.124**	**0.018**	**0.003**	*<0.25*	*<0.65*	*<1.23*	**0.835**	**1.098**
Fe15e07	*<0.51*	*<0.18*	*<0.03*	*<0.25*	**5.712**	**2.114**	**2.153**	**0.334**
Fe15e08	**0.041**	**BDL**	**0.005**	*<0.06*	**0.414**	*<0.80*	**0.401**	**0.190**
Fe15e09	*<0.09*	**0.010**	*<0.01*	*<0.05*	*<0.32*	**0.863**	**0.899**	**0.630**
Fe15e10	*<0.07*	**0.014**	**0.012**	*<0.08*	**1.499**	**0.760**	**0.811**	**1.563**
Fe15e11	*<0.14*	*<0.03*	**0.001**	*<0.05*	*<0.17*	**0.963**	**0.776**	**0.548**

Table A4: Continued

Filter = <3 X LLD	Re	Os	Ir	Pt	Au	Pb	Pb	Pb
Isotopic mass	185	189	193	195	197	204	206	207
Fe15b08	**0.003**	**BDL**	*<0.01*	*<0.03*	**0.782**	**28.006**	**27.615**	**25.704**
Fe15b09	*<0.02*	**0.002**	*<0.01*	**0.005**	**0.735**	**18.173**	**20.513**	**18.324**
Fe15b10	*<0.02*	**0.002**	**0.001**	*<0.03*	**0.771**	**7.440**	**7.992**	**7.328**
Fe15b11	**0.002**	**0.002**	**BDL**	*<0.03*	**2.888**	**25.790**	**25.847**	**24.118**
Fe15b12	**0.001**	**0.003**	**0.000**	**0.002**	**0.785**	**5.765**	**6.271**	**5.600**
Fe15b13	**0.001**	**0.003**	**0.000**	*<0.02*	**0.697**	**11.261**	**8.158**	**7.167**
Fe15b14	*<0.01*	*<0.06*	*<0.01*	*<0.01*	**1.713**	**8.858**	**9.352**	**8.379**
Fe15b15	**0.015**	**0.014**	**BDL**	**0.005**	**9.801**	*<40.85*	**38.439**	**37.577**
Fe15b16	**0.018**	*<0.16*	*<0.04*	*<0.12*	**3.287**	*<26.79*	**10.097**	**9.556**
Fe15C05	**0.006**	**BDL**	**BDL**	**0.004**	**15.632**	**17.304**	**9.098**	**8.417**
Fe15C06	*<0.01*	**0.001**	**BDL**	*<0.01*	**2.359**	**14.535**	**15.245**	**14.169**
Fe15C07	**0.012**	*<0.11*	**0.001**	**BDL**	**5.201**	**24.190**	**26.305**	**22.766**
Fe15C08	**0.001**	*<0.04*	**BDL**	**0.002**	**3.423**	**27.659**	**26.165**	**22.944**
Fe15C09	**0.007**	**0.003**	**0.001**	*<0.07*	**14.767**	**54.483**	**56.960**	**49.571**
Fe15e05	*<0.06*	*<0.12*	**0.002**	**BDL**	**<0.58**	**49.622**	**30.168**	**26.753**
Fe15e06	*<0.11*	**BDL**	*<0.04*	**BDL**	**<0.91**	**107.538**	**101.563**	**87.843**
Fe15e07	*<0.05*	**BDL**	**0.001**	**<0.05**	**<0.49**	**390.423**	**364.404**	**331.579**
Fe15e08	*<0.03*	**BDL**	**0.001**	**<0.03**	**<0.35**	**60.117**	**59.050**	**53.725**
Fe15e09	**0.001**	**0.002**	**BDL**	**<0.05**	**<0.26**	**30.326**	**13.372**	**11.790**
Fe15e10	*<0.02*	*<0.03*	**0.001**	**<0.02**	**<0.21**	**256.617**	**227.608**	**207.621**
Fe15e11	*<0.01*	*<0.02*	**BDL**	**0.004**	**<0.17**	**5.738**	**5.628**	**5.140**

Table A4: Continued

Filter = <3 X LLD	Pb	Cd
Isotopic mass	208	111
Fe15b08	**27.239**	**0.095**
Fe15b09	**18.472**	**0.062**
Fe15b10	**7.517**	**0.040**
Fe15b11	**24.580**	*<0.30*
Fe15b12	**5.861**	*<0.17*
Fe15b13	**7.568**	**0.035**
Fe15b14	**8.538**	**0.150**
Fe15b15	**36.091**	**0.126**
Fe15b16	**9.283**	*<1.04*
Fe15C05	**8.826**	*<0.17*
Fe15C06	**14.653**	**0.037**
Fe15C07	**24.225**	**0.069**
Fe15C08	**23.993**	**0.143**
Fe15C09	**52.965**	*<0.82*
Fe15e05	**27.735**	*<0.36*
Fe15e06	**97.488**	**0.084**
Fe15e07	**346.529**	**1.208**
Fe15e08	**55.801**	**0.137**
Fe15e09	**12.371**	**0.391**
Fe15e10	**216.304**	**0.988**
Fe15e11	**5.175**	**0.446**

Table A4: Continued

Filter = <3 X LLD	Pb	Cd
Isotopic mass	208	111
Fe14a05	20.424	-
Fe14a06	29.612	-
Fe14a07	21.404	-
Fe14a08	56.287	-
Fe14a09	64.859	-
Fe14a10	26.491	-
Fe14a11	48.253	-
Fe14a12	57.263	-
Fe14a13	49.879	-
Fe14a14	21.866	-
Fe14a15	54.316	-
Fe14b05	54.556	-
Fe14b06	124.121	-
Fe14b07	339.002	-
Fe14b08	296.131	-
Fe14b09	265.933	-
Fe14b10	526.475	-
Fe14b11	78.415	-
Fe14b12	58.838	-
Fe14b13	21.870	-
Fe14b14	63.193	-
Fe14b15	23.082	-
Fe14b16	53.035	-
Fe14b17	49.615	-
Fe14c05	16.798	-
Fe14c06	175.983	-
Fe14c07	105.684	-
Fe14c08	107.608	-
Fe14c09	56.386	-
Fe14c10	79.919	-
Fe14c11	185.843	-
Fe14c12	31.380	-
Fe14c13	78.587	-
Fe14d05	5.515	-
Fe14d06	0.141	-
Fe14d07	0.318	-
Fe14d08	0.269	-
Fe14d09	0.684	-
Fe14d10	43.196	-
Fe14d11	45.644	-
Fe14d12	48.169	-
Fe15b05	194.532	0.778
Fe15b06	85.307	*<0.33*
Fe15b07	57.720	*<0.25*

REFERENCES

Atwater, Tanya, 1970, Implications of plate tectonics for the Cenozoic tectonic evolution of western North America. Bull. *Geol. Soc. Amer*., **81**, 3513-3536.

Baragar, W. R. A., Ernst, R. E., Hulbert, L., & Peterson, T., 1996, Longitudinal petrochemical variation in the Mackenzie dyke swarm, northwestern Canadian Shield, *Journal of Petrology*, ***37*(2)**, 317-359.

Brueseke, M.E., Heizler, M.T., Hart, W.K., Mertzman, S.A., 2007. Distribution and geochronology of Oregon Plateau (U.S.A.) flood basalt volcanism: the Steens Basalt revisited, *Journal of Volcanology and Geothermal Research*, **161**, 187–214.

Camp, V.E., and Hanan, B.B., 2008, A Plume-triggered Delamination Origin for the Columbia River Basalt Group, *Geosphere*, **4,** no. 3, 480-495.

Camp, V.E., and Ross, M.E, 2004, Mantle dynamics and genesis of mafic magmatism in the intermontane Pacific Northwest, *Journal of Geophysical Research*, **109**, B08204.

Christiansen, R.L., Foulger, G.R., and Evans, J.R., 2002, Upper-mantle origin of the Yellowstone hotspot: *Geological Society of America Bulletin*, **114**, 1245–1256.

Coble, M.A., and Mahood, G.A., 2012, Initial impingement of the Yellowstone plume located by widespread silicic volcanism contemporaneous with Columbia River flood basalts, *Geology*, **40**, no. 7; 655–658.

Cole, D. R., & Drummond, S. E.,1986, The effect of transport and boiling on Ag/Au ratios in hydrothermal solutions: a preliminary assessment and possible implications for the formation of epithermal precious-metal ore deposits. *Journal of Geochemical Exploration*, ***25*(1)**, 45-79.

Conrad, J. E., McKee, E. H., Rytuba, J. J., Nash, J. T., & Utterback, W. C., 1993, Geochronology of the Sleeper Deposit, Humboldt County, Nevada; epithermal gold-silver mineralization following emplacement of a silicic flow-dome complex. *Economic Geology*, **88(2)**, 317-327.

Day, J.M.D., 2013, Hotspot volcanism and highly siderophile elements, *Chemical Geology*

Dickinson, W.R., and Snyder, W.S., 1979, Geometry of Subducted Slabs Related to San Andreas transform, *The Journal of Geology*, **87**, 609-627.

Dickinson, W. R., 2006, Geotectonic evolution of the Great Basin, *Geosphere,* **2**, 353–368.

Dussubieux, L., & Van Zelst, L., 2004, LA-ICP-MS analysis of platinum-group elements and other elements of interest in ancient gold, *Applied Physics A*, ***79***, *no.* 2, 353-356.

Geist, D., and Richards, M., 1993, Origin of the Columbia River plateau and Snake River plain: Deflection of the Yellowstone plume, *Geology*, **21**, 789–792.

Glen, J.M.G., and Ponce, D.A., 2002, Large-scale fractures related to inception of the Yellowstone hotspot, *Geology*, **30**, 647–650.

Hames, W., Unger, D., Saunders, J., & Kamenov, G., 2009, Early Yellowstone hotspot magmatism and gold metallogeny. *Journal of Volcanology and Geothermal Research*, **188(1)**, 214-224.

Hart, S. R., & Kinloch, E. D., 1989), Osmium isotope systematics in Witwatersrand and Bushveld ore deposits. *Economic Geology*, **84(6)**, 1651-1655.

Hedenquist, J. W., & Lowenstern, J. B., 1994, The role of magmas in the formation of hydrothermal ore deposits. *Nature*, ***370*(6490)**, 519-527.

Hofstra, A. H., & Creaser, R. A., 2009, Re–Os isotope results for electrum from three low sulfidation epithermal Au–Ag deposits in the Great Basin. In *Geological Society of America Abstracts with Programs*, **41**, No. 6, 20.

John, D.A., and Wallace, A.R., 2000, Epithermal gold-silver mineral deposits related to the northern Nevada rift: Geological Society of Nevada, Geology and Ore Deposits 2000: the Great Basin and Beyond Symposium, May 15–18, 2000, Reno-Sparks, Nevada, Proceedings, 155–175.

John, D.A., 2001, Miocene and early Pliocene epithermal gold-silver deposits in the northern Great Basin, western United States: Characteristics, distribution, and relationship to magmatism, *Economic Geology*, **96**, 1827–1853.

John, D.A., Hofstra, A.H., Fleck, R.J., Brummer, J.E., Saderholm, E.C., 2003A, Geologic setting and genesis of the Mule Canyon low-sulfidation epithermal gold-silver deposit, north-central Nevada, *Economic Geology*, **98**, 425–464.

John, D.A., Hofstra, A.H., Theodore, T.G., 2003B, A Special Issue Devoted to Gold Deposits in Northern Nevada: Part 1. Regional Studies and Epithermal Deposits, *Economic Geology*, **98**, no. 2, 225-234.

Kamenov, G. D., Saunders, J. A., Hames, W. E., & Unger, D. L., 2007, Mafic magmas as sources for gold in middle Miocene epithermal deposits of the northern Great Basin, United States: evidence from Pb isotope compositions of native gold. *Economic Geology*, **102(7)**, 1191-1195.

Leavitt, E.D., Spell, T.L.,Goldstrand, P.M., and Arehart, G.B., 2004, Geochronology of the Midas Low-Sulfidation Epithermal Gold-Silver Deposit, Elko County, Nevada, *Economic Geology*, **99**, 1665-1686.

Liu, L., and Stegman, D.R., 2012, Origin of Columbia River flood basalt controlled by propagating rupture of the Farallon slab, *Nature*, **482**, 386-389.

Mabey, D. R., 1966, Regional gravity and magnetic anomalies in part of Eureka County, Nevada, *Soc. Exploration Geophysics Mining Geophysics Case History*, **1**, 77-83.

MacDougall, R. E., Rogers, G. R., Sumner, J. S., and Ward, S. H., eds., Mining geophysics, **1**: Tulsa, Oklahoma, Society of Exploration Geophysicists, 77-83.

McLemore, V. T., 1994, Vocanic-epithermal deposit in the Mogollon-datil volcanic field, west-central New Mexico.

McQueen, K. G., 2005, Ore Deposit Types and their Primary Expressions, *Regolith Expression of Australian Ore Systems;*(Eds) CRM Butt, IDM Robertson, KM Scott, M. Cornelius. CRC LEME.

Noble, D.C., McCormack, J.K., McKee, E.H., Silberman, M.L., and Wallace, A.B., 1988, Time of mineralization in the evolution of the McDermitt caldera complex, Nevada-Oregon, and the relation of middle Miocene mineralization in the northern Great Basin to coeval regional basaltic magmatic activity, *Economic Geology*, **83**, 859–863.

Pirajno, F., 2009, *Hydrothermal processes and mineral systems*. *Springer*.

Ponce, D. A., & Glen, J. M. G., 2002, Relationship of epithermal gold deposits to large-scale fractures in northern Nevada. *Economic Geology*, **97(1)**, 3-9.

Price, J.G., 2003, Geology of Nevada: 39th Forum on the Geology of Industrial Minerals, May 18-24, 2003, Reno, Nevada, 38-39. Robinson et al., 1970.

Raven, W., Ullmer, E., Hawthorn, G.W.,2011, Update Technical Report and Resource Estimation on the Fire Creek Gold Property Lander Co., Nevada, Klondex Mines Ltd.

Rickard D, Luther GW, 2006, Metal sulfide complexes and clusters. Rev Mineral *Geochem*, **61**, 421–504.

Robinson, E. S., 1970, Relations between geological structure and aeromagnetic anomalies in central Nevada. *Geological Society of America Bulletin*, **81(7)**, 2045-2060.

Saunders, J.A., Unger, D.L., Kamenov, G.D., Hames, W.E., Utterback, W.C., 2008. Genesis of mid-Miocene Yellowstone-hotspot-related bonanza epithermal Au–Ag deposits, Northern Great Basin region, USA. *Mineralium Deposita*, **43**, 715–734.

Serenko, T.J., 1992, Epithermal alteration and mineralization at Mule Canyon, Nevada, U.S.A. [abs.], in Foster, R.P., ed., Mineral deposit modeling in relation to crustal reservoirs of the ore-forming elements [abs.]: Keyworth, United Kingdom, abstracts volume, unpaginated.

Shirey, S. B., & Walker, R. J., 1998, The Re-Os isotope system in cosmochemistry and high-temperature geochemistry, *Annual Review of Earth and Planetary Sciences*, ***26*(1)**, 423-500.

Sillitoe, R. H., Hannington, M. D., & Thompson, J. F., 1996, High sulfidation deposits in the volcanogenic massive sulfide environment. *Economic Geology*, ***91*(1)**, 204-212.

Sillitoe, R. H., & Hedenquist, J. W., 2003, Linkages between volcanotectonic settings, ore-fluid compositions, and epithermal precious metal deposits. *Special Publication-Society of Economic Geologists*, **10**, 315-343.

Simmons, S. F., & Browne, P. R., 2000, Hydrothermal minerals and precious metals in the Broadlands-Ohaaki geothermal system: Implications for understanding low-sulfidation epithermal environments, *Economic Geology*, ***95*(5)**, 971-999.

Stewart, J.H., 1980. Geology of Nevada: Nevada Bureau of Mines and Geology Special Publication, **4**, 126.

Steiner, A., 1970, Genesis of hydrothermal K-feldspar (adularia) in an active geothermal environment at Wairakei, New Zealand. *Mineral. Mag*, ***37*(292)**, 916.

Tauxe, L., Butler, R. F., Van der Voo, R., & Banerjee, S. K., 2010, Essentials of paleomagnetism, University of California Press.

Theodore, T.G., Armstrong, A.K., Harris, A.G., Stevens, C.G., and Tosdal, R.M., 1998, Geology of the northern terminus of the Carlin trend, Nevada—links between crustal shortening during the Late Paleozoic Humboldt orogeny and northeast-striking faults, U.S.Geological Survey Open- File Report **98**-338, 69–105.

Vikre, P. G., 1985, Precious metal vein systems in the National district, Humboldt County, Nevada. *Economic Geology*, **80(2)**, 360-393.

Wagner, T., Klemd, R., Wenzel, T., & Mattsson, B., 2007, Gold upgrading in metamorphosed massive sulfide ore deposits: Direct evidence from laser-ablation–inductively coupled plasma–mass spectrometry analysis of invisible gold. *Geology*, ***35*(9),** 775-778.

Wallace, A.R., 2003, Geology of the Ivanhoe Hg-Au district, northern Nevada: Influence of Miocene volcanism, lakes, and active faulting on epithermal mineralization, *Economic Geology*, **98**, p. 409–424.

Walker, R. J., Shirey, S. B., Hanson, G. N., Rajamani, V., & Horan, M. F., 1989, Re-Os, Rb-Sr, and O isotopic systematics of the Archean Kolar schist belt, Karnataka, India. Geochimica et Cosmochimica Acta, **53(11)**, 3005-3013.

Ward, P.L., 1995, Subduction cycles under western North America during the Mesozoic and Cenozoic eras, *Geological Society of America,* special paper 299.

White, N. C., & Hedenquist, J. W., 1995, Epithermal gold deposits: styles, characteristics and exploration. *SEG Newsletter*, ***23*(1)**, 9-13.

Yilmaz, H., Sonmez, N. F., Akay, E., Şener, A. K., & Tufan, S. T., 2013, Low-Sulfidation Epithermal Au-Ag Mineralization in the Sındırgı District, Balıkesir Province, Turkey. *Turkish Journal of Earth Sciences*, **22.**

Zehner, R.E., and Gustin, M.S., 2002, Estimate of Mercury Vapor Flux from Natural Substrate in Nevada, Environ. Sci. Technol., **36**, 4039-4045.

Zoback, M. L., & Thompson, G. A., 1978, Basin and Range rifting in northern Nevada: Clues from a mid-Miocene rift and its subsequent offsets, *Geology*, ***6*(2)**, 111-116.

Zoback, M.L., McKee, E.H., Blakely, R.J., and Thompson, G.A., 1994, The northern Nevada rift: Regional tectono-magmatic relations and middle Miocene stress direction, *Geological Society of America Bulletin*, **106**, 371–382.